

**Functional analysis of the anion transporter Slc4a8 with
the help of constitutive knockout mouse models**

Dissertation

zur Erlangung des akademischen Grades

doctor rerum naturalium (Dr. rer. nat.)

vorgelegt dem Rat der Medizinischen Fakultät

der Friedrich-Schiller-Universität Jena

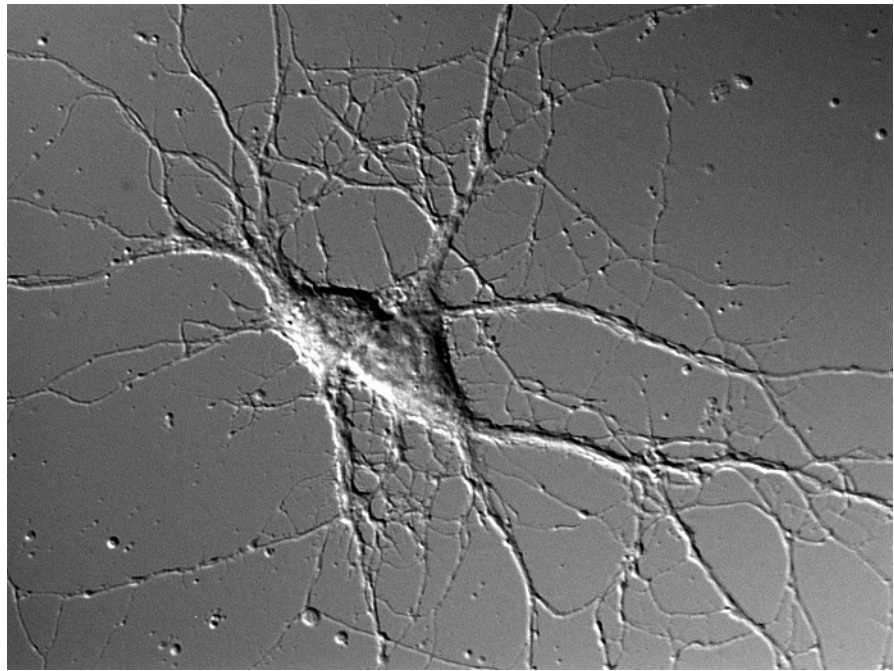
von Anne Sinning (M.sc.)

geboren am 10.05.1983 in Kassel

Gutachter

- 1. Prof. Dr. Christian A. Hübner (Institut für Humangenetik/Universität Jena)**
- 2. Prof. Dr. Otto W. Witte (Klinik für Neurologie/Universität Jena)**
- 3. Prof. Dr. Valentin Stein (Institut für Physiologie/ Universität Bonn)**

Tag der öffentlichen Verteidigung: 04.09.2012



List of abbreviations

aCSF	Artificial cerebrospinal fluid
AE	Anion exchanger
AM	Acetoxymethyl
AMPA	2-Amino-3-(5-methyl-3-oxo-1,2-oxazol-4-yl)propanoic acid
ANOVA	Analysis of variance
ATP	Adenosine-5'-triphosphate
BBS	Bicarbonate-buffered solution
BCECF	2',7'-Bis-(2-carboxyethyl)-5-(and-6)-carboxyfluorescein
CA	Carbonic anhydrase
<i>CAI-3</i>	Cornu Ammonis
Ca ²⁺	Calcium
CCD	Cortical collecting duct
cDNA	Complementary deoxyribonucleic acid
Cl ⁻	Chloride
CNQX	6-Cyano-7-nitroquinoxaline-2,3-dione
CO ₂	Carbon dioxide
D/L-APV	(2R)-Amino-5-phosphonovaleric acid
DAB	Diaminobenzidine
DAPI	4',6-Diamidino-2-phenylindole
<i>DG</i>	Dentate gyrus
DIDS	4,4'-Diisothiocyanatostilbene-2,2'-disulfonate
DNA	Deoxyribonucleic acid
DOCP	Desoxycorticosterone
eEPSC	Evoked excitatory postsynaptic current
ENaC	Epithelial sodium channel
fEPSP	Field excitatory postsynaptic potential
GABA	γ-Aminobutyric acid
GAD	Glutamate Decarboxylase

GAPDH	Glyceraldehyde-phosphate dehydrogenase
GFAP	Glial fibrillary acidic protein
H ⁺	Proton
HBSS	Hank's balanced salt solution
HCO ₃ ⁻	Bicarbonate
HCTZ	Hydrochlorothiazide
J _{ex}	Acid extruder
J _{load}	Acid loader
K ⁺	Potassium
KO	Knockout
MAP2	Microtubule-associated protein 2
MCT	Monocarboxylate transporter
mEPSC	Miniature excitatory postsynaptic current
MF	Mossy fibres
mIPSC	Miniature inhibitory postsynaptic current
mRNA	Messenger ribonucleic acid
Na ⁺	Sodium
NaCl	Sodium chloride
NBC	Sodium/bicarbonate co-transporter
NCC	Sodium chloride co-transporter
NDAE	Sodium-dependent anion exchanger
NDCBE	Sodium-dependent Chloride/Bicarbonate Exchanger
NF	Neurofilament
NH ₄ Cl	Ammoniumchloride
NHA	Sodium/proton antiporter
NHE	Sodium/proton exchanger
NMDA	N-Methyl-D-aspartic acid
PB	Phosphate buffer
PBS	Phosphate-buffered solution
PCMA	Plasma membrane Ca ²⁺ ATPase
pCO ₂	Partial pressure of carbon dioxide
PCR	Polymerase chain reaction

pH _i	Intracellular pH
pO ₂	Partial pressure of oxygen
PP	Perforant path
PSD	Postsynaptic density
RNA	Ribonucleic acid
ROMK	Renal outer medullary potassium channel
RT	Room temperature
SC	Schaffer collaterals
SDS	Sodium dodecyl sulfate
SEM	Standard error of the mean
SLC	Solute carrier
<i>Slc4a8</i> ^{-/-}	Homozygous knockout for <i>Slc4a8</i>
<i>Slc4a10</i> ^{-/-}	Homozygous knockout for <i>Slc4a10</i>
SL-M	Stratum lacunosum-moleculare
SNAP	Synaptosomal-associated protein
SOr	Stratum oriens
SPyr	Stratum pyramidale
SRad	Stratum radiatum
TBST	Tris-buffered saline added with Tween 20
TriMA	Trimethylamine-chloride
TSA	Tyramide signal amplification
vGAT	Vesicular GABA transporter
vGLUT	Vesicular glutamate transporter
WT	Wild-type
β _i	Buffering capacity
τ	Time constant

Table of contents

Summary.....	1
Zusammenfassung	3
Introduction	5
Cellular pH regulation	5
Ion transporters regulate cellular pH.....	6
Passive and active transport	6
Proton Transporters	7
Bicarbonate transporters and the Slc4 family	8
pH regulation in the brain	10
pH homeostasis as a prerequisite for brain function	10
Regulators of neuronal pH	11
Slc4a10 in the brain	14
Slc4a8 in the brain	15
Na ⁺ and HCO ₃ ⁻ transporters in the kidney	17
Renal Na ⁺ transport	18
Na ⁺ coupled HCO ₃ ⁻ transporters	19
Aim of this study	21
Material and methods	22
Molecular biology.....	22
Genotyping.....	22
Isolation of RNA from murine tissue.....	24
Reverse transcription.....	24
Realtime PCR.....	25
Reverse transcription PCR	25

Protein biochemistry	26
Protein preparation for Western blot analysis	26
Subcellular fractionation	26
Immunoblotting	27
Immunohistochemistry	28
Freeze-fracture replica immunolabeling	29
Cell culture and live cell imaging	31
Hippocampal neuron culture	31
Intracellular pH recordings.....	31
Calibration of BCECF fluorescence signal	32
Analysis of cell volume regulation.....	34
FM recordings	34
Electrophysiology	36
Slice preparation for electrophysiological recordings.....	36
Field potential recordings.....	36
Patch clamp recordings	38
<i>In vivo</i> analysis.....	40
Physiological studies	40
NaCl restriction	40
Metabolic experiments	40
Statistics	42
Data analysis	42
Results	43
Expression of Slc4a8 in non-neuronal, murine tissues	43
Slc4a8 mediates an electroneutral Na ⁺ reabsorption in the murine kidney	44
Compensatory changes in <i>Slc4a8</i> ^{-/-} mice under Na ⁺ restricted conditions	47

Expression of Slc4a8 in the murine brain	49
Broad expression of Slc4a8 in neurons, but not in glial cells of the WT mouse brain	49
Slc4a8 localizes to presynaptic, glutamatergic nerve endings in the hippocampus	50
Slc4a8 is important for the regulation of pH _i in hippocampal neurons	53
Normal cell volume regulation in <i>Slc4a8</i> ^{-/-} neurons	56
Slc4a8 modulates glutamate release	57
Altered excitability in <i>Slc4a8</i> ^{-/-} pyramidal cells of the hippocampus	57
pH dependent modulation of mEPSC frequency in WT and <i>Slc4a8</i> ^{-/-} neurons	61
Slc4a8 modulates presynaptic vesicle release	62
Pyramidal cells and interneurons express Slc4a10	65
Slc4a10 deletion alters field excitability and paired pulse depression	67
Discussion	70
Physiological role of Slc4a8 in the mouse kidney	70
Renal function of Slc4a8	70
Physiological role of Slc4a8 in the mouse brain	72
Slc4a8 localizes to presynaptic nerve endings	72
Role of Slc4a8 in neuronal pH _i regulation	72
Glutamatergic vesicle release is modulated by Slc4a8	74
How can disruption of Slc4a8 affect neurotransmitter release?	75
Clinical relevance of these findings	77
Role of Slc4a10 in cortical brain regions	78
Comparison of hippocampal expression patterns of Slc4a10 and Slc4a8	78
Deletion of Slc4a10 alters neuronal excitability antithetic to Slc4a8	79
Outlook	81
Conclusions	84
Literature	85

Appendix	97
Curriculum Vitae	97
Publications.....	99
Acknowledgements.....	100
Ehrenwörtliche Erklärung.....	102

Summary

Cellular ion homeostasis and pH regulation critically depend on the activity of ion exchangers. This is of special importance in the brain, where pH modulates neuronal excitability and neuronal activity in turn can cause changes in pH. The objective of this thesis was the investigation of the physiological function of the Na⁺-coupled anion-exchanger Slc4a8 in the mammalian brain and kidney, as well as a comparative analysis of the closely related transporter Slc4a10 with the help of knockout mouse models that had previously been generated in the group.

Slc4a8 showed a broad neuronal expression pattern but was absent from glial cells. Supporting an important role of Slc4a8 for neuronal pH regulation, cultured hippocampal neurons of mice with a targeted disruption of Slc4a8 showed a reduced steady-state pH_i and recovered more slowly from an acute acid load. In accordance with enrichment of Slc4a8 in presynaptic nerve endings of pyramidal neurons, the electrophysiological analysis revealed a pH-dependent presynaptic defect with impaired glutamate release. Whereas, release of the inhibitory neurotransmitter GABA was not affected. The decrease of hippocampal excitability in Slc4a8^{-/-} slices *in vitro* was reflected by an increased seizure threshold *in vivo*. Accordingly, these results propose that Slc4a8 in the brain modulates glutamate release and thus synaptic strength in a pH-dependent way.

In contrast, Slc4a10 is mostly localized postsynaptically in excitatory pyramidal cells and it was also abundantly expressed in most interneurons. Electrophysiological analysis revealed an increase in field excitability in the Slc4a10^{-/-} hippocampal slices and a more pronounced GABA_B-receptor mediated short term plasticity in the cortex of Slc4a10^{-/-} mice.

Besides the neuronal expression, Slc4a8 transcripts and protein were also detected in other murine tissues including the renal cortex. The renal expression of Slc4a8 was up-regulated under conditions of increased salt reabsorption. However, Slc4a8^{-/-} mice were able to adapt normally to a low sodium diet, which most likely is caused by a compensatory up-regulation of the Na⁺/Cl⁻ co-transporter NCC.

The results of this thesis suggest important roles of Slc4a8 and Slc4a10 for brain function and support their importance as possible targets for clinical applications e.g. in the future treatment of epilepsy. Besides its neurobiological function, Slc4a8 is also involved in Na⁺ transport in the renal cortex.

Zusammenfassung

Ionenhomöostase sowie zelluläre pH-Regulation hängen stark von der Aktivität einzelner Ionenaustauscher ab. Von besonderer Bedeutung ist dies im Gehirn, da hier der zelluläre pH die Erregbarkeit von Neuronen beeinflusst, aber neuronale Aktivität wiederum auch Veränderungen im pH hervorrufen kann. Ziel dieser Arbeit war die Untersuchung der physiologischen Bedeutung des Na⁺-abhängigen Anionenaustauschers Slc4a8 im Säugerhirn und der Niere, sowie die vergleichende Analyse des verwandten Transporters Slc4a10. Dies geschah mit Hilfe von *Knockout*-Mausmodellen für beide Gene, die im Vorfeld in der Arbeitsgruppe generiert worden.

Slc4a8 zeigte ein breites neuronales Expressionsmuster, wurde aber nicht in Gliazellen nachgewiesen. Erste Hinweise für eine wichtige Rolle von Slc4a8 bei der neuronalen pH-Regulation lieferten kultivierte hippocampale Neurone von Mäusen mit einer gezielten Deletion des *Slc4a8*-Genes. Diese wiesen einen verminderten basalen intrazellulären pH auf und erholten sich langsamer als *Wildtyp*-Neurone von einer Ansäuerung. In Übereinstimmung mit dem Nachweis von Slc4a8 an präsynaptischen pyramidalen Nervendigungen ergaben elektrophysiologische Untersuchungen zudem einen pH-abhängigen Defekt der Präsynapse. Dieser zeichnete sich durch eine gestörte Freisetzung des exzitatorischen Neurotransmitters Glutamat aus. Die Abgabe des inhibitorischen Neurotransmitters GABA blieb hingegen unverändert. Die verminderte Erregbarkeit in *Slc4a8*^{-/-}-Hirnschnitten *in vitro* spiegelte sich auch in einer erhöhten Krampfschwelle *in vivo* wieder. Diese Ergebnisse weisen auf eine wichtige Funktion von Slc4a8 für die Glutamat-Ausschüttung im Gehirn hin. Slc4a8 moduliert somit die synaptische Transmission über den intrazellulären pH.

Slc4a10 hingegen lokalisierte hauptsächlich an Postsynapsen von exzitatorischen Pyramidenzellen, wird jedoch auch von den meisten inhibitorischen Interneuronen exprimiert. Erste elektrophysiologische Untersuchungen ergaben eine Steigerung der Erregbarkeit in *Slc4a10*^{-/-}-Hirnschnitten des Hippokampus und eine verstärkte GABA_B-Rezeptor-vermittelte Kurzzeitplastizität im Kortex von *Slc4a10*^{-/-}-Mäusen.

Neben der neuronalen Expression konnte Slc4a8 auf Transkriptions- und Proteinebene auch in anderen Geweben der Maus nachgewiesen werden, unter anderem im Kortex der Niere. Die

renale Expression von Slc4a8 wurde unter Bedingungen verstärkter Salzurückresorption herauf reguliert. Trotzdem konnten sich *Slc4a8*^{-/-}-Mäuse normal an eine Niedrig-Salz-Diät anpassen. Diese Adaptation wird wahrscheinlich durch eine kompensatorische Regulation des Na⁺/Cl⁻-Kotransporters NCC ermöglicht.

Die Ergebnisse dieser Arbeit weisen auf eine wichtige Rolle von Slc4a8 und Slc4a10 für die Hirnfunktion hin und unterstützen deren Bedeutung als mögliche Ziele für therapeutische Anwendungen z.B. bei der zukünftigen Behandlung von Epilepsien. Neben der neurobiologischen Funktion ist Slc4a8 auch am Na⁺-Transport in der Niere beteiligt.

Introduction

Cellular pH regulation

The regulation of cellular pH is a vital homeostatic function of all cell types. pH is defined as the negative decadic logarithm of the proton (H^+) concentration:

$$pH = -\log_{10}[H^+].$$

Because of its paramount importance, intracellular pH (pH_i) is regulated at various levels:

$$pH_i = \beta_i + J_{ex} + J_{load}$$

(β_i -buffering capacity; J_{ex} -acid extrusion; J_{load} -acid load).

The first line of regulation is the inherent buffering capacity (β_i) of the intracellular and extracellular space that helps to reduce rapid localized pH shifts (Casey et al., 2010). The most important intracellular buffer is bicarbonate (HCO_3^-), which is generated by hydration of carbon dioxide (CO_2) and subsequent deprotonation of carbonic acid (Cordat and Casey, 2009). This generation of HCO_3^- from CO_2 is catalyzed by carbonic anhydrases (CAs), which thereby help to dissipate local pH gradients (for review see Supuran, 2008).

16 CAs have been described in mammals (Gilmour, 2010). CA activity was first described in red blood cells (Nyman, 1961) and later became evident in many other organs. In the mammalian brain at least 10 catalytically active isoforms or CAs have been described, which differ in cellular (Agnati et al., 1995; Parkkila et al., 2001) and sub-cellular (Langley et al., 1980; Tong et al., 2000) localization.

Furthermore, active H^+ and HCO_3^- transport mechanisms play a key role for intra- and extracellular pH regulation in many organs (Kopito et al., 1989; Gluck et al., 1996; Romero et al., 1997; Karmazyn et al., 1999; , including the brain (Chesler, 2003). Depending on the

transport direction and the transported ions, mostly HCO_3^- and H^+ , transporters are classified as acid extruders (J_{ex}) and acid loaders (J_{load}).

Ion transporters regulate cellular pH

Transport mechanisms are necessary to maintain ion concentration gradients which are essential prerequisites for the function of most mammalian cells, e.g. epithelial cells in the kidney or neurons in the central nervous system. For almost all cellular functions a tight regulation of asymmetric ion gradients is of great importance. The transport of H^+ and HCO_3^- across the cell membrane regulates the pH homeostasis. The well-balanced ion and pH homeostasis is facilitated by many different cellular transport mechanisms. In general, cellular transport can be classified as active and passive transport.

Passive and active transport

Passive transport enables the movement of molecules along its concentration gradient and ion fluxes along their electrochemical gradient. Thus, passive transport does not directly require energy. Diffusion, osmosis and filtration facilitate the membrane passage of only a minor fraction of molecules. But, passive transporters aid the translocation of molecules that cannot diffuse freely across membranes and thereby accelerate the overall transport rate. Passive transporters, such as ion channels can transport ions at rates approaching several thousand ions per second (Berg et al., 2002).

In contrast to the fast mode of action of passive transporters, energy consuming active transport mechanisms depend on the complex formation with the transported ions and are therefore relatively slow processes with a transport rate of a 10^{-10} ions per second (Lodish et al., 2000).

In mammalian cells one can distinguish two different types of active ion transporters, which differ in their primary energy source. On the one hand, ion pumps use adenosine-5'-triphosphate (ATP) as their direct energy source to carry ions against the electrochemical gradients (Purves et al., 2001). The most important ion pumps are the main determinants of the neuronal resting membrane potential, the sodium/potassium (Na^+/K^+) ATPase (Lingrel, 1992),

and the calcium/proton ($\text{Ca}^{2+}/\text{H}^+$) ATPase, which regulates pH in different cellular compartments (Schwiening et al., 1993).

The second class of active transporters on the other hand comprises of coupled carriers which are called ion exchangers. Ion exchangers use the electrochemical gradient of one co-transported ion to actively transport another. They can be classified as uniporters, symporters and antiporters depending on the number and the transport direction of the transported ions (Alberts et al., 2002).

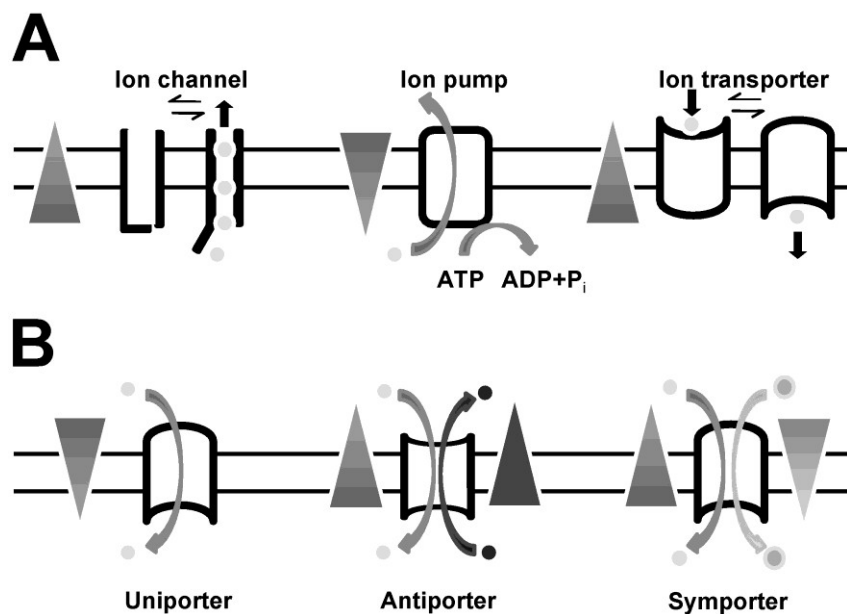


Figure 1. Cellular transport mechanisms. **A**, Ion channels enable passive transport of ions along their electrochemical gradient. Active transport against the gradient is mediated via ATP-dependent ion pumps or transporters. **B**, Transporters can be divided into uniporters, allowing the transport of single ions along their gradient and antiporters, which facilitate transport of ions against the gradient by concurrent transport of ions along its gradient. Symporters allow rectified transport of two or more ions, one along and the other against its gradient.

Proton Transporters

In general, ATP-dependent ion pumps can extrude protons from the cell, e.g. the vacuolar type H^+ ATPase (Blake-Palmer and Karet, 2009) or p-type H^+/K^+ ATPase in epithelial cells of the kidney (Codina and DuBose, 2006). ATPases also serve to acidify cellular organelles, e.g. the

H⁺ ATPase in synaptic vesicles or vacuolar ATPases in the Golgi complex (Buch-Pedersen et al., 2009).

In contrast, most protons are extruded from the cell by ion transporters via counter-transport with cations, mostly of Na⁺ or K⁺. 11 orthologues of H⁺ transporters are described in humans, 9 distinct isoforms of Na⁺-H⁺ exchangers (NHE1-9) and two isoforms of the Na⁺-H⁺ antiporter (NHA1/2) (Casey et al., 2010). The ubiquitously expressed Nhe1/Slc9a1 is a multifunctional protein that is shown to be important not only for ion exchange and intracellular pH regulation but also for cell volume regulation, cell migration and cytoskeletal anchoring (Malo and Fliegel, 2006).

Additionally, protons are co-transported with monocarboxylic acids, predominantly with lactate, mediated by monocarboxylate transporters (MCTs), a mechanism of special importance in tissues with high energy demands like brain, muscles or tumors (Halestrap and Meredith, 2004).

Bicarbonate transporters and the Slc4 family

The constant production of CO₂ by cellular respiration and concomitant generation of HCO₃⁻ renders the HCO₃⁻ concentration in the extracellular space of mammalian cells relatively high (approximately 25 mM) (Casey, 2006). In contrast to the membrane permeable CO₂, transport mechanisms are necessary for the larger, anionic HCO₃⁻ ions. An inward transport increases intracellular pH by increasing the buffering capacity for protons. The outward transport is of special importance when the impermeable HCO₃ accumulates due to rise in CO₂ concentration and jeopardizes cellular osmolarity and electroneutrality e.g. in erythrocytes or under conditions of alkaline shifts in neurons (Casey, 2006).

Known transporters for HCO₃⁻ mediate either Na⁺/HCO₃⁻ co-transport (NBC), anion exchange (AE) of HCO₃⁻ and chloride (Cl⁻) or Na⁺-dependent exchange of Cl⁻ and HCO₃⁻ (NDCBE) and can be divided into two families by their sequence homology, the Slc4 and the Slc26 family (Sterling and Casey, 2002).

Four members of the Slc26 family have been shown to mediate HCO_3^- transport: Dra/Slc26a3, Pendrin/Slc26a4, Sat-1/Slc26a1 and Pat-1/Slc26a6. At least three further homologues of this family (Slc26a7, Tat1/Slc26a8 and Slc26a9) may mediate HCO_3^- transport (Sterling and Casey, 2002). Slc26 family members transport sulfate or share homology with sulfate transporters (Markovich, 2001) and mutations in some of the family members are connected to rare genetic diseases, e.g. Pendred syndrome with mutations in *PENDRIN* (Everett et al., 1997) or congenital chloride diarrhea with mutations in the *SLC26A3* gene (Höglund et al., 1996).

The largest group of HCO_3^- transporters belongs to the Slc4 family which includes 10 different members (see Fig. 2). Most of the Slc4 members catalyse either Na^+ -independent $\text{Cl}^-/\text{HCO}_3^-$ exchange (Slc4a1-a3) or Na^+ -dependent HCO_3^- -transport (Slc4a4-a8 and Slc4a10). Additional members of this group are the borate transporter Btr1/Slc4a11 (Park et al., 2004) and Ae4/Slc4a9, a kidney specific homologue (Ko et al., 2002). The topology of all family members is relatively similar: each containing 10-14 transmembrane segments, long N- and C-terminals with hydrophilic and intracellular domains. All show similar glycosylation patterns and most are inhibited by stilbene derivatives such as 4,4'-diisothiocyanatostilbene-2,2'-disulfonate (DIDS, for review see Romero et al., 2004 or Alper, 2006).

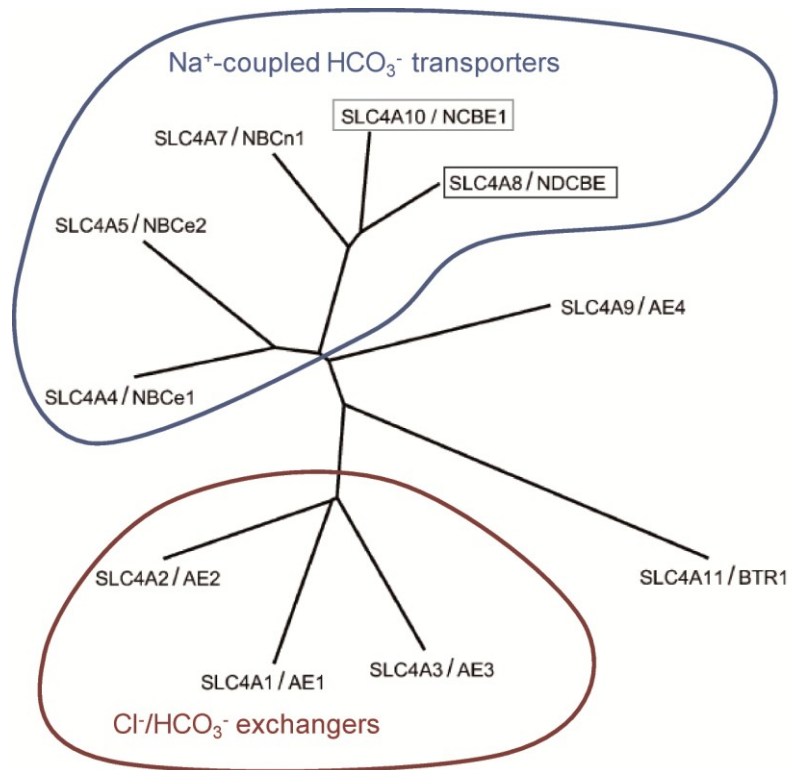


Figure 2. The SLC4 gene family. Phylogenetic analysis of representative human splice variants for all members of the *SLC4* gene family. Note the close phylogenetic proximity of *SLC4A8* and *SLC4A10*. Adapted from Romero et al. (2004).

pH regulation in the brain

pH homeostasis as a prerequisite for brain function

Given that numerous ion channels are influenced by pH (Tombaugh and Somjen, 1996; Kiss and Korn, 1999), a role of intra- and extracellular pH transients in relation to membrane potential and excitability has often been considered (Somjen and Tombaugh, 1998). This is of particular relevance in the brain, where changes in pH can on one hand influence neuronal activity and neuronal activity on the other hand can elicit rapid changes of pH. As a general rule, it appears that a rise in brain pH is associated with increased neuronal excitability, whereas a fall in pH has been shown to have the opposite effect (Chesler, 2003). The high energy demand of the brain and the concomitant production of metabolic acids as well as the negative membrane potential, which drives protons in and anions out of the cell aggravate the

need for a tight pH regulation in the brain. In this respect, the mechanisms that generate and regulate changes in pH are of considerable neurobiological interest.

CO₂ is constantly produced by metabolism, readily traverses biological membranes and can be controlled by ventilation. Importantly, hyperventilation and the associated decrease of the partial pressure of CO₂ (pCO₂) results in an increase of the pH in the blood and thus appears to be a key event in the induction of febrile seizures in the immature brain (Schuchmann et al., 2006). Febrile seizures are defined as epileptic convulsions which occur in association with febrile illness in children (peak incidence 18 month) and affect approximately 5-10 % of children in Western countries (Shinnar and Glauser, 2002). In general, epilepsies are characterized by recurrent seizures caused by abnormal neuronal activity mostly in cortical brain regions which can cause sensory, motor, cognitive, psychological or autonomic disturbances. Albeit seizure incidence in adults is generally lower than in children, epilepsies are still the most common neurological disease in humans (Hirtz et al., 2007). Interestingly, hypercarbic acidosis can terminate epileptic activity in humans (Lennox, 1928) or rodents (Mitchell and Grubbs, 1956; Ziemann et al., 2008) and might be used as a therapeutic option in the future (Tolner et al., 2011).

Regulators of neuronal pH

Because of the continuous generation of acid equivalents together with the transport of ions that alter pH, dynamic and sustained mechanisms are required to ensure long-term pH homeostasis in neurons. The neuronal regulatory machinery in principal comprises Na⁺/H⁺ exchange (Luo and Sun, 2007), monocarboxylate transport (Hertz and Dienel, 2005), Ca²⁺/H⁺-ATPase activity (Schwiening et al., 1993), passive Cl⁻/HCO₃⁻ exchange (Alper, 2009), Na⁺-driven Cl⁻/HCO₃⁻ exchange and Na⁺/HCO₃⁻ co-transport (Boron et al., 2009). A schematic overview is shown in figure 3 (Casey et al., 2010).

The acid regulation machinery may differ among different types of neurons; however, the overlapping expression of pH-relevant transporters and the lack of specific inhibitors have precluded a detailed analysis to date. Nevertheless, indirect studies have suggested that Na⁺-driven Cl⁻/HCO₃⁻ exchange contributes to acid extrusion mechanisms in hippocampal neurons (Baxter and Church, 1996; Bevensee et al., 1996; Schwiening and Boron, 1994; Bonnet et al., 2000), but the molecular correlate and its physiological relevance remained unclear. Both

Ndcbe/Slc4a8 (encoded by *Slc4a8*) and Ncbe/Slc4a10 (encoded by *Slc4a10*) are members of the Slc4a family of solute carriers (for review, (Alper, 2009) and have been shown to mediate Na^+ -driven $\text{Cl}^-/\text{HCO}_3^-$ exchange (Wang et al., 2000; Grichtchenko et al., 2001; Damkier et al., 2010). The inward bicarbonate transport classifies Slc4a8 and Slc4a10 to the group of acid extruders.

The intracellular HCO_3^- concentration, which is much higher in neurons as expected on the basis of a passive distribution, further contributes to the significant depolarizing HCO_3^- current across γ -aminobutyric acid- type A receptors (GABA_A) receptors (Kaila and Voipio, 1987). Hence, changes in neuronal HCO_3^- concentration modulate the neuronal excitation-inhibition balance in a comparable manner as it was previously shown for Cl^- transporters (Hübner et al., 2001; Ben-Ari, 2002; Dzhala et al., 2005). Accordingly, intracellular CAs have been shown to be essential for synchronous firing of hippocampal neurons by enabling tonic GABA_A ergic excitation (Ruusuvuori et al., 2004), whereas the functional importance of HCO_3^- transporters for GABA_A ergic signalling remains unclear. Since HCO_3^- transporters often catalyze concomitant transport of Cl^- , their activity can influence transmembrane Cl^- gradients and thus also the Cl^- dependent GABA_A signalling. By both mechanisms, activity of acid extruding HCO_3^- transporters such as Slc4a8 can influence neuronal excitability.

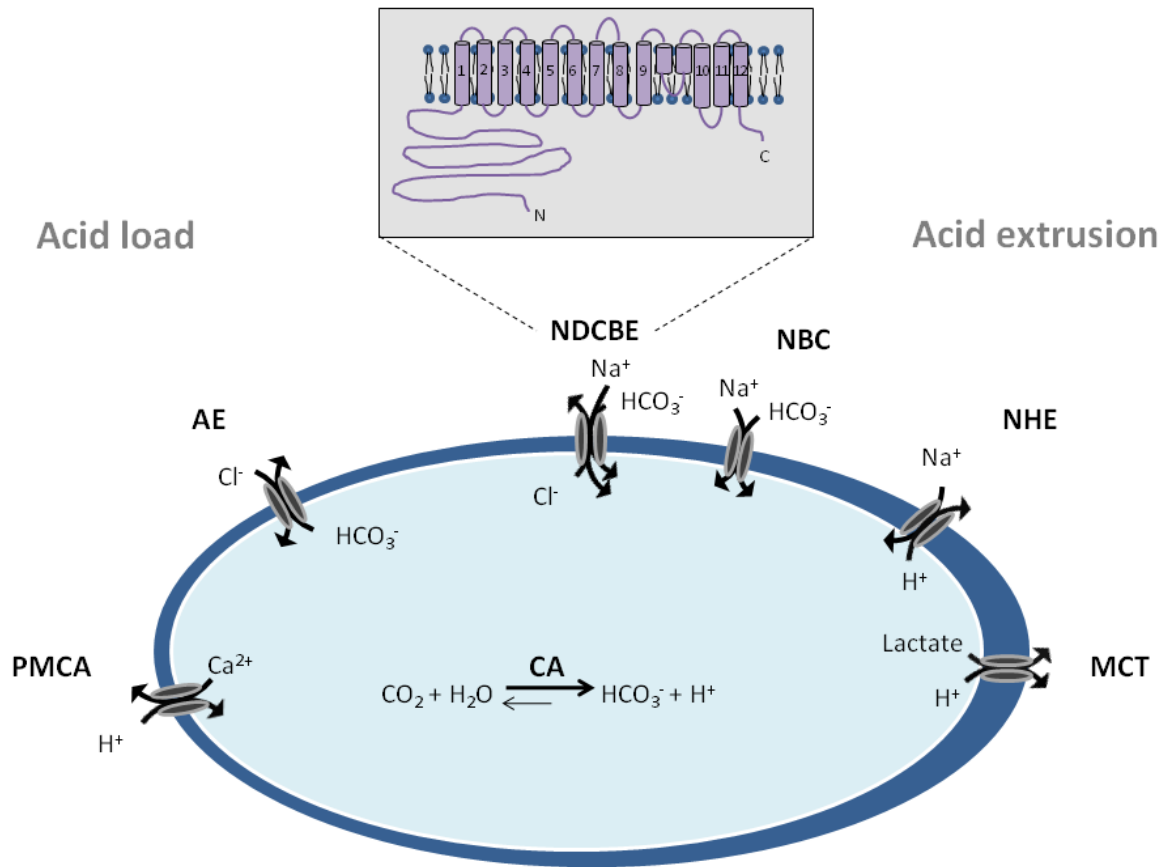


Figure 3. Intracellular and membrane-bound regulators of neuronal pH. Due to the concomitant production of metabolic acids several acid extrusion mechanisms counteract the intracellular acid load. Intracellular CAs catalyze the rapid inter-conversion of carbon dioxide and water to bicarbonate and protons. Protons are extruded from the cytoplasm mainly via the plasma membrane NHEs or co-transported with monocarboxylates by the MCTs. Inwardly directed bicarbonate transporters such as Na⁺/HCO₃⁻ co-transporters or Na⁺-dependent HCO₃⁻/Cl⁻ exchangers increase the intracellular buffering capacity and thereby elevate intracellular pH. The topology of the Na⁺-dependent HCO₃⁻/Cl⁻ exchanger Slc4a8 with its intracellular N- and C-terminal domains and the 12 transmembrane stretches is illustrated in the inset. Counterbalancing acid loading mechanisms ensure the pH homeostasis mainly via anion exchangers as well as the plasma membrane Ca²⁺/H⁺ ATPase (PCMA), which is activated under conditions of increased intracellular Ca²⁺ load. Adapted from (Casey et al., 2010).

Slc4a10 in the brain

The *Slc4a10* gene was first cloned in 2000 (Wang et al., 2000) and is mainly expressed in the central nervous system as shown at ribonucleic acid (RNA) and protein levels on adult and embryonic tissues of mouse, rat and human (Hübner et al., 2004; Praetorius et al., 2004b; Damkier et al., 2007; Chen et al., 2008b; Jacobs et al., 2008). Besides strong expression in the choroid plexus, expression was confirmed in the cerebellum, cortex and the hippocampus (Praetorius et al., 2004b; Chen et al., 2008b).

The hippocampus is part of the limbic formation in the mammalian brain and has a fundamental role in the formation of long-term memory. It is organized in a strict laminar manner with a well-defined neuronal architecture in three major areas which include the regions of the *cornu ammonis* (CA1-3), the *dentate gyrus* (DG) and the subiculum (Fig. 4).

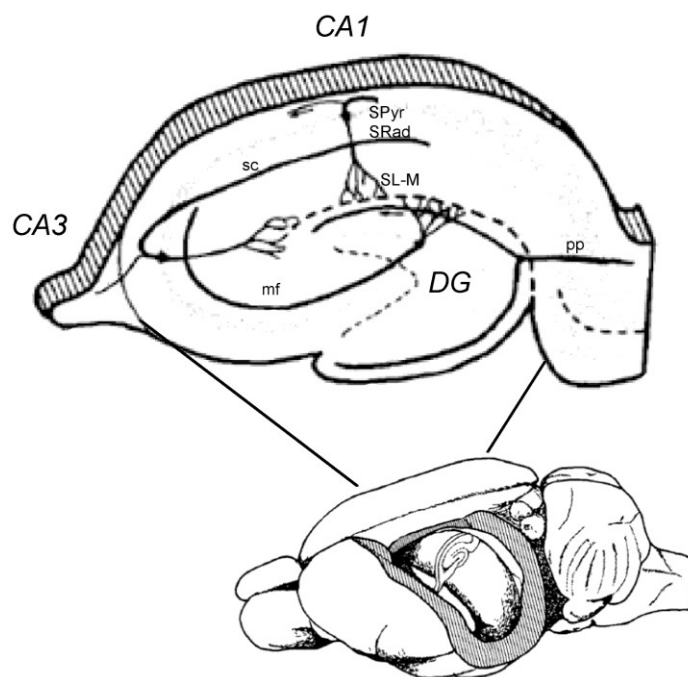


Figure 4. The hippocampal formation. The hippocampus is a c-shaped elaboration of the cerebral cortex. All major components (CA1-3 and the DG) and intrinsic connections (Mossy fibres, mf, Schaffer collaterals, sc, and parts of the perforant path, pp) are preserved in hippocampal slice preparations. Cell bodies form the stratum pyramidale (SPyr). The sc terminates in the stratum radiatum (SRad) and the pp in the stratum lacunosum-moleculare (SL-M). Adapted from Amaral and Witter (1989).

Neurons in the hippocampus can be divided into excitatory principal cells (called granule cells in *DG* or pyramidal cells in the *CA* regions) and different classes of inhibitory interneurons (for review see Mann and Paulsen, 2007). The major neurotransmitter used by excitatory principal neurons is glutamate and the major inhibitory neurotransmitter is GABA. The hippocampus is further surrounded by the parahippocampal region (e.g. ento-, peri- and postrhinal cortices), which mainly conveys output and input information between neocortex and the hippocampal formation (Burwell, 2000). The input to the hippocampus is processed through the entorhinal cortex and sent via the direct temporoammonic path or through the well-characterized trisynaptic pathway to the *CA1* pyramidal cells. In the trisynaptic pathway signals enter the hippocampus via the perforant path on *DG* granule cells, are transmitted from *DG* to *CA1* pyramidal neurons via the Mossy fibres and finally reach *CA1* pyramidal neurons via the Schaffer collaterals. Ascending projections originate in the *CA1* and the subicular region and project to the neocortex and subcortical regions (for review see van Strien et al., 2009).

On the sub-cellular levels, SLC4A10 protein is enriched at the postsynaptic side, in dendrites and dendritic spines (Jacobs et al., 2008). Disruption of the *Slc4a10* gene in mice (*Slc4a10*^{-/-}) drastically reduced brain ventricle volume and protected from fatal seizures *in vivo*. On the cellular level, disturbances in intracellular pH regulation were shown in *Slc4a10* knockout (KO) epithelial cells of the choroid plexus and in *CA3* pyramidal neurons (Jacobs et al., 2008). In contrast, previous reports from patients with heterozygous deletions in genomic regions spanning the *SLC4A10* locus reported epileptic phenotypes and mental retardation (Gurnett et al., 2008; Krepischi et al., 2010).

Slc4a8 in the brain

From early pH recordings in the squid giant axon and in snail neurons it became evident, that Na⁺-dependent Cl⁻/HCO₃⁻ exchange was the first described acid-base transport mechanism shown to play a role in pH_i regulation of neurons (Boron and De Weer, 1976; Thomas, 1976). The molecular correlate of Na⁺-dependent Cl⁻/HCO₃⁻ transport was first cloned from *Drosophila* (*ndae1*; Romero et al., 2000) and later also cloned as *Slc4a8/Ndcbe* from human and mouse brain (Grichtchenko et al., 2001; Wang et al., 2000). Whereas the stoichiometry of

Slc4a10 transport activity is under debate (Parker et al., 2008b; Damkier et al., 2010), transport activity of Slc4a8 was shown to be electroneutral with the stoichiometry 1:2:1 ($\text{Na}^+:\text{HCO}_3^-:\text{Cl}^-$) (Grichtchenko et al., 2001).

pH regulation in the brain differs among different types of neurons. The existence of a Na^+ -dependent $\text{Cl}^-/\text{HCO}_3^-$ transport was shown in 1994 in hippocampal neurons of the rat. It has already then been concluded that besides a less active Na^+ dependent, HCO_3^- independent transport mechanism, a DIDS-sensitive, Na^+ -dependent $\text{Cl}^-/\text{HCO}_3^-$ transport is the major physiological pathway of recovery from acid load and increases steady-state pH_i (Schwiening and Boron, 1994). The physiological importance of Na^+ dependent $\text{Cl}^-/\text{HCO}_3^-$ transport for hippocampal pH_i regulation was confirmed by later studies, albeit the molecular correlate remained unknown (Baxter and Church, 1996; Bevensee et al., 1996). Cloning of the human *SLC4A8* homologue and expression analysis demonstrated *SLC4A8* transcripts in the human brain (Grichtchenko et al., 2001). Several studies confirmed expression of the Slc4a8 protein in different areas of the human, mouse and rat brain, amongst others in pyramidal neurons of the hippocampus (Chen et al., 2008a; Damkier et al., 2007; Kougioumtzes, 2006). A previously generated constitutive KO mouse model for *Slc4a8* (*Slc4a8*^{-/-}) showed no obvious phenotype, but closer behavioral analysis revealed a prolonged latency till seizure onset in different *in vivo* models of epilepsy, as well as an increased body weight due to a decrease in locomotor activity.

The well-described expression of Slc4a8 and Slc4a10 in the hippocampus and the detailed characterization of neurons and connections in the hippocampus (see Fig.4) are suggestive of *in vitro* experiments on acute brain slice as used in this study amongst other techniques for the analysis of the role of Slc4a8 and Slc4a10 for nerve cell function.

Na⁺ and HCO₃⁻ transporters in the kidney

The extracellular volume is the main determinant of arterial blood pressure and it is tightly controlled by the kidney. In the kidney blood is filtrated and the primary filtrate is then modified during its passage along the nephron. Approximately 14,000 nephrons in the cortex of the mouse kidney and approximately 1 million nephrons in a human kidney warrant the fluid and electrolyte homeostasis in the mammalian body. Paracellular transport of ions along the nephron is limited to specific segments of the nephron (proximal tubulus, and the thick ascending loop of Henle). Therefore most ions are transported transcellularly (Boron and Boulpaep, 2003). Transport mechanisms for Na⁺ and HCO₃⁻ vary on the apical and basolateral side of the epithelial cells and also differ in the various sections of each nephron as well as their regulatory mechanisms (e.g. for Na⁺ transport, see Fig. 5) (Boron and Boulpaep, 2003).

Especially the reabsorption of Na⁺ plays an important role for the maintenance of the body extracellular fluid volume and thereby impacts the systemic blood pressure by regulating blood volume (Dahl and Love, 1954; Guyton et al., 1984). Increased salt retention can cause abnormal increases in blood pressure (hypertension), which are normally counteracted by the so-called pressure-natriuresis (Guyton et al., 1972; Franco et al., 2008). Hypertension affects approximately 20-50 % of the population in economically developed countries today and the worldwide prevalence is believed to increase strongly in the future (Kearney et al., 2004; Kearney et al., 2005) . Persistent hypertension is a major risk factor for stroke, myocardial infarction, as well as heart- and kidney failure (Pierdomenico et al., 2009). Therefore, pharmacological regulators of ion transporters are of great clinical relevance. Drugs that block renal ion transport and thereby increase urinary volume are called diuretics. Thiazides e.g. hydrochlorthiazides (HCTZ) or thiazide-like drugs like chlortalidone are still first line anti-hypertensive treatments (Chobanian et al., 2003). Nevertheless the development of more specific and effective diuretics in the future requires a detailed understanding of ion transport mechanisms in the kidney as well as the molecular targets of diuretics already in clinical use.

Renal Na⁺ transport

As epithelial cells in the kidney have to absorb massive amounts of sodium chloride (NaCl) from the ultrafiltrate, e.g. 1.7 kg per day in humans, several transport mechanisms facilitate the Na⁺ reabsorption and secretion along the nephron (Greger, 2000).

In the proximal part of the mammalian nephron two transporters reabsorb approximately 90 % of Na⁺: the Na⁺/H⁺ exchanger 3 (NHE3) in the proximal tubulus and the Na⁺/K⁺/2 Cl⁻ co-transporter 2 (NKCC2) in the thick ascending limb of Henle. In the distal part of the nephron the ‘classical’ Na⁺- transporters are the Na⁺/Cl⁻ co-transporter (NCC) in the distal convoluted tubule (DCT) and the epithelial Na⁺-channel (ENaC) in the cortical collecting duct (CCD; Fig. 5; (Eladari and Hübner, 2011; Greger, 2000).

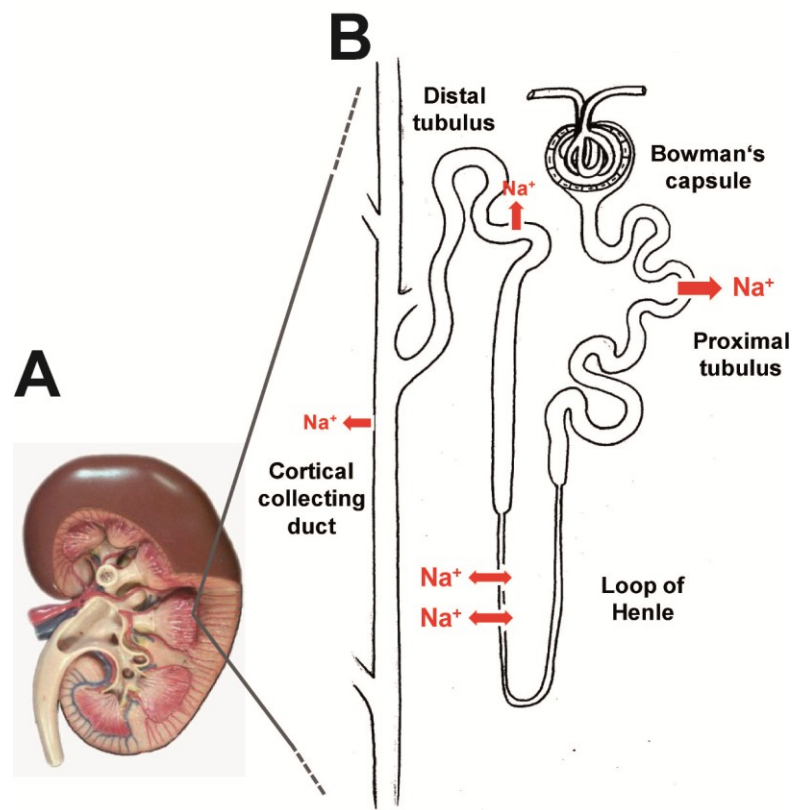


Figure 5. Schematic overview of Na⁺ reabsorption in the nephron. A, Illustration of a mammalian kidney. B, Most of the NaCl is reabsorbed from the ultrafiltrate in the proximal part of the nephron, by NHE3 in the proximal tubulus and by NKCC2 in the ascending limb of the loop of Henle. In the distal part, NCC and ENaC are the classical transport mechanisms. Adapted from <http://www.ronenvet.com/kidneydz/> and <http://www.aic.cuhk.edu.hk/web8/Kidney.htm>.

Only approximately 3 % of Na^+ is reabsorbed in the collecting duct. Nevertheless, it is of great physiological significance since it is tightly regulated by the mineralocorticoid aldosterone (for review see, Eladari and Hübner, 2011). The renal collecting duct is a highly specialized epithelium that is mainly formed by two cell types: principal and intercalated cells (Frömter, 1988). Intercalated cells, which can be divided into α -, β - and non α -non β type cells, are important regulators of the urinary pH (Wagner et al., 2009). Principal cells express the channel ENaC on the apical side and the Na^+/K^+ ATPase on the basolateral side, which together form the major mechanism of Na^+ reabsorption in this segment of the nephron. Na^+ transport by ENaC is electrogenic and therefore generates a driving force for K^+ secretion via the apical K^+ channel ROMK (Konstas et al., 2002).

Different pharmacological diuretics target the described Na^+ transport mechanism and thereby increase the urinary salt and water concentration. For example, so-called loop diuretics target the NKCC2 transporter in the loop of Henle (Shankar and Brater, 2003), amiloride blocks ENaC activity (Hummler, 2003) and the already mentioned thiazides are thought to target NCC in the CCD (Glover et al., 2011).

Although the major Na^+ transport mechanisms are well-described and already useful targets in the clinic, Slc4a8 transport activity might play an additional, yet unknown, role for renal salt reabsorption. Thus, a better understanding of the renal Slc4a8 function could improve clinical treatments in the future.

Na^+ coupled HCO_3^- transporters

Transepithelial Na^+ transport in the kidney is also often coupled to HCO_3^- transport via several ion transporters which are mainly involved in renal acid-base regulation. The extrusion of acid with the urine formed in the kidney combined with the excretion of CO_2 by the lungs ensures external pH regulation of the body.

Reabsorption of bicarbonate e.g. by α -intercalated cells in the cortical collecting duct or the excretion of fixed acids, both result in a strong acidification of the urine (Wagner and Geibel, 2002). Active HCO_3^- transport mechanisms in conjunction with carbonic anhydrase activity

therefore play an important role in the regulation of intracellular pH in the epithelial cells but also of blood and urinary pH.

Besides $\text{Cl}^-/\text{HCO}_3^-$ exchange, $\text{Na}^+/\text{HCO}_3^-$ co-transport and Na^+ dependent $\text{Cl}^-/\text{HCO}_3^-$ exchange are described in the kidney (Aalkjaer et al., 2004). Slc4a4/NBCE1 and Slc4a5/NBCE2 facilitate $\text{Na}^+/\text{HCO}_3^-$ co-transport mostly in the proximal tubules with a stoichiometry of 1:2 or 1:3 and thus are electrogenic (Abuladze et al., 2004; Boron and Boulpaep, 1983; Maunsbach et al., 2000). Also, the electroneutral $\text{Na}^+/\text{HCO}_3^-$ co-transporter Slc4a7/NBCN1 and the Na^+ dependent $\text{Cl}^-/\text{HCO}_3^-$ exchanger Slc4a8/NDCBE (also named kNBC3) are expressed in the kidney albeit their exact localizations and their physiological role remain unclear (Praetorius et al., 2004a; Pushkin et al., 1999b; Wang et al., 2001). Transport activity of Slc4a8 could theoretically support a role in renal pH regulation. But coupling of different ion transporters is a common mechanism in the kidney. Thus, Slc4a8 could also function as a sole Na^+ and/or Cl^- transporter and influence urinary and blood osmolarity as well as arterial blood pressure.

Aim of this study

A tight regulation of intra- and extracellular pH is of special relevance in the brain, where on one hand neuronal activity can evoke changes in pH and on the other hand alterations in pH influence excitability. Na⁺ dependent Cl⁻/HCO₃⁻ exchange has repeatedly been shown to be a key regulator of neuronal pH (Schwiening and Boron, 1994; Baxter and Church, 1996; Bonnet et al., 2000). Indeed, mice with a targeted disruption of either the Na⁺ dependent Cl⁻/HCO₃⁻ exchanger Slc4a10 or Slc4a8 displayed an increased seizure threshold (Jacobs et al., 2006; Kougioumtzes, 2006). Similar transport characteristics and overlapping expression of Slc4a10 and Slc4a8 in the brain suggested a comparative analysis of the closely related transporters.

A major aim of this thesis therefore was to unravel the physiological significance of the Na⁺ dependent Cl⁻/HCO₃⁻ exchanger Slc4a8 for neuronal pH_i regulation. For this purpose the cellular and sub-cellular localization of Slc4a8 protein in the brain had to be resolved. In the next step its role for the regulation of the intracellular pH of neurons should be addressed. In addition the impact of disruption of Slc4a8 on synaptic transmission should be analyzed by electrophysiological characterization of acute brain slices.

As Slc4a8 had already been shown to be expressed in the kidney (Pushkin et al., 1999a; Wang et al., 2001; Praetorius et al., 2004a), part of this thesis was the basic characterization of kidney function in mice with a targeted disruption of the Slc4a8.

Material and methods

Molecular biology

Genotyping

Genomic deoxyribonucleic acid (DNA) was isolated from tail biopsies of mice by alkaline lysis (25 mM NaOH, 0.2 mM EDTA; 30 min; 95°C). The alkaline buffer was neutralized by adding 40 mM Tris-HCl (2 min; 0°C) and DNA was stored at 4°C. Appropriate amounts of solved DNA were used for genotyping by polymerase chain reaction (PCR).

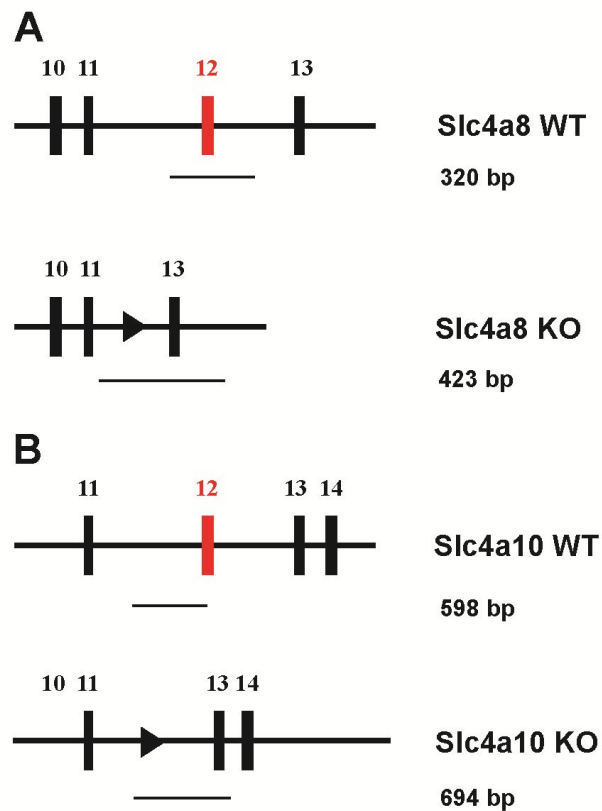


Figure 6. Genotyping strategy for *Slc4a8* and *Slc4a10* knockout mice.

A, In WT mice, primers amplified a 320 bp PCR product and genomic DNA of *Slc4a8*^{-/-} mice without exon 12 allowed amplification of a 423 bp long product. **B**, Genotyping PCR for *Slc4a10*^{-/-} mice was designed to yield a 598 bp product on WT DNA and a longer (694 bp) product on DNA from tail biopsies of *Slc4a10*^{-/-} mice.

PCR (35 cycles with 95°C for 30 sec, 59°C for 30 sec and 1 min for 72°C) with the respective primers (*Slc4a8 rev*, *Slc4a8 forw 1*, *Slc4a8 forw 2*; see table 1) results in amplification of a 423 bp band for the *Slc4a8* KO allele and of 320 bp fragment for the *Slc4a8* wild-type (WT) allele (Fig. 6A). For genotyping of the conditional *Slc4a8* mouse line PCR was performed using the *Slc4a8 rev* and the *Slc4a8 forw cond* primer, and the resulting bands were 674 bp for the WT allele and 708 bp for the floxed allele.

Table 1. Overview of used PCR primers.

Primer	Sequence (5'-3')
<i>Slc4a8 rev</i>	ggcaatccccgtcatgcacg
<i>Slc4a8 forw 1</i>	tgtagtgggtgggaactacatc
<i>Slc4a8 forw 2</i>	ggctaggcagttcttatctttccc
<i>Slc4a8 forw cond</i>	gcctgcatgtcggcccgttatac
<i>Slc4a10 forw 1</i>	ctgcaagcaatgtgtgaggag
<i>Slc4a10 rev 1</i>	gagcagcccagatgtacaccagc
<i>Slc4a10 rev 2</i>	ctccctacagacctccaacagcg
<i>Slc4a4 forw realtime</i>	aggaatctgacatcctccagtctc
<i>Slc4a4 rev realtime</i>	cagttctctgtagttcttcacagtca
<i>Gapdh forw realtime</i>	gatgcccccatggttgatg
<i>Gapdh rev realtime</i>	tggcatggactgtggtcatga
<i>Scl4a10 forw realtime</i>	cgcaatcgatctgccaatct
<i>Slc4a10 rev realtime</i>	gagctgtggttgcctttgtca
<i>Slc9a1 forw realtime</i>	gatgaagcaggccattgagct
<i>Slc9a1 rev realtime</i>	gcaagatgccgtctgaagtca
<i>Slc4a3 forw realtime</i>	ttcatgccagcaaagcacc
<i>Slc4a3 rev realtime</i>	agaagtgcaatgcagccca
<i>Slc4a7 forw realtime</i>	tgcacctcccattcgaaag
<i>Slc4a7 rev realtime</i>	ggcagttttggccatatcat
<i>Slc4a8 forw realtime</i>	gcctaaaaccacggtctggaa
<i>Slc4a8 rev realtime</i>	ggcacctcatggtccaatct
<i>Slc4a8 forw reverse transcription PCR</i>	cgtgcaagtagcatagaggag
<i>Slc4a8 rev reverse transcription PCR</i>	gtatccacctctcccaccag
<i>Gapdh forw reverse transcription PCR</i>	caacagcaactcccactcttc
<i>Gapdh rev reverse transcription PCR</i>	aaggagtaagaaaccctggacc

Mice from the constitutive KO mouse line for *Slc4a10* (*Slc4a10*^{-/-}) were genotyped with one forward and two reverse primers (see table) and the resulting PCR products were 598 bp for the WT allele and 694 bp for the *Slc4a10* KO allele (Fig. 6B).

PCR products were separated by horizontal gel electrophoresis (1-1.5 % agarose in running buffer, containing 40 mM Tris, 0.11 % acetic acid and 1 mM EDTA). DNA fragments were visualized by addition of ethidium bromide to the gel (0.05 ng/ml). Samples were added with loading dye (25 % ficoll 400, 100 mM EDTA, 0.25 % bromphenolblue) and gels were loaded in tris acetate EDTA buffer. Fragment sizes were determined by application of a 1 kb-ladder (Gene graft, Germany). Depending on fragment sizes, bands were separated at constant voltage of 120 V for 30-60 min and evaluated under ultraviolet light.

Isolation of RNA from murine tissue

Brains of adult mice were removed and rinsed with ice-cold phosphate-buffered solution (PBS; 140 mM NaCl, 3.2 mM Na₂HPO₄, 2.7 mM KCl, 1.5 mM KH₂PO₄; pH 7.4). Tissue was grinded with mortar and pestle in liquid nitrogen and trizol reagent (1 ml/50 mg tissue, Invitrogen, USA) was added (5 min, room temperature, RT). Cell debris was removed by centrifugation (5,000 g, 8 min, RT). Chloroform (200 µl/ml; Merck, Germany) was added (2 min RT), the mixture centrifuged (13,000 g, 15 min, 4°C), and the aqueous phase was collected. To precipitate the RNA, isopropanol was added (13,000 g; 10 min). The pellet was rinsed with 75 % ethanol and the RNA dissolved in diethylpyrocarbonate-treated H₂O. RNA was flash frozen in liquid nitrogen and stored at -80°C until use.

Reverse transcription

RNA concentration was determined by spectrometric absorption measurement of 260 nm with a Nanodrop system (ThermoScientific, USA) and 1 µg of RNA was used for reverse transcription. First strand complementary DNA (cDNA) synthesis was performed using random hexanucleotide primers and the Superscript III kit according to the manufacturer's instructions (Invitrogen, USA). cDNA was diluted with DEPC-treated H₂O to 5 ng/µl transcribed RNA and stored at -20°C.

Realtime PCR

cDNA of 40 ng transcribed RNA of whole brains, primers (each 5 pmol; see also Table 1) and the QuantiTect SYBR Green PCR Kit (Quiagen, Netherlands) were used for quantitative real time analysis with the Lightcycler 2 (Roche, Switzerland). Transcript abundance in tissue of three independent animals per genotype was analyzed.

Glyceraldehyde 3-phosphate dehydrogenase (*Gapdh*) served as a reference. All PCR reactions were completed with a melting-curve analysis to confirm the amplification specificity. The relative quantification was calculated with the analysis software of the Lightcycler 2. For analysis the $2^{-\Delta\Delta C(T)}$ method was used and the standard error was determined as described by Livak and Schmittgen (2001).

Reverse transcription PCR

Semi-quantitative PCR was performed on cDNA using intron-spanning primers (*Slc4a8 forw reverse transcription PCR*, *Slc4a8 rev reverse transcription PCR*, *Gapdh forw reverse transcription PCR*, *Gapdh rev reverse transcription PCR*; see table 1) and a standard PCR program (35 cycles; 94 °C for 20 s, 57 °C for 30 s and 72 °C for 30 s). Amplified fragments (*Slc4a8* 376 bp, *Gapdh* 164 bp) were visualized on a 2 % agarose gel as described for analysis of genotyping.

Protein biochemistry

Protein preparation for Western blot analysis

Membrane fractions were isolated from tissue lysates by addition of ice cold homogenization buffer (125 mM NaCl, 18 mM Tris, 4.5 mM EDTA), sonification and brief centrifugation (2x 1,000 g; 10 min; 4°C) to remove cell debris and nuclei. Ultracentrifugation of the supernatant (13,500 g; 30 min; 4°C) was performed and the pellet was dissolved in lysis buffer (1% Triton X-100 in PBS) or RIPA buffer (25 mM Tris, 250 mM NaCl, 1% NP-40, 0.1% sodium dodecyl sulfate, SDS).

Preparation of membrane fractions from renal cortices were performed as described previously (Quentin et al., 2004). In short, kidneys were cut into 5-mm slices and the renal cortex was excised under a stereoscopic microscope and placed into ice-cold isolation buffer (250 mM sucrose, 20 mM Tris-HEPES, pH 7.4) containing protease inhibitors (1x *complete* protease inhibitor cocktail, Roche, Switzerland). Minced tissues were homogenized with a teflon douncer (Sartorius, Germany). The homogenate was centrifuged at 1,000 g for 10 min and the supernatant was centrifuged at 100,000 g for 20 min at 4°C. The pellet was resuspended in isolation buffer.

Total lysates from cell culture were prepared by applying RIPA buffer to detach and solve the cells. Cell lysates were centrifuged (1,000 g; 10 min; 4°C) to remove the cell debris.

All buffers were substituted with *complete* protease inhibitor cocktail (1x) and *pefabloc* (4 mM, both Roche, Switzerland) according to the manufacturer's instructions. Protein amounts were determined by use of the bicinchoninic acid protein assay (Pierce, USA) and subsequent spectral measurements with the Nanodrop system. Protein concentration was adjusted with the respective buffer. Laemmli buffer (63 mM Tris-HCl, 10 % glycerol, 2 % SDS, 0.0025 % bromphenol Blue, 1 % β -mercaptoethanol) was added and proteins were denatured at 60 °C for 20 min.

Subcellular fractionation

Synaptic proteins were prepared as described previously (Carlin et al., 1980) with minor modifications. Whole brains of adult mice (≥ 2 brains per preparation) were homogenized in

homogenization buffer (0.32 M sucrose, 5 mM HEPES, pH 7.4) with a teflon douncer and centrifuged twice (1,000 g, 10 min at 4°C) to remove cell debris and nuclei. For all following centrifugation steps except the final step, a preparative ultracentrifuge (L-90K, rotor JA25.50, Beckman Coulter, USA) was used. The crude membrane fractions were pelleted from the supernatants (12,000 g, 20 min) and solved in homogenization buffer. The cytosolic fractions were harvested from the supernatant by ethanol precipitation and ultracentrifugation (100,000 g, 1 h at 4°C). The synaptosome fractions were isolated from the membrane fractions by a discontinuous sucrose gradient (0.85/1/1.2 M sucrose; 85,000 g; 2 h at 4°C) and harvested in the interface of 1.0 M and 1.2 M sucrose. The synaptosomal membrane fractions were prepared by osmotic lysis (1 mM Tris-HCl, pH 8.1, 30 min at 0°C) and centrifugation (33,000 g; 30 min at 4°C). Synaptic junction plasma membranes were enriched by a subsequent second sucrose gradient (0.85/1/1.2 M sucrose; 85,000 g; 2 h at 4°C). For the final isolation of the postsynaptic density (PSD) fraction, two triton X-100 purification steps (0.32 M Sucrose, 0.5 mM EDTA, 7.5 mM Tris-HCl, 0.5 % triton X-100, pH 8.1; 15 min at 0°C) were performed with subsequent centrifugation of the insoluble (PSD) fractions (32,000 g; 30 min at 4°C). To isolate the final PSD fraction, the pellet was resuspended (0.32 M Sucrose, 1 mM EDTA, and 5 mM Tris-HCl), applied on 1.5 M Sucrose and centrifuged for at least 2 h at 202,000 g (Optima™ TLX, rotor SW 41, Beckman Coulter, USA). The final pellets as well as all other fractions were solved in RIPA buffer substituted with protease inhibitors and prepared for Western blot analysis as described.

Immunoblotting

For immunoblotting, 10 µg of protein (or otherwise indicated) was separated by reducing SDS 8 % polyacrylamide gel electrophoresis and transferred to nylon membranes (Mini Trans-Blot Cell, Biorad, USA). After blocking with 5 % non-fat dry milk in Tris-buffered solution added with tween 20 (Sigma-Aldrich; TBST) for 1 h at RT, blots were incubated with the respective primary antibodies (over-night, 4°C). Detection was achieved using peroxidase-coupled secondary antibodies (2 h, RT). The signals were visualized with an enhanced chemoluminescence Kit (Amersham Biosciences, Germany) and autoradiography films (AGFA, Medical X-Ray films, Germany). The following primary antibodies were used: rabbit anti-Slc4a8 (1:500), mouse monoclonal anti-PSD-95 (1:1,000; Abcam, USA) and mouse

monoclonal anti-synaptophysin (1:1,000; Millipore). β -Actin (1:40,000; Santa Cruz, USA) served as a loading control. If needed, quantification of bands was performed by densitometry using the National Institute of Health Image software (*Image J*, USA). Densitometric values were normalized to the mean for the control group that was defined as 100 %.

Immunohistochemistry

Immunohistochemical stainings were performed mostly as described previously (Jacobs et al., 2008). For immunohistochemistry, the brain of an adult mouse (WT or *Slc4a8*^{-/-}, 6-8 weeks of age) was removed after transcardial, consecutive perfusion of anesthetized mouse with phosphate buffer (PB; 155 mM Na₂HPO₄, 22.6 mM NaH₂PO₄) and 2 % paraformaldehyde/0.25 % glutaraldehyde in PB. The tissue was postfixed for 2 h at RT. Tissue was incubated in 30 % sucrose overnight for cryoprotection. Free-floating cryosections (50 μ m) were cut with a sliding microtome (-20 °C; Leica, Germany) and stored in PB (4 °C) until used for immunostainings. Non-specific staining was avoided by incubating the slices in blocking solution (1 h, RT). Blocking solution contained 5 % normal goat serum (Millipore, USA) in wash buffer (PBS with 0.25 % Triton X-100, Sigma-Aldrich, Germany). Slices were stained with the primary antibody diluted in blocking solution overnight at 4 °C. For most stainings polyclonal antibodies against SLC4A8 protein (Leviel et al., 2010) were used, which were raised in rabbits immunized against a c-terminal epitope (ALSINSGNTKEKSPFN-COOH) encoding exon 24 (aa 1074-1089) of *Slc4a8* and (accession number Q8JZR6, UniProt) and affinity purified (Eurogentech, Belgium). For diaminobenzidine (DAB) staining, coronal and sagittal brain sections were incubated with a biotinylated anti-rabbit immunoglobulin G secondary antibody using the vectastain ABC-kit (Vector Laboratories, USA). The peroxidase stain was visualized by 0.05 % DAB, 0.04 % nickel ammonium sulfate and 0.03 % H₂O₂ dissolved in 0.01 M PB.

For immunofluorescence studies on sagittal and coronal brain sections (n \geq 6 from at least two independent preparations and stainings), the *Slc4a8* signal was amplified with a tyramide signal amplification (TSA) kit according to the manufacturer's instructions (Invitrogen, Germany). For co-stainings, the following primary antibodies were used: monoclonal mouse anti-neurofilament 68 (NF68; 1:500, Sigma-Aldrich), monoclonal mouse anti- glutamate decarboxylase 67 (GAD67; 1:500, Millipore), polyclonal guinea pig anti-vesicular glutamate

transporter 1 (vGLUT1; 1:500, Synaptic Systems, Germany), monoclonal mouse anti-vGLUT 2 (1:250; Millipore), monoclonal mouse anti-vGLUT3 (1:5,000; Millipore), polyclonal guinea pig anti-vesicular GABA transporter (vGAT; 1:500; Synaptic Systems), monoclonal mouse anti-synaptophysin (1:500; Millipore), mouse anti-parvalbumin (1:2,000; Swant, Switzerland), monoclonal mouse anti-microtubule-associated protein 2 (MAP2; 1:500; Sigma-Aldrich), monoclonal mouse anti-PSD protein 95 (PSD-95; 1:1,000; Abcam; USA), monoclonal mouse anti-glial fibrillary acidic protein (GFAP; 1:500; Chemicon; Germany) and a rabbit polyclonal antibody against Slc4a10 protein (1:500). The Slc4a10 antiserum was raised in rabbits against the epitope KHRKRDRERDSGLED (amino acids 71–85 of the SLC4A10 protein; accession no. NM 033552), coupled by a C-terminal cysteine to keyhole limpet hemocyanin and affinity-purified (Jacobs et al., 2008).

For co-stainings with primary antibodies of different specificity raised in the same species, slices were sequentially stained with the two different antibodies similar as described previously by (Tóth and Mezey, 2007). First, staining against the first epitope was performed using the TSA kit as described. After this staining, the antibodies were removed by heating the slices (5 min, 100°C) in citrate buffer (0.1 M Na₂HPO₄, 0.1 M citric acid, pH 6.0). Slices were then stained with antibodies against the second epitope and fluorescently labeled by corresponding secondary antibody.

Alexa Fluor 488- and 555-coupled goat anti-rabbit, goat anti-guinea pig and goat anti-mouse (1:500 or 1:1,000 in blocking buffer, Molecular Probes, Netherlands) were used as secondary antibodies (2 h, RT) and slices were washed with washing buffer (3x 10 min) between and after the incubation with the secondary antibodies. Cell nuclei were stained by 4',6-diamidino-2-phenylindole (DAPI; 1 µg/mL; Sigma-Aldrich). Analysis was performed by confocal microscopy (LSM 510; Zeiss, Germany) and representative pictures were chosen.

Freeze-fracture replica immunolabeling

The ultrastructural analysis was performed in close collaboration with PD Dr. Martin Westermann from the Electron Microscopy Center of the University of Jena.

For freeze-fracture replica immunogold labeling aliquots of isolated synaptosomes were enclosed between two 0.1 mm copper sandwich profiles. The profiles were rapidly frozen by plunge-freezing in liquid ethane/propane (1:1) cooled by liquid nitrogen. Freeze-fracture was

performed in a BAF400T (BAL-TEC, Liechtenstein) freeze-fracture unit at -150°C using a double-replica stage. The fractured samples were replicated by perpendicularly evaporation of carbon (15-25 nm) as first layer, followed by platinum/carbon (2 nm) shadowing at an angle of 35° . The SDS freeze-fracture replica labeling technique was performed as described (Westermann et al., 2005), using specific primary antibodies against Slc4a8 (1:100), Syntaxin (mouse monoclonal, 1:50 Sigma-Aldrich) and the synaptosomal-associated protein 25 (SNAP25; guinea pig polyclonal, 1:50; Synaptic Systems) followed by gold-conjugated second antibodies goat anti-rabbit (diameter 10 nm), goat anti-mouse (diameter 5 nm) or goat anti-guinea pig (diameter 5nm) (British Biocell International, UK). After immunolabeling the replicas were fixed with 0.5 % glutaraldehyde, washed with distilled water and finally picked onto Formvar coated grids. Images were taken as digital pictures in an EM 902 A electron microscope (Zeiss, Germany) using a 1 k FastScan-CCD-camera (TVIPS camera and software, Germany).

Cell culture and live cell imaging

Hippocampal neuron culture

Mixed hippocampal cultures were prepared similar as described previously (Kaeck and Banker, 2006). Mice from homozygous WT or *Slc4a8*^{-/-} matings were sacrificed at postnatal day 0.5–1.5. Brains were removed and hippocampi dissected in ice-cold Hank's buffered salt solution (HBSS) supplemented with penicillin-streptavidin/HEPES (pH 7.25). Hippocampi were rinsed three times with HBSS and trypsinized with 0.05 % trypsin/EDTA (Invitrogen) for 25 min at 37°C. The supernatant was removed and rinsed with HBSS. The tissue was placed in 2 mL of HBSS containing 20 µL DNase (1 µg/µL in HBSS) and dissociated into single cells by trituration with folded Pasteur pipettes of decreasing diameters. Approximately 50,000 cells were plated onto coated coverslips (ø 18 mm) in plating medium (Modified eagle medium, GIBCO, Germany; 10 % horse serum, 0.6 % glucose). Coverslips were coated with poly-L-lysine (1 mg/ml, Sigma-Aldrich) overnight and subsequently washed three times with HBSS before use.

Cells were allowed to settle for 10–20 min at 37 °C/5 % CO₂. Finally, coverslips were transferred to 6 cm culture dishes containing neurobasal medium (GIBCO) supplemented with 1 mM L-glutamine (Invitrogen), 0.2 % horse serum and B27 supplement (Invitrogen). Neurobasal medium supplemented with B27 was added once a week to maintain the initial volume. For pure glial culture, astrocytes were cultured with Dulbeccos modified eagle medium supplemented with 10 % fetal calf serum and penicillin-streptavidine and split at least 3 times. pH measurements were performed after 21–28 days in culture, analysis of cell volume regulation after 7-14 days and FM measurements at day 14 *in vitro*.

Intracellular pH recordings

The fluorescent indicator 2',7'-bis-(2-carboxyethyl)-5-(and-6)-carboxyfluorescein (BCECF; Rink et al., 1982) was used for non-invasive measurement of pH_i in cultured hippocampal neurons. BCECF is a commonly used dual-excitation indicator, which is pH sensitive when excited by light of a wavelength of 495 nm, and nearly pH insensitive when the excitation wavelength is shifted to 440 nm (isobestic point). It thereby allows ratiometric monitoring of

the pH_i independent of photobleaching and dye leakage in cell culture (Boyarsky et al., 1988). All carboxylate groups of BCECF are esterified by acetoxymethyl (AM) groups which are removed by unspecific intracellular esterases and thereby render the lipophilic, fluorescent dye trapped within the cell (Grynkiewicz et al., 1985).

Primary hippocampal cultures were loaded with BCECF-AM (Molecular Probes, Netherlands) at a final concentration of 1 μM with 0.002 % Pluronic F127 in bicarbonate-buffered solution (BBS, containing in mM: 125 NaCl, 3 KCl, 1.2 CaCl₂, 1.2 MgSO₄, 1.25 NaH₂PO₄, 10 glucose and 26 NaHCO₃, gassed with 95 % O₂/5 % CO₂, pH 7.3; (Yao et al., 1999)) for 5–10 min at 37 °C. For recordings, coverslips were mounted onto a perfusion chamber (350 μl volume, ChamSlide EC, Live Cell Instruments, Korea) and superfused with BBS (32 \pm 0.2°C) at a linear flow rate of 1.5–2.0 ml/s corresponding to \sim 4 bath changes per min. A subset of experiments was performed in the nominal absence of bicarbonate and presence of 30 mM HEPES (pH adjusted to 7.3 with NaOH). Light emission (510–535 nm) upon alternating excitation with 495 nm and 440 nm was recorded with a 10 \times objective every 10 s with a charge-coupled device camera (AxioCam MRm, Zeiss). The F_{495}/F_{440} ratio was converted into pH_i values using the nigericin single-point calibration technique (Boyarsky et al., 1988). After defining the region of interest (somata of pyramidal neurons) and 10 min of baseline recordings, the basal pH_i was calculated as mean pH_i over 30 s. Cells were acid loaded by the ‘rebound acidification’ technique (Boron and De Weer, 1976) with a 20 mM ammonium chloride (NH₄Cl) pulse (BBS with equimolar substitution of Na⁺ by NH₄⁺) and NH₄Cl induced alkalosis was quantified as $\text{pH}_{\text{Maximum}} - \text{pH}_{\text{Baseline}}$. The rate of pH_i recovery (dpH_i/dt) was determined over the first minute after peak acidification upon withdrawal of NH₄Cl and at pH_i 7.7–7.8. Data from ≥ 20 neurons (2–7 cells/experiment) cultured from at least three independent preparations per genotype were averaged. For NH₄Cl pulse experiments in the presence of HEPES ≥ 10 cells were analyzed from at least two independent preparations per genotype.

Calibration of BCECF fluorescence signal

The calibration curve was constructed using HEPES-buffered solutions (containing in mM: 105 KCl, 20 N-methyl-D-glucamin, 5 MgSO₄, 10 glucose, 30 HEPES, 0.010 nigericin). The proton ionophore nigericin allows exchange of H⁺ for K⁺ ions across their concentration

gradients. Thus, if external K^+ concentration is strongly increased protons can move freely across the cell membrane and equilibrate intracellular pH with the extracellular pH (Thomas et al., 1979).

The pH of the calibration solution was adjusted to different pH values in the range of 6.0 to 8.0 with HCl. Calibration data from ≥ 8 experiments were analyzed and a common equation was obtained from a regression fit. The non-linear regression analysis for the construction of a calibration curve (Fig. 7) was performed with the help of Prof. Dr. Alt (Institute for Applied Mathematics, University Jena) and yielded the following equation: $pH_i = 7 - (1 / (\text{TAN}((6,29 * F_{495nm} / F_{400nm}) / (4 * F_{495nm \text{ pH } 7.0} / F_{400nm \text{ pH } 7.0}))))$.

For conversion of F_{495nm} / F_{400nm} values into actual pH_i values, F_{495nm} / F_{400nm} at pH 7.0 in the presence of nigericin was determined after each measurement and the entire set of F_{495nm} / F_{400nm} values from a single cell was then normalized to the F_{495nm} / F_{400nm} ratio at pH 7.0 via the above mentioned equation (one-point calibration; Boyarsky et al., 1988)

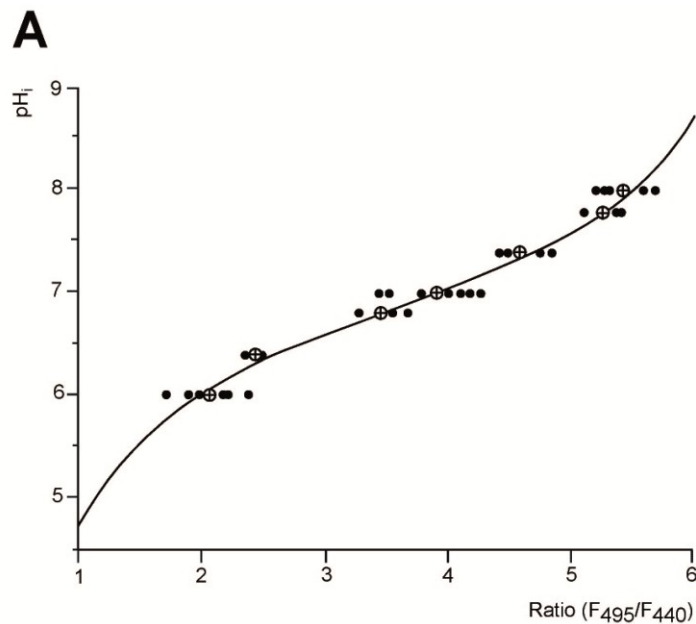


Figure 7. Calibration curve for the conversion of the fluorescence ratio F_{495nm} / F_{400nm} into pH_i values. A, Ratios of F_{495nm} / F_{400nm} gathered by different measurements (closed circles) and mean values at distinct extracellular pH values (crossed open circles) in the presence of nigericin. In grey, non-linear regression analysis resulted in good fit and allowed conversion of F_{495nm} / F_{400nm} into actual pH_i values by the help of a one-point calibration after each measurement.

Analysis of cell volume regulation

Mixed hippocampal cultures were loaded with AM ester of calcein blue (Molecular Probes, Invitrogen, 4 μ M, pre-diluted in dimethyl sulfoxide) for 30-40 min at 37°C. During the measurement, cells were continuously superfused with isotonic BBS (containing in mM: 135 NaCl, 5 KCl, 1 CaCl₂, 1.2 MgCl₂, 1.7 KH₂PO₄, 5 glucose and 26 NaHCO₃, 32±2°C gassed with 5 % CO₂/ 95 % O₂; flow rate 2 ml/min). For hypo- and hyper-osmotic conditions, NaCl concentration was decreased or increased by 50 mM NaCl, respectively. Optical recordings were performed as described for pH measurements except for changes in the excitation (Exc = 370 nm) and emission wavelength (Em = 445 ± 25 nm, Zeiss filterset 49) and use of a 25x objective. Fluorescence intensity was corrected for bleaching by negative slope analysis. Two regions of interests within the soma were analyzed for each pyramidal neuron. For analysis of cell volume (V), mean fluorescence intensity over time per region of interest (F(t)) and the fluorescence intensity under iso-osmotic, resting conditions (F(0)) were used to calculate the relative cell volume (V(t)) following the equation : $V(t) = (F(0)/F(t))/1$ (Loo and McNamara, 2006).

FM recordings

For analysis of presynaptic vesicle release in WT and *Slc4a8*^{-/-} hippocampal neurons, synaptic vesicles were labeled with a fluorescent FM dye and vesicle exocytosis upon electrical field stimulation was investigated by quantification of fluorescence intensity decline (Gaffield and Betz, 2006).

Coverslips with hippocampal cultures at day 14 *in vitro* were mounted onto an optical recording chamber supplied with a pair of platinum electrodes for field stimulation (Chamlide EC). During the recording cells were continuously superfused with BBS (pH 7.3, flow rate 1.1 ml/min at room temperature) supplemented with 6-cyano-7-nitroquinoxaline-2,3-dione (CNQX, 10 μ M, Tocris, UK) and (2R)-amino-5-phosphonovaleric acid (D/L-APV, 50 μ M, Sigma-Aldrich) in an optical recording chamber supplied with a pair of platinum electrodes for field stimulation. After 5 min, the cells were exposed to high potassium BBS (containing in mM: 68 NaCl, 60 KCl, 1.2 CaCl₂, 1.2 MgSO₄, 1.25 NaH₂PO₄, 10 glucose and 26 NaHCO₃) supplemented with 10 μ M FM1-43 (Molecular Probes) for 1 min followed by 1 min BBS supplemented with 5 μ M FM1-43 and washed with BBS for 10 min. Fluorescence was

recorded with a 63× water-immersion objective at a frequency of 1 Hz (Exc=480 nm, Em=445±25 nm). Following the baseline recording, 1 ms current pulses were applied for 150 s at a frequency of 10 Hz (corresponding to ~1,500 action potentials). Sub-threshold stimulus intensity (80 V) was determined in a subset of pilot experiments in which hippocampal cells were loaded with the calcium-sensitive dye Oregon-green BAPTA-AM (Molecular Probes, Netherlands) and stimulation intensity was increased till each stimulus resulted in an uniform increase in calcium, representing an action potential. Regions of interest corresponding to nerve terminals (≥ 25 , \varnothing 1.5 μm) were analyzed (6 recordings from three independent preparations per genotype). Bleaching effects were corrected by negative slope analysis. Puncta that did not show a reduction of the corrected fluorescence intensity of more than 30% after stimulation or that could not be fitted by a mono-exponential fit were excluded from analysis of the destaining time constant (τ).

Electrophysiology

Slice preparation for electrophysiological recordings

Immediately after decapitation, brains from adult mice (WT, *Slc4a8*^{-/-} or *Slc4a10*^{-/-}; 4-8 weeks or 3-6 weeks of age, males and females) were removed from the skull and chilled (at ~4°C) in artificial cerebrospinal fluid (aCSF) containing (in mM): NaCl 120, KCl 3.5, MgSO₄ 1.3, NaH₂PO₄ 1.25, CaCl₂ 2.5, D-glucose 10 and NaHCO₃ 25, gassed with 95 % O₂/5 % CO₂, pH 7.3. Frontal lobes and cerebellum were removed. Coronal slices were prepared with a vibroslicer (VT 1000S, Leica Instruments, Germany) as described previously (Liebmann et al., 2009). Slices (350 μm) were stored at RT in aSCF for at least 1h until use.

Field potential recordings

After a 1 h equilibration period, slices were transferred to an interface recording chamber and perfused with gassed aCSF (2–3 mL/min) at 32°C. Slices were allowed to equilibrate to the recording conditions for 1 hr. Bipolar stimulating electrodes with a tip diameter of 100 μm (SNE-200X, Science-Products, Germany) were placed onto the sc fibers in the hippocampus or in layer 6, close to the corpus callosum, of the cortex (see also Fig. 8). Data of field potential recordings were collected with an extracellular amplifier (EXT-02, NPI, Germany), low pass filtered at 4 kHz and digitally stored with a sample frequency of 10 kHz. Data acquisition and analysis of population spike amplitudes were performed using the software Signal (Cambridge Electronic Design, UK). Upon stimulation (pulse duration 50 μs), field excitatory postsynaptic potentials (fEPSPs) were recorded using glass microelectrodes (2–5 MΩ, filled with aCSF) impaled into the SPyr or the SRad of hippocampal CA1 region, as well as layer 2/3 of the corresponding cortical positions. Slopes of fEPSPs were determined for recordings in the SRad and for all other recording positions amplitudes were analyzed using the Signal software.

The maximal population spike amplitude was determined by gradually increasing the stimulus intensity (0-70 V) for each experiment (interstimulus interval 30 s) until the responses saturated. The relationship between stimulus intensity and the evoked response was fitted by a

sigmoid function: $R_{(i)} = R_{\max} / (1 + \exp(i - i_h))$, where $R_{(i)}$ is the response at intensity (i), R_{\max} is the maximal response and i_h is the intensity at which half-maximal response was observed.

Following determination of the half-maximal stimulation intensity, paired-pulse stimuli were applied with interstimulus intervals of 15, 20, 30, 50, 80, 120, 180, 280, 430, 650 and 1,000 ms to investigate possible changes in short term plasticity. Depending on timing and brain region the response to the second stimulus can be 5 times in size of the response to the first stimulus. In the hippocampus a conditioning pulse (fEPSP1) leads to an increase of intracellular calcium via voltage dependent calcium channels in the nerve terminals of neurons (Katz and Miledi, 1968; Wu and Saggau, 1994). A sustained increase in intracellular calcium levels then facilitates a second fEPSP. In the cortex, response to the second stimulus is smaller than the first response (paired-pulse depression). The paired pulse ratio (fEPSP2/fEPSP1) is therefore a measure for the paired pulse paradigm.

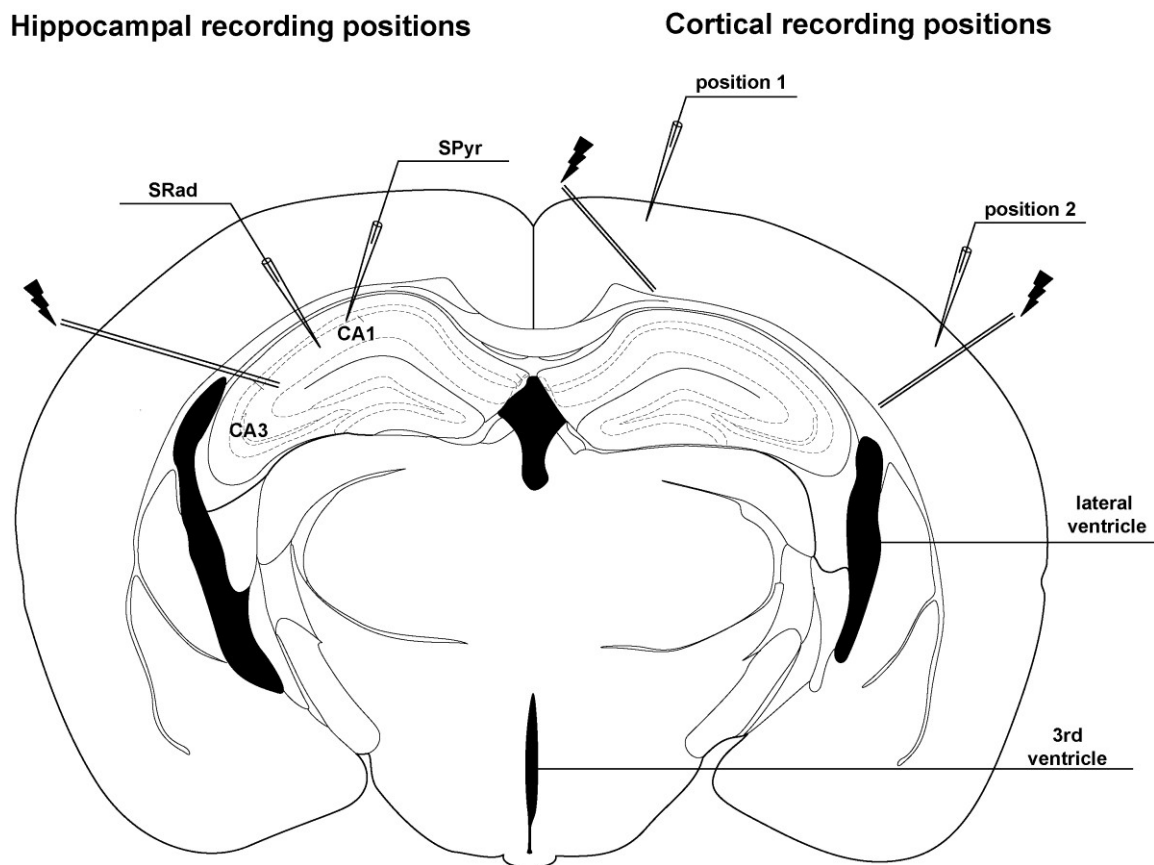


Figure 8. Stimulation and recording sites of field potentials. Cortical positions depicted on right site and hippocampal sites on the left sites. Stimulation sites are indicated by flashes.

Patch clamp recordings

Single cell recordings were performed in close collaboration with Dr. Lutz Liebmann from the Institute of Clinical Chemistry/Human Genetics at the University Hospital Jena.

Hippocampal slices were placed in a submerged-type recording chamber mounted on an upright microscope (BX51WI, Olympus, Germany). Slices were continuously superfused with gassed aCSF (5% CO₂/95 % O₂, 2–3 mL/min, 32°C, pH 7.2). Patch clamp recordings were performed under visual control with differential interference contrast and a 40x water-immersion objective. *CA1* neurons with a pyramidal-shaped cell body were selected for recordings. The membrane patch under the electrode was ruptured by gentle suction after seal formation (resistance >1 GΩ). Only recordings with an access resistance of <15 MΩ and a resting membrane potential more negative than –55 mV were included in this study. Signals were recorded using a patch clamp amplifier (Multiclamp 700B, Molecular Devices, USA). Responses were filtered at 4 kHz and digitized at 20 kHz (Digidata 1440, Molecular Devices). All data were acquired, stored and analyzed on a PC using pClamp 10.2 and Clampfit 10.2 (Axon Instruments). Patch pipettes with an impedance of 3–4 MΩ were pulled from borosilicate glass (outer diameter 1.5 mm, Science Products, Germany) on a Sutter micropipette puller (P-97, Sutter Instrument, USA). Spontaneous miniature excitatory currents (mEPSCs) and spontaneous miniature inhibitory currents (mIPSCs) were recorded at a holding potential of –70 mV for at least 5 min. Data analysis was performed off-line with the detection threshold levels set to 5 pA for mEPSCs and mIPSCs. mEPSCs were isolated by adding tetrodotoxin (0.5 μM, Tocris) and bicuculline methiodide (20 μM, Biomol, Germany) to block action potential-induced glutamate release and GABA_A receptor-mediated mIPSCs, respectively. D/L-APV (30 μM) was added to suppress N-methyl-D-aspartic acid (NMDA) currents. The pipette solution contained (in mM): 120 CsMeSO₄, 17.5 CsCl, 10 HEPES, 5 BAPTA, 2 Mg-ATP, 0.5 Na-GTP, 10 QX-314, pH 7.3, adjusted with CsOH.

Recordings of mIPSCs were performed using a CsCl-based intracellular solution (in mM): 122 CsCl, 8 NaCl, 0.2 MgCl₂, 10 HEPES, 2 EGTA, 2 Mg-ATP, 0.5 Na-GTP, pH adjusted to 7.3 with CsOH. D/L-APV (30 μM), CNQX (10 μM) and tetrodotoxin (0.5 μM) were added to the perfusate. The currents were identified as event when the rise time was faster than the decay time. The following parameters were determined: inter-event interval, frequency, rise time, peak amplitude and τ of decay. The decay of each event was fitted with a mono-exponential

curve in pClamp. Only residual standard deviations below 0.3 were accepted as a criterion for the quality of the fit. In a subset of mEPSC recordings, the extracellular pH was adjusted to 6.9 or 7.5 using aCSF gassed with carbogen containing 10 or 2.5 % CO₂, respectively. In a subset of experiments, pH_i was alkalinized by substitution of 20 mM NaCl by trimethylamine-chloride (*TriMA*, Sigma-Aldrich).

To study the regulation of presynaptic release, the open-channel blocker of the NMDA receptor MK-801 maleate (40 μM, Tocris) was used. CNQX (10 μM) was added to block 2-amino-3-(5-methyl-3-oxo-1,2-oxazol-4-yl) propanoic acid (AMPA) receptor responses. NMDA receptor-mediated excitatory postsynaptic currents (eEPSCs) were evoked in CA1 pyramidal neurons by electrical stimulation (Stimulator Model 2100, A-M-Systems, USA) of Schaffer collaterals with a frequency of 0.1 Hz. EPSCs were recorded in response to stimulation with half-maximal stimulus intensity at +40 mV holding potential. MK-801 was added after establishment of a stable baseline. Stimulation was resumed and eEPSCs were recorded for an additional 100 stimuli. Pulses were normalized to the first pulse given in the presence of MK-801. τ of NMDA-receptor blockade were estimated by mono-exponential fit and defined as timepoint where amplitudes dropped to 37% of baseline. Furthermore, action potential properties and spike frequency accommodation were recorded under current clamp conditions. Prolonged current steps (600 ms) were applied from the resting membrane potential in the range of 0 to 560 pA with 40 pA increments. Patch pipettes were filled with (in mM): 140 K-methane-sulfonate, 10 HEPES, 0.1 EGTA, 4 Mg-ATP and 0.3 Na-GTP, pH 7.3.

***In vivo* analysis**

All physiological studies on the renal function of *Slc4a8* were performed in close collaboration with Dr. D. Eladari and Dr. R. Chambrey at the INSERM U872/ University Paris Descartes in Paris (France).

Physiological studies

Physiological experiments were performed at the Institute des Cordeliers (INSERM U652, IFR58, Paris, France) and all animals used in this study were treated in full compliance with the French government animal welfare policy. Mice were housed at constant room temperature ($24\pm 1^\circ\text{C}$) with 12 h light/dark cycle. For convenience, the 12:12 light/dark cycle was inverted. Mice were given deionized water *ad libitum* and pair-fed with standard laboratory chow containing 0.3 % of Na^+ (Institut National de la Recherche Agronomique, France).

NaCl restriction

WT mice were divided into three groups (n=6 animals per group). One group received 1.7 mg desoxycorticosterone (DOCP; diluted in 0.3 % NaCl, Ciba-Geigy Animal Health, Novartis, Switzerland) by intramuscular injection 7 days before sacrifice. The second group of treated mice received a low sodium diet (0.009 % Na^+). Control mice were fed *ad libitum* with standard laboratory mouse chow and all mice had free access to distilled water for the same period of time. After 7 days mice were sacrificed and kidney cortices were removed and used for preparation of protein extraction as described earlier.

Metabolic experiments

All experiments were performed by using age- and sex-matched *Slc4a8*^{-/-} mice (3 to 5 months of age). Animals were housed in metabolic cages (Techniplast, Italy) and were first allowed to adapt for 5 d to the cages. Food and water intake as well as body weight were monitored throughout the experiment. At steady-state, urine collection was performed daily under

mineral oil in the urine collector for electrolyte measurements. Urine creatinine (modified kinetic Jaffé colorimetric method) was measured with a Konelab 20i auto-analyzer (Thermo Scientific) and urinary Na^+ and K^+ concentrations were measured by flame photometry (IL943; Instruments Laboratory). Experimental outline for Na^+ restriction and phenotypical analysis is depicted in Fig. 9. Urinary aldosterone was measured under baseline (day -1) or low Na^+ (day +5) conditions by radioimmunoassay (DPC Dade Behring, France). After two weeks on low Na^+ diet, blood was sampled from the tail vein and blood pH, pCO_2 and oxygen pressure (pO_2) were measured with an ABL 77 1 pH/blood-gas analyzer (Ratiometer, Denmark).

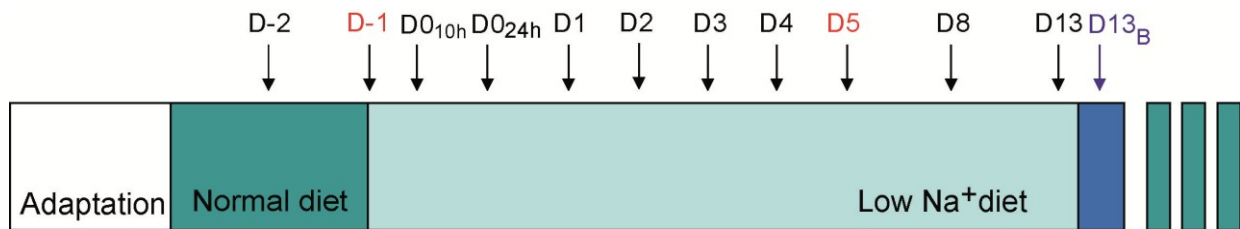


Figure 9. Experimental outline of metabolic experiments. Days of urinary analysis denoted in black, time points of additional aldosterone measurements in red and the time point of blood withdrawal in blue.

For the analysis of possible compensatory mechanisms, 50 mg/kg body weight HCTZ or amiloride (1.45 mg/kg of body weight) were injected subcutaneously in mice after adaptation to low Na^+ diet. Analysis of urinary content as described earlier was performed 18, 12 and 0 hours prior to injection of pharmacological blockers and 6, 12 and 24 hours after treatment.

Statistics

Data analysis

Data are presented as mean±standard error of mean (SEM). Statistical analysis of two experimental groups was performed using the un-paired, parametric two-tailed Student's t-test. If more than two groups were compared, one-way analysis of variance (ANOVA) and subsequent Newman-Keuls tests for post-hoc analysis were performed. In experiments, which include repeated measurements, differences between groups were tested by repeated measures ANOVA. In a subset of experiments two-way ANOVA was applied. Cumulative distributions were tested using the Kolmogorov-Smirnov test. Significance was considered at p-values <0.05 (* indicates p<0.05; ** indicates p<0.01; *** indicates p<0.001).

Results

Expression of Slc4a8 in non-neuronal, murine tissues

Previous data on Slc4a8 expression obtained by Northern blot and *in situ* hybridization showed strong expression of Slc4a8 in the murine central nervous system and in the testis. Lower expression was also detected in parts of the intestinal tract as well as renal and lung tissue amongst others (Kougioumtzes, 2006; Leviel et al., 2010). The expression of *Slc4a8* messenger ribonucleic acid (mRNA) was analysed in more detail by semi-quantitative PCR on cDNA of different murine tissues. Besides strong expression of Slc4a8 in total RNA isolated from brain, lower expression levels were confirmed in samples from kidney, thyroid and aorta of adult mice. No *Slc4a8* mRNA could be detected in pancreas samples from adult or neonatal mice (Fig.10A). At the protein level, Slc4a8 was detected in lysates from murine WT kidney (Fig.10B), as well as lysate from kidney cortices (Fig. 11) and from isolated cortical collecting ducts. No specific signals for Slc4a8 were obtained in immunohistochemical stainings of kidney sections with any of the protocols tested. Thus, the cellular as well as the sub-cellular localization of Slc4a8 in the kidney remain unclear. However, the expression data together with functional evidence from *in vitro* analysis of transport activity in cortical collecting ducts (Leviel et al., 2010) prompted us to analyse the role of Slc4a8 for kidney function in more detail.

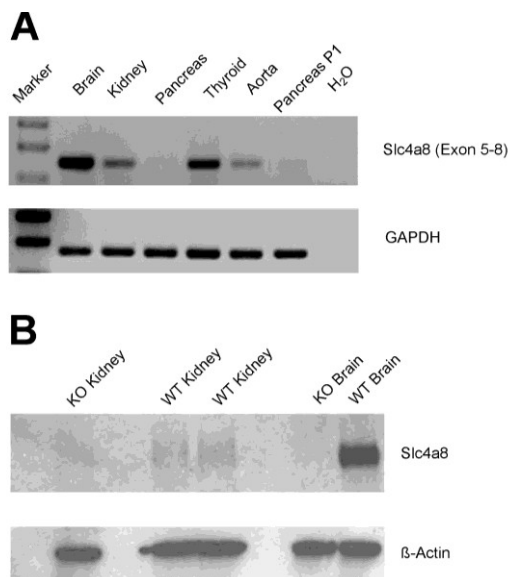


Figure 10. Expression of Slc4a8 in non-neuronal, murine tissues. **A**, PCR on cDNA from different murine tissues confirmed expression of Slc4a8 in brain, kidney, thyroid and aorta, but not in the pancreas of newborn or adult mice. **B**, Slc4a8 protein was detected in whole kidney lysates of WT mice, but not of a *Slc4a8*^{-/-} mouse by Western Blot analysis.

Slc4a8 mediates an electroneutral Na⁺ reabsorption in the murine kidney

Results of this thesis in collaboration with Dr. D. Eladari suggest an important role of Slc4a8 for thiazide-sensitive Na⁺ reabsorption in the renal collecting ducts of mice (Leviel et al., 2010). Differences in ion transport activity between genotypes in isolated cortical collecting ducts described in this study were most prominent in Na⁺ depleted mice. Considering that in general renal Na⁺ reabsorption under normal feeding conditions is relatively low and that only 1-3 % of filtrated sodium enters the connecting tubule and the collecting duct, we decided to analyze expression of Slc4a8 in kidneys of mice under conditions of NaCl restriction. Cortices of kidneys of WT mice were dissected after 7 days under Na⁺ free diet, or 7 days after injection of the aldosterone analogue DOCP and Slc4a8 protein amount was analysed by Western blot analysis (Fig. 11A). In both conditions a significant up-regulation of Slc4a8 protein expression could be detected (Fig. 11B, Relative expression of Slc4a8 protein: control 100.00±3.15 %; low Na⁺ 122.69±4.93 %; Students t-test: p=0.005; n= 5/6; control 100.00±4.46 %; DOCP treatment 154.81±10.04 %; Students t-test: p=0.001; n=5/6). These results corroborate the functional importance of Slc4a8 for salt reabsorption in the kidney.

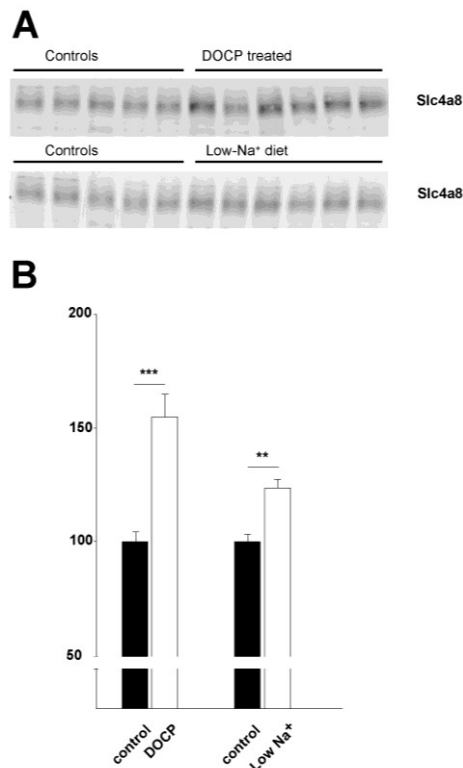


Figure 11. Renal expression of Slc4a8 is increased under Na⁺ restriction. **A**, Under conditions of increased Na⁺ reabsorption, induced by application of the aldosterone analogue, DOCP, or by maintenance of mice under Na⁺ restriction, Slc4a8 protein expression was increased in Western Blot analysis. **B**, Quantification of expression levels (n=5/5/5; p<0.001/p<0.01).

To test the functional significance of *Slc4a8* for kidney function, *in vivo* metabolic experiments were performed in which we monitored food and water intake as well as blood and urinary composition under normal and Na⁺ restricted diet. No differences in food (basal KO: 3.00±0.19 g; WT: 2.95±0.19 g; Students t-test: p>0.05; low Na⁺ KO: 3.32±0.28 g; WT: 3.37±0.09; Students t-test: p>0.05; n =10/10) and water intake (basal KO: 4.89±0.55 ml; WT: 4.30±0.52 ml; Students t-test: p>0.05; low Na⁺ KO: 4.92±0.38 ml; WT: 4.05±0.63; Students t-test: p>0.05; n =10/10) were detected. Mice of both genotypes were able to maintain their weight under both experimental conditions. However, the previous finding of an increased bodyweight in *Slc4a8*^{-/-} mice was confirmed. WT and *Slc4a8*^{-/-} mice were both able to conserve Na⁺ rapidly after Na⁺ depletion (Fig. 12A; repeated measures ANOVA: F=4.01, p=0.06). Also, urinary K⁺ concentration during the treatment was monitored, as alterations in urinary K⁺ excretion can indicate compensatory mechanisms in *Slc4a8*^{-/-} mice. *Slc4a8*^{-/-} mice did not show long-lasting alterations of urinary K⁺ excretion, although there was a significantly increased K⁺ excretion in *Slc4a8*^{-/-} mice at day 5 under NaCl restriction (Fig. 12B; repeated measures ANOVA: F=4.56, p=0.046; Bonferroni post test: D5 p<0.01; all other time points: p>0.05).

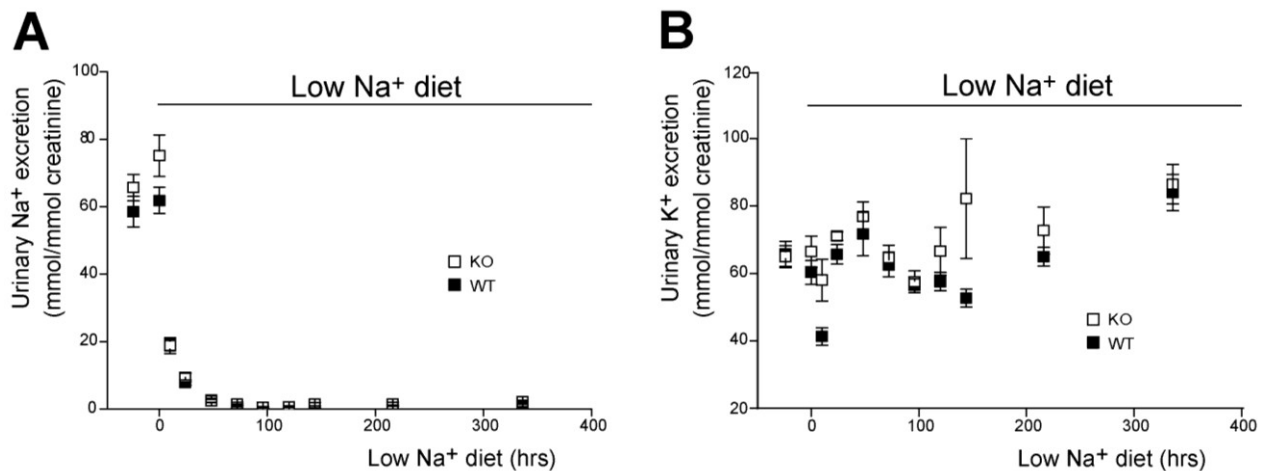


Figure 12. *Slc4a8* deletion does not alter urinary Na⁺ or K⁺ composition under Na⁺ restriction. A, *Slc4a8*^{-/-} and WT mice did not differ significantly in the amount of excreted Na⁺ under normal conditions and both genotypes were able to adapt normally to Na⁺ restriction (n=10/10; p=0.06). **B,** Urinary K⁺ excretion was normal in *Slc4a8*^{-/-} mice at most time points during the metabolic experiments (n=10/10; p=0.05).

Additionally, different blood parameters (e.g. pH, pCO₂, pO₂) were analysed under Na⁺ restricted conditions (day 13) but no significant differences between WT and *Slc4a8*^{-/-} mice could be detected in any of the parameters analysed (Tab. 2).

Table 2. Blood and plasma composition under Na⁺ restricted conditions.

	KO (n=10)			WT (n=10)			p-value
<i>Blood</i>							
<i>pH</i>	7.25	±	0.01	7.24	±	0.01	0.45
<i>pCO₂ (mmHg)</i>	53.20	±	1.81	58.90	±	1.99	0.23
<i>pO₂ (mmHg)</i>	84.30	±	7.19	86.80	±	6.86	0.83
<i>HCO₃⁻ (mM)</i>	22.70	±	0.70	24.20	±	0.70	0.36
<i>Plasma</i>							
<i>[Na⁺] (mM)</i>	146.70	±	1.08	143.90	±	2.69	0.56
<i>[K⁺] (mM)</i>	3.74	±	0.15	3.65	±	0.13	0.33
<i>[Cl⁻] (mM)</i>	116.60	±	1.09	116.50	±	0.97	0.94
<i>[Ca²⁺] (mM)</i>	1.29	±	0.02	1.31	±	0.02	0.18
<i>Hematocrit (%)</i>	44.6	±	3.71	42.30	±	3.77	0.56

It is well established that a sodium-deficient diet stimulates aldosterone biosynthesis in mammals (Müller, 1995). Accordingly, a rise in relative aldosterone content in urine samples under low Na⁺ diet compared to baseline was measured in both genotypes (Fig. 13; urinary aldosterone excretion WT baseline: 1.97±0.24 mmol/mmol creatinine; WT low Na⁺: 7.73±1.00 mmol/mmol creatinine; KO baseline: 2.45±0.59 mmol/mmol creatinine; KO low Na⁺: 15.95±2.8 mmol/mmol creatinine; two-way ANOVA: F=21.13, p<0.0001; n=9/9/5/5). Interestingly, the aldosterone concentration under Na⁺ restriction was significantly increased in *Slc4a8*^{-/-} mice (two-way ANOVA: F=18.46, p<0.0001; Bonferroni post test: basal: p>0.05, low Na⁺: p<0.001).

In conclusion, the data suggest that *Slc4a8* is expressed in kidney cortices of WT mice under basal conditions and that its expression is up-regulated under conditions of increased Na⁺ reabsorption. Albeit *in vitro* results from recordings on isolated cortical collecting ducts propose that *Slc4a8* is an essential component for NaCl reabsorption, *Slc4a8*^{-/-} mice adapted normally to NaCl restriction *in vivo*. The normal adjustment of *Slc4a8*^{-/-} mice may be facilitated by compensatory changes.

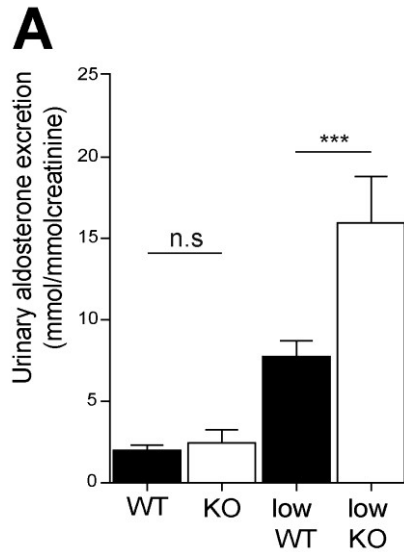


Figure 13. Na⁺ restriction increases urinary aldosterone concentration more strongly in *Slc4a8* depleted mice. A, Na⁺ restriction increased urinary aldosterone in WT and *Slc4a8*^{-/-} mice (n=9/9/5/5; p<0.0001), but to a larger extent in *Slc4a8*^{-/-} mice (p<0.001).

Compensatory changes in *Slc4a8*^{-/-} mice under Na⁺ restricted conditions

An impaired activation of *Slc4a8* could be compensated by increased activity of NCC in the distal convoluted tubule or of ENaC in the CCD. To analyse the physiological activity of both ion transport proteins *in vivo* pharmacological blockers, amiloride to block ENaC and HCTZ to inhibit NCC, were acutely injected under Na⁺ restricted conditions and the acute Na⁺ excretion in the urine was compared between genotypes. An increase in Na⁺ excretion indicates an increased activity of the transport mechanism blocked.

Acute injection of amiloride resulted in a strong increase in urinary Na⁺ excretion in both genotypes (Urinary Na⁺ excretion 0-6 hours post injection KO 29.63±7.8 mmol/mmol creatinine; WT 43.14±7.2 mmol/mmol creatinine; Students t-test WT: p<0.001; KO: p<0.01; n=10/10), but there was no significant difference between genotypes in the magnitude of the increase (Students t-test: p=0.21). Similar results were observed 6-12 hours and 12-24 hours after injection (see also Fig. 14B). To analyze the activity of NCC, HCTZ was injected (Fig. 14B). Under Na⁺ restricted conditions, HCTZ injection increased the amount of excreted Na⁺

in both genotypes, *Slc4a8*^{-/-} (Urinary Na⁺ excretion 0-6 hours post injection KO 55.44±7.24 mmol/mmol creatinine; Students t-test: p<0.05, n=10) and WT mice (WT 31.71±5.06 mmol/mmol creatinine; p<0.001; n=10). Interestingly, the increase in urinary Na⁺ concentration was significantly higher in *Slc4a8*^{-/-} animals compared to WT within the first 6 hours after injection (Students t-test: p=0.02).

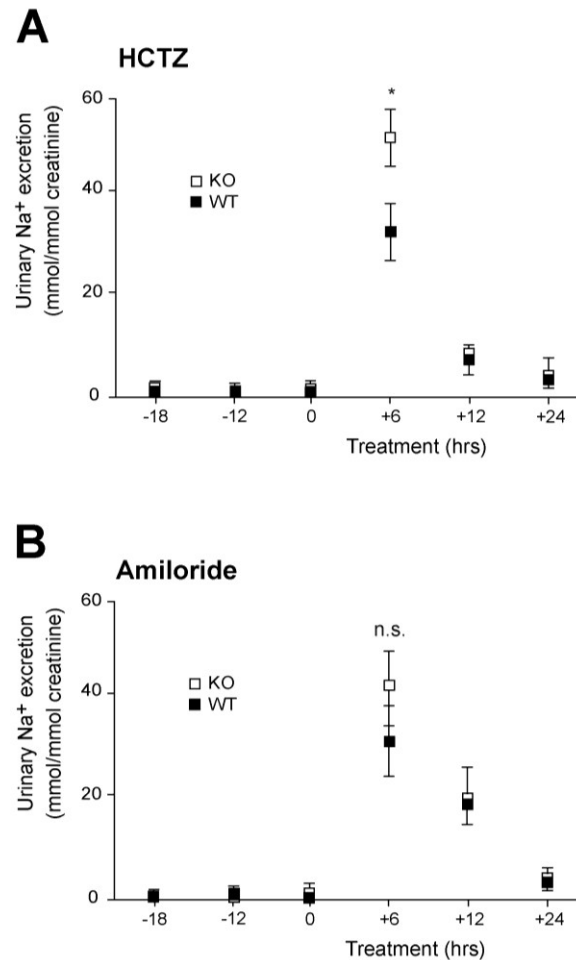


Figure 14. Administration of thiazides under Na⁺ restriction evokes stronger response in *Slc4a8*^{-/-} mice. **A**, Acute injection of HCTZ under Na⁺ restricted conditions results in excretion of a significantly larger amount of urinary Na⁺ in KO compared to WT (p<0.001). **B**, No differences between genotypes were detected in urinary Na⁺ excretion upon blockade of ENaC upon injection of amiloride.

These results suggest an increased activity of thiazide-sensitive transport mechanisms, probably mainly mediated via NCC, in *Slc4a8*^{-/-} mice under Na⁺ restricted conditions, which may explain why *Slc4a8*^{-/-} mice adapt normally to Na⁺ restriction.

Expression of Slc4a8 in the murine brain

Broad expression of Slc4a8 in neurons, but not in glial cells of the WT mouse brain

DAB stainings of WT brain sections demonstrated that Slc4a8 was broadly expressed in the central nervous system (Fig. 15AB). Signals were most prominent in cortical and midbrain structures, whereas large fiber tracts like the corpus callosum were almost spared. In the hippocampus, all layers stained positive including the SPyr and the SL-M of the *CA1* region (Fig. 15C). The specificity of our antibody and the staining procedure was confirmed by the absence of signals on tissue of *Slc4a8*^{-/-} mice (Fig. 15D).

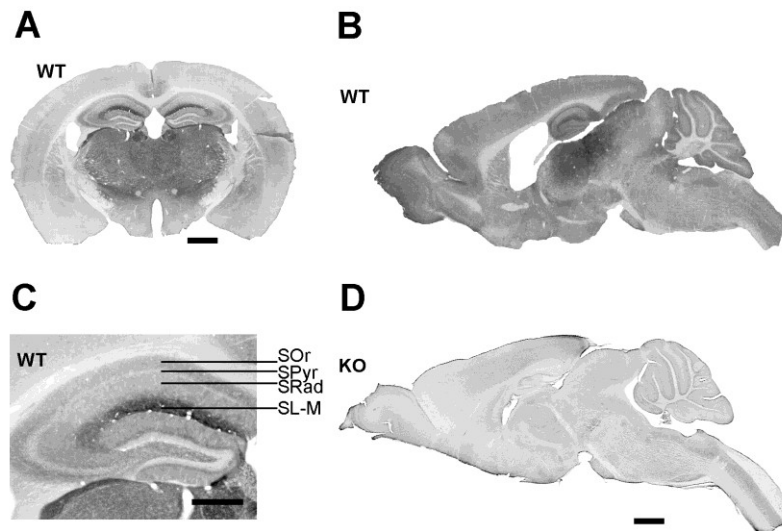


Figure 15. Expression of Slc4a8 in mouse brain. **A**, DAB staining of a coronal WT brain section with an antibody raised against Slc4a8 protein (scale bar 1000 μm). **B**, Slc4a8 staining of a sagittal WT brain section (scale bar 1000 μm). **C**, All hippocampal layers stained positive for Slc4a8 (scale bar 500 μm ; SOr: stratum oriens). **D**, The specificity of the antibody was verified by the absence of signals in brain sections of *Slc4a8*^{-/-} mice (scale bar 1000 μm).

Slc4a8 protein was detected in protein lysates of mixed neuron/glia cell cultures, but not of cultured glia cells (Fig. 16). The neuronal localization of Slc4a8 in different areas of the brain was confirmed by fluorescent immunostainings of brain sections. Accordingly, no overlap of Slc4a8 protein was noted in a fluorescent double staining with the astrocyte marker GFAP. Thus, the neuron-specific expression of Slc4a8 in the mouse brain was confirmed and

subsequently the sub-cellular expression pattern in the hippocampus was analysed in more detail.

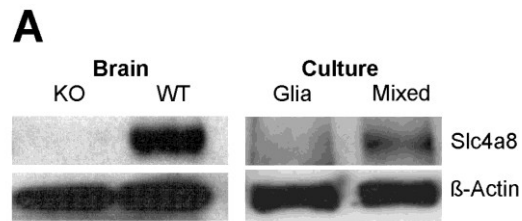


Figure 16. Neuronal expression of Slc4a8. A, The ~120 kD band for Slc4a8 protein was absent in *Slc4a8*^{-/-} brain lysate. Slc4a8 protein was detected in mixed hippocampal cultures, but was not detectable in lysates from pure glia cell cultures from WT mice.

Slc4a8 localizes to presynaptic, glutamatergic nerve endings in the hippocampus

The somata of Slc4a8 stained neurons were labelled variably, most displaying a clear plasma membrane bound signal and some a more intracellular vesicular staining (see close up from SPyr Fig. 17H). Slc4a8 did not co-localize with the dendritic marker MAP2 (Fig 17A). Co-staining with the axonal marker NF68 revealed that Slc4a8 rather localized to axons than dendrites (Fig. 17B). Slc4a8 overlapped with the presynaptic marker synaptophysin (Fig. 17C, close up from SRad C'-C''') and, more specifically, with glutamate transporters vGLUT1 (Fig. 17D) and vGLUT2 (Fig. 17E), but much less with the postsynaptic marker PSD-95 (Fig. 17F).

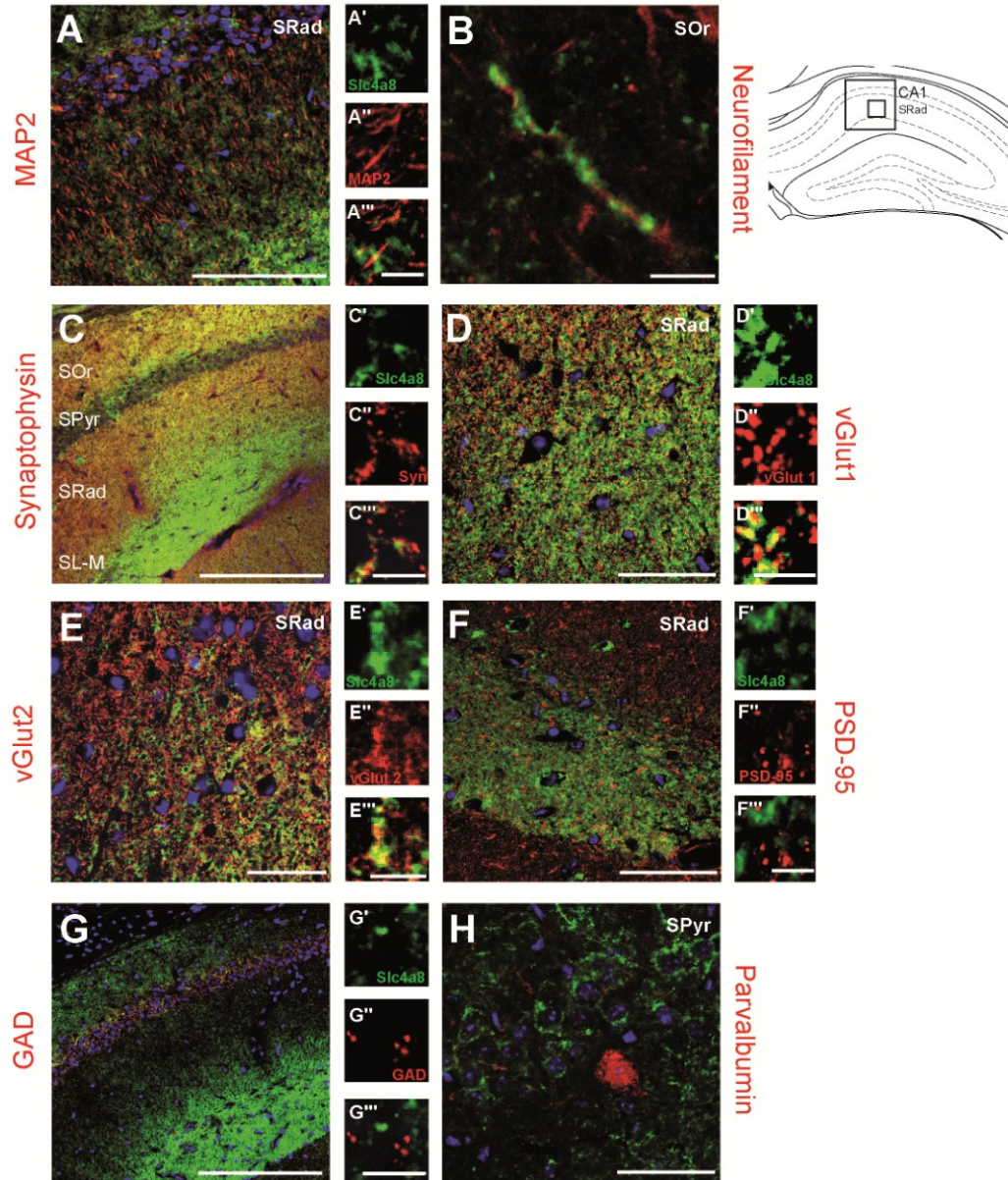


Figure 17. Presynaptic localization of Slc4a8 in the hippocampus. A, A'-A''', Co-staining for Slc4a8 (green) and the dendritic marker MAP2 showed no significant overlap (scale bar 200/5 μ m). Slc4a8 localized along axons labeled with NF68 (B, scale bar 5 μ m). C, C'-C''', Staining with the presynaptic marker synaptophysin revealed a significant overlay (scale bar 200/5 μ m). D, D'-D''', Slc4a8 overlapped with the vesicular glutamate transporter vGLUT1 (, scale bars 50/5 μ m). Similar results were obtained for vGLUT2 (E, E'- E''', scale bars 50/5 μ m). F, F'-F''', Slc4a8 and the postsynaptic protein PSD-95 (SRad, scale bars 50/5 μ m) did not co-localize. G, G'- G''', Co-staining of Slc4a8 and GAD revealed that Slc4a8 was not detected in most GABAergic nerve endings (scale bars 200/5 μ m). H, Parvalbumin-positive interneurons did not express Slc4a8 (scale bar 50 μ m). Nuclei were labeled with DAPI (blue).

Overlap between Slc4a8 and GAD67 as a marker of GABAergic presynapses in the hippocampus was marginal (Fig. 17G) and Slc4a8 protein was absent from most parvalbumin-positive inhibitory interneurons in the hippocampus (Fig. 17H).

The presynaptic localization of Slc4a8 was further confirmed by fractionation studies from mouse brain lysates. Slc4a8 protein was increasingly enriched in synaptosomes, synaptosomal membranes and synaptic junction plasma membranes but absent from the postsynaptic density (Fig. 18).

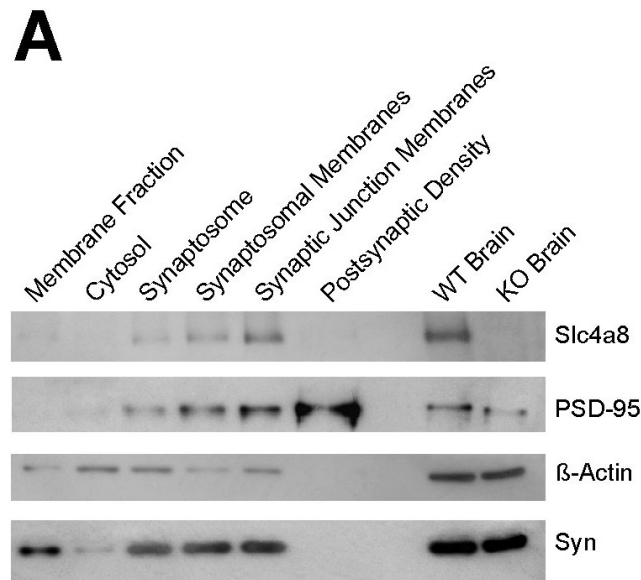


Figure 18. Enriched expression of Slc4a8 in synaptic fractions. A, Immunoblot analysis of a density fractionation of WT mouse brain lysates. Slc4a8 protein was enriched in synaptosomes, synaptosomal membranes and the synaptic junction plasma membrane fraction, but was not detectable in the postsynaptic density fraction. The postsynaptic protein PSD-95 and the presynaptic marker synaptophysin served as positive controls and β-actin as a loading control.

In collaboration with Dr. Martin Westermann immunogold labeling of freeze-fractured synaptosome preparations from WT and *Slc4a8*^{-/-} mice were performed and those confirmed strong expression of Slc4a8 in isolated nerve terminals (Fig. 19AB). Finally, double labeling studies in WT synaptosome preparations proved that Slc4a8 localized to the same compartment as the well-established presynaptic proteins syntaxin (Bennett et al., 1992) and SNAP-25 (Oyler et al., 1989) (Fig. 19CD).

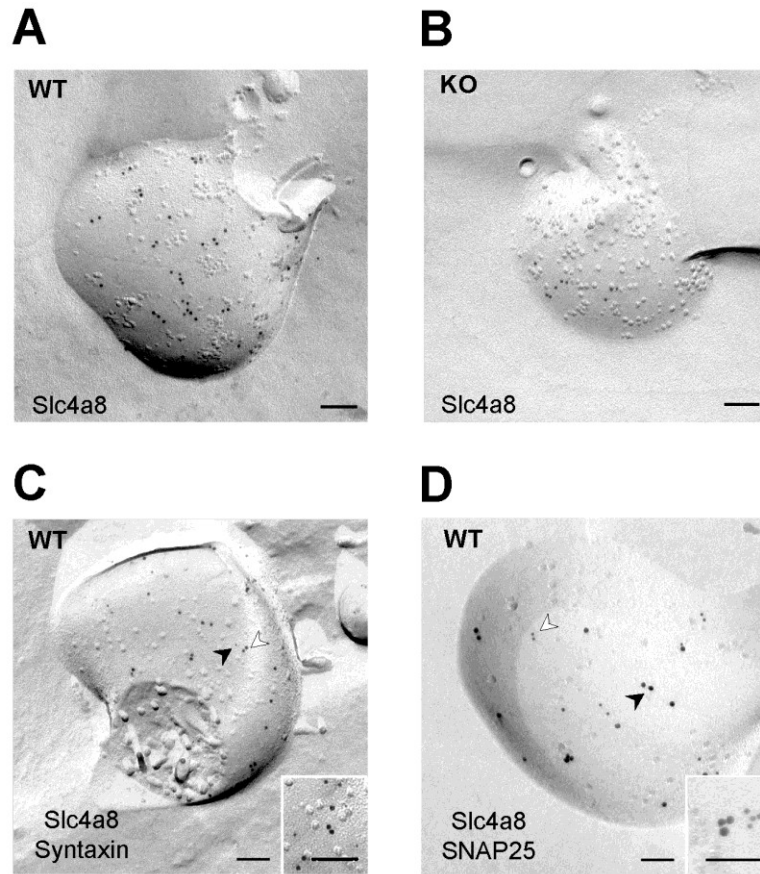


Figure 19. Expression of Slc4a8 in synaptosomes. **A-D**, Transmission electron microscopy of a freeze-fractured WT (**A**) synaptosome immunogold labeled for Slc4a8 (large grains, 10 nm). **B**, KO control confirmed specificity of Slc4a8 antibody. **C**, Co-labeling of Slc4a8 (10 nm, white arrow) and the presynaptic marker syntaxin (small grains, 5 nm, black arrow) of freeze fractured WT synaptosomes confirmed presynaptic localization of Slc4a8 protein. Inset: higher magnification; scale bar 100 nm. **D**, Similar results were obtained by double labelling of SNAP25 and Slc4a8. All images show the protoplasmic fracture face of a synaptosome membrane. All scale bars correspond to 100 nm.

Slc4a8 is important for the regulation of pH_i in hippocampal neurons

Since Slc4a8 appeared to be broadly expressed in neurons and sodium-dependent chloride-bicarbonate exchangers had repeatedly been proposed to be key regulators of neuronal pH_i (Bevensee et al., 1996; Romero et al., 2000; Russell and Boron, 1976; Schwiening and Boron,

1994), the role of *Slc4a8* in neuronal pH homeostasis was investigated by BCECF fluorescence imaging of cultured hippocampal neurons from *Slc4a8*^{-/-} and WT mice.

In bicarbonate-buffered solutions, the resting p*H*_i of *Slc4a8*^{-/-} neurons was significantly lower compared to WT (Fig. 20AB; p*H*_i KO: 6.88±0.02; WT: 6.97±0.03; one-way ANOVA: F=7.65, p=0.0001; Newman-Keuls test: p<0.05; n=35/35), whereas it was unchanged in HEPES-buffered and nominally bicarbonate-free solution (p*H*_i KO: 6.75±0.05; WT: 6.78±0.03; Newman-Keuls test: p>0.05; n=9/16). To challenge neuronal p*H*_i regulation, cells were alkali loaded with an extracellular NH₄Cl pulse. Entry of NH₃ causes a rise in p*H*_i, which is followed by a slower, variable fall in pH caused by the slower, passive entry of NH₄⁺ as well as efflux of bicarbonate via membrane transporters. Upon withdrawal of NH₄⁺ from the extracellular solution, p*H*_i falls drastically, as the intracellular NH₄⁺ exits the cells in form of NH₃ and leaves a cytosolic H⁺ load behind. This acid load is then counteracted by acid extruders (Roos and Boron, 1981). In the presence of bicarbonate, NH₄Cl-induced peak alkalosis compared to baseline (Δ p*H*_{Maximum-Basal}) was significantly raised in *Slc4a8*^{-/-} neurons compared to WT (Fig. 20C; Δ p*H*_{Maximum-Basal} KO: 0.50±0.03; WT: 0.33±0.02; one-way ANOVA: F=30.88; p<0.0001; Newman-Keuls tests: p<0.001; n=35/35), whereas rebound acidosis upon withdrawal of NH₄Cl compared to baseline (Δ p*H*_{Basal-Minimum}) was unaltered (Fig. 20C; Δ p*H*_{Basal-Minimum} KO: 0.22±0.03; WT: 0.17±0.03; one-way ANOVA: F=0.08; p=0.97; n=35/35) albeit the absolute minimum p*H*_i (p*H*_{Minimum}) was slightly more acidic in *Slc4a8*^{-/-} neurons (p*H*_{Minimum} KO: 6.67±0.03; WT: 6.79±0.03; Students t-test: p=0.005; n=35/35).

Acid extrusion within the first minute after the maximal acid load was diminished in the absence of *Slc4a8* (Fig. 20D; Δ p*H*/min_{1min} KO: 0.09±0.01; WT: 0.15±0.01; Students t-test: p<0.001; n=35/35) as was the recovery in a time frame of two minutes (Δ p*H*/min_{2min} KO: 0.10±0.01; WT: 0.13±0.01; Students t-test: p=0.019; n=35/35). To evaluate the net proton fluxes independently of the p*H*_i, the mean slope for both genotypes was additionally calculated between p*H*_i 6.7 and 6.8, which was decreased as well (Δ p*H*/min_{p*H*6.7-6.8} KO: 0.11±0.01; WT: 0.15±0.01; one-way ANOVA: F=4.24, p=0.007; Newman-Keuls test: p<0.01).

In the nominal absence of bicarbonate no significant differences were observed between genotypes in any of the parameters analysed (NH₄Cl-induced alkalosis Δ p*H*_{Maximum-Basal} KO:

0.83±0.08; WT 0.74±0.07; Newman-Keuls test: $p>0.05$; acid load $\Delta\text{pH}_{\text{Basal-Minimum}}$ KO: 0.24±0.06; WT 0.38±0.07; Newman-Keuls test: $p>0.05$; recovery from acid load $\Delta\text{pH}/\text{min}_{\text{pH } 6.7-6.8}$ KO: 0.09±0.01; WT: 0.10±0.01; Newman-Keuls test: $p>0.05$; $n=9/16$).

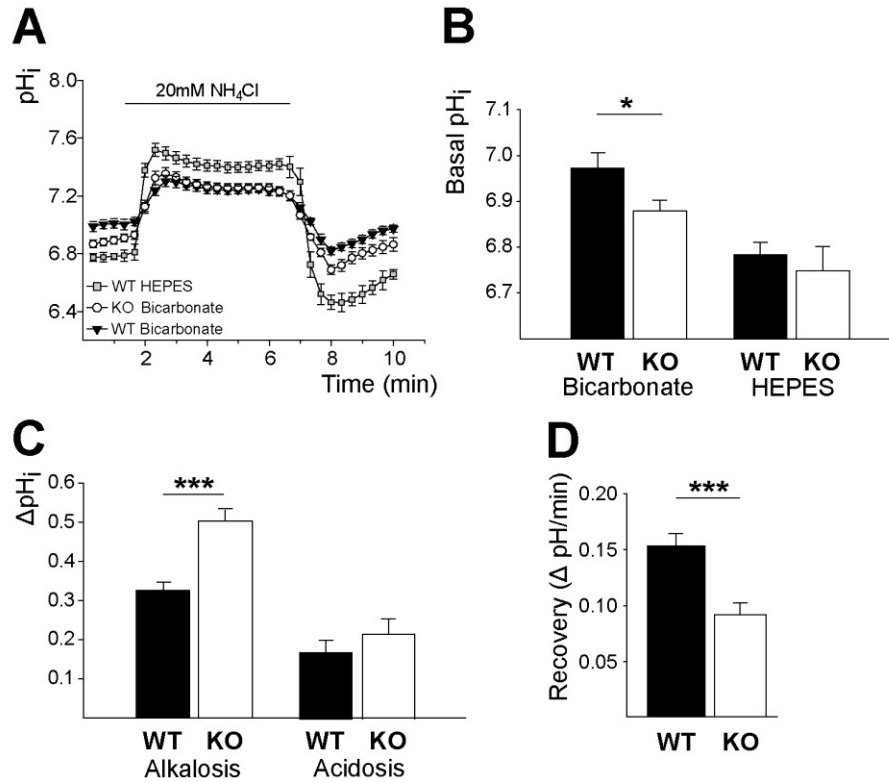


Figure 20. Impaired pH regulation in cultured hippocampal neurons of *Slc4a8*^{-/-} mice. **A**, Mean pH_i of *Slc4a8*^{-/-} and WT neurons challenged with NH₄Cl ($n=9/35/35$). **B**, Steady-state pH_i was only reduced in *Slc4a8*^{-/-} neurons in the presence of bicarbonate (bicarbonate: $p<0.05$; $n=35/35$; HEPES: $p>0.05$; $n=9/16$). **C**, Peak alkalosis by NH₄Cl was increased in *Slc4a8*^{-/-} neurons ($\Delta\text{pH}_{\text{Maximum-Basal}}$ $p<0.001$; $n=35/35$) but net acid load upon withdrawal of NH₄Cl did not differ between genotypes ($\Delta\text{pH}_{\text{Basal-Minimum}}$ $p=0.97$; $n=35/35$). **D**, Recovery from acid load in the first min after maximal acid load was slower in *Slc4a8*^{-/-} neurons compared to WT ($\Delta\text{pH}/\text{min}_{1\text{min}}$ $p=0.0001$, $n=35/35$).

These results did not suggest a major compensatory regulation of other acid extruders in *Slc4a8*^{-/-} mice. In accordance, transcript abundance of *Slc9a1*, *Slc4a3*, *Slc4a4*, *Slc4a7* and *Slc4a10* quantified by real-time PCR did not differ significantly between genotypes (fold changes in transcript abundance KO vs. WT: *Slc9a1* 0.92±0.2; *Slc4a3* 1.14±0.08; *Slc4a4* 1.15±0.43; *Slc4a7* 0.85±0.12; 1.21±0.15; one-way ANOVA: $F=2.526$, $p=0.875$; $n=3/3$).

Slc4a8 transcript abundance served as a control (KO vs. WT: 0.0007 ± 0.0006 ; Students t-test: $p < 0.0001$).

In conclusion, acid extrusion via *Slc4a8* appears to play an important role for the steady state pH_i and for the control of pH_i to an acute acid load.

Normal cell volume regulation in *Slc4a8*^{-/-} neurons

Slc4a8 transports one Na^+ and two HCO_3^- ions in exchange for one Cl^- ion into the cell (Grichtchenko et al., 2001). As a result *Slc4a8* activity could theoretically affect cell volume. Therefore, cell volume regulation in response to exposure to hypo- and hyperosmolar bicarbonate buffered solution was analysed in cultured hippocampal neurons from WT and *Slc4a8*^{-/-} mice by calcein fluorescence imaging.

No difference between genotypes was detected in maximal cell shrinkage upon exposure to hypoosmolar solution (V_{Minimum} KO: 92.69 ± 0.74 %; WT: 91.78 ± 0.07 %; Students t-test: $p = 0.42$; $n = 13/12$) or cell swelling upon application of hyperosmolar solution (V_{Maximum} KO: 109.04 ± 0.78 %; WT: 109.04 ± 0.40 %; Students t-test: $p = 0.74$; $n = 17/15$). Regulatory cell volume increase in response to cell shrinkage was normal in *Slc4a8*^{-/-} neurons (Fig. 21A; repeated measures ANOVA: $F = 2.58$, $p = 0.12$). Also, regulatory cell volume decrease upon cellular swelling induced by hyperosmolar solution did not differ in neurons lacking the *Slc4a8* transporter (Fig. 21B; repeated measures ANOVA: $F = 3.426$, $p = 0.08$).

Thus, these results do not suggest a major role of *Slc4a8* for cell volume regulation in hippocampal neurons.

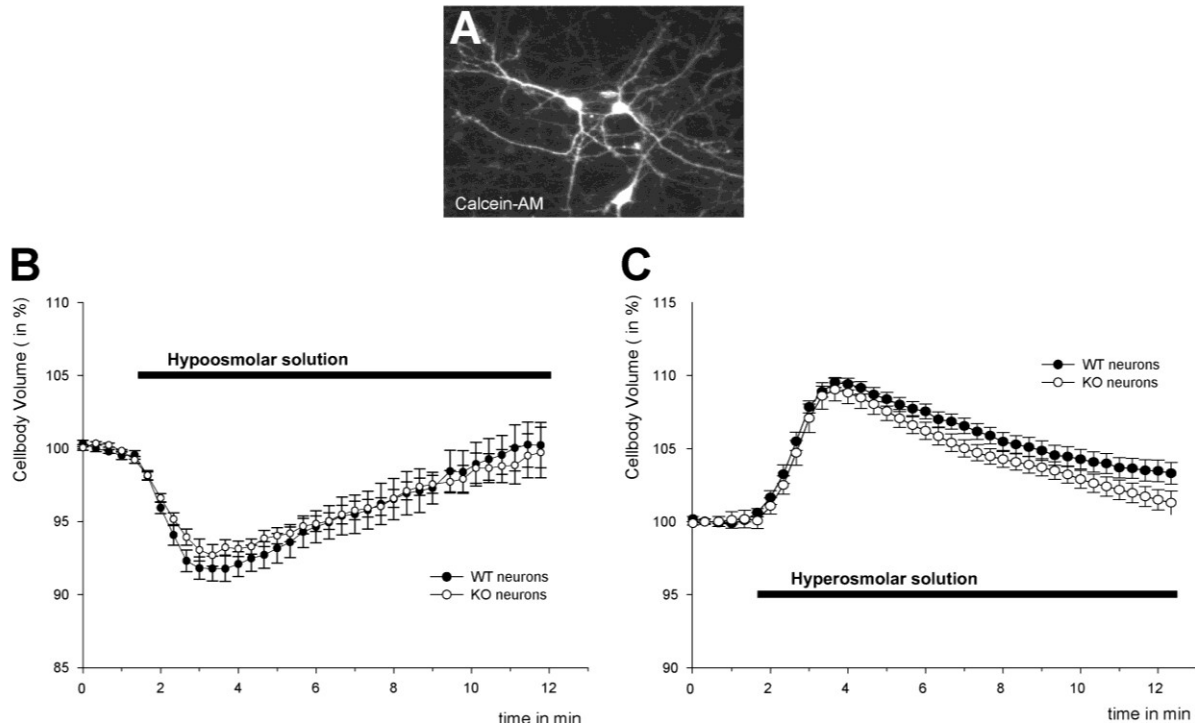


Figure 21. No differences in cell volume regulation between genotypes. **A**, Calcein-labelled neurons. **B**, Regulatory cell volume increase upon exposure to hypoosmolar solution was normal in *Slc4a8*^{-/-} neurons (n=13/12; p>0.05) as was the regulatory cell volume decrease (n=17/15; p>0.05).

Slc4a8 modulates glutamate release

Altered excitability in *Slc4a8*^{-/-} pyramidal cells of the hippocampus

Because of the localization of Slc4a8 to glutamatergic boutons and its impact on neuronal pH regulation, field potentials were measured in the *CA1* region of acute WT and *Slc4a8*^{-/-} slice preparations upon stimulation of Schaffer collaterals. Fiber volley amplitudes analysed at half-maximal stimulus intensities (WT: 33.6±2.1 V; KO: 35.5±3.3 V, Students t-test: p=0.65; n=22/19) did not differ between the genotypes (Fig. 22A; KO: 0.68±0.06 mV; WT: 0.72±0.08 mV; Students t-test: p=0.63; n=22/19). Population spike amplitudes in the pyramidal layer were strongly decreased in *Slc4a8*^{-/-} mice (Fig.22B; e.g. at half maximal stimulus intensity KO 4.27±0.62 mV; WT: 6.81±0.67 mV; Students t-test: p=0.01; and input/output curve: repeated

measures ANOVA: $F=4.56$, $p=0.04$ $n=22/19$). In support of a presynaptic defect, paired-pulse facilitation was increased in fEPSP recordings of *Slc4a8*^{-/-} slices (Fig. 22C; repeated measures ANOVA: $F=5.04$, $p=0.03$). Comparable results were obtained from field potential recordings in the SRad, where paired pulse ratios upon stimulation with half-maximal stimulus intensity were also increased in *Slc4a8*^{-/-} slices (Fig. 22D; repeated measures ANOVA: $F=4.44$, $p=0.04$; $n=37/41$).

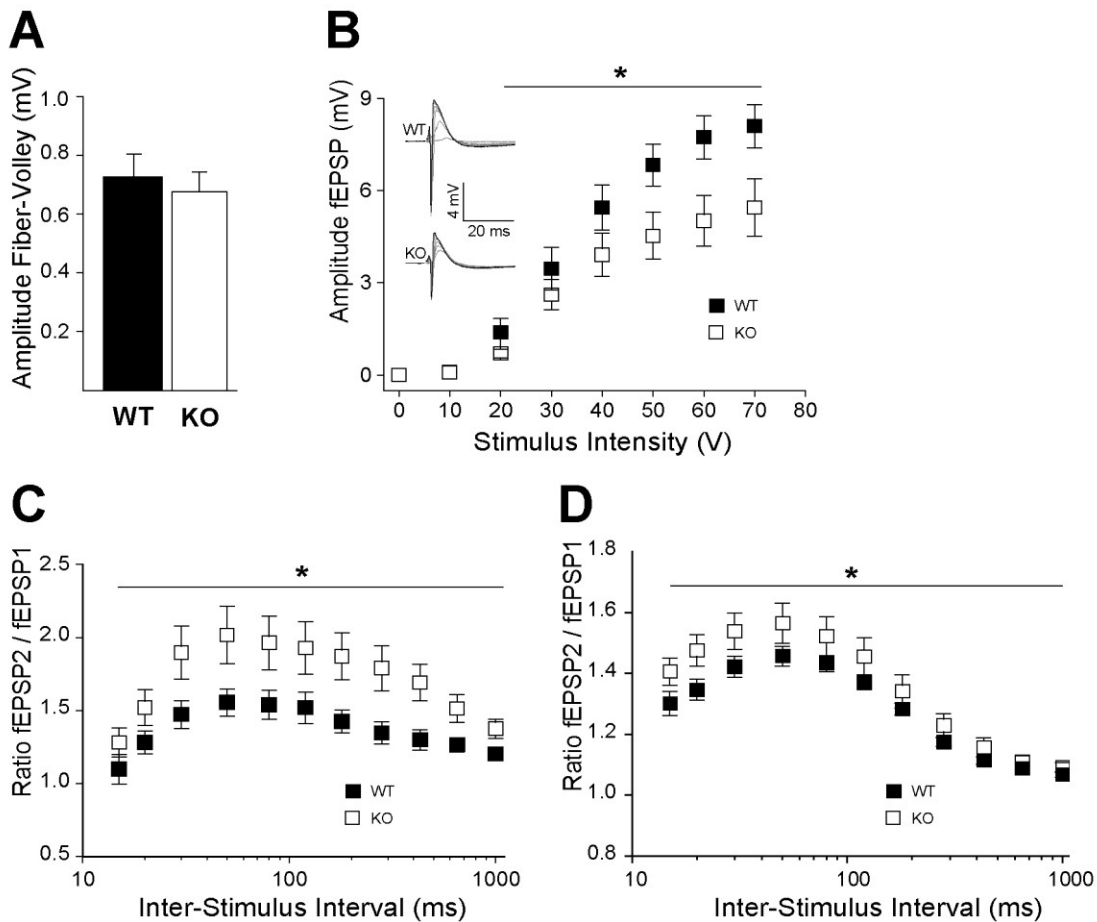


Figure 22. Reduction of network excitability in hippocampal slices from *Slc4a8*^{-/-} mice. **A**, Fibre volley amplitude at half maximal stimulus intensity was normal in *Slc4a8*^{-/-} slices ($n=22/19$; $p>0.05$). **B**, *CA1* population spike amplitudes upon stimulation of Schaffer collaterals were decreased in *Slc4a8*^{-/-} slices ($p=0.04$; $n=22/19$). Inset: sample traces of somatic field recordings, stimulus artifacts were omitted for clarity. **C**, Paired-pulse facilitation in the SPyr was significantly increased in slices of *Slc4a8*^{-/-} mice at 30–1,000 ms inter-stimulus intervals ($p=0.03$; $n=22/19$). Similar results were found in the SRad (**D**, $n=37/41$, $p=0.04$).

Passive (input resistance, capacity, resting membrane potential) and active (e.g. action potential height, spike frequency accommodation) membrane properties were unaltered in *CA1* pyramidal neurons (Table 3; n=12/12) patched in the current clamp mode in collaboration with Dr. L. Liebmann.

Table 3. Passive and active membrane properties in principal neurons of the *CA1* region.

	KO (n=12)	WT (n=13)	p-value
<i>Capacity [pF]</i>	19.1 ± 1.7	17.1 ± 1.1	0.45
<i>Resting Membrane Potential [mV]</i>	-66.5 ± 1.3	-64.4 ± 1.0	0.26
<i>Input Resistance [MΩ]</i>	62.6 ± 6.1	73.5 ± 7.8	0.28
<i>Action Potential Threshold [mV]</i>	-44.7 ± 1.0	-42.2 ± 2.0	0.28
<i>Action Potential Height [mV]</i>	97.0 ± 2.9	97.1 ± 2.9	0.98
<i>Action Potential Halfwidth [ms]</i>	0.7 ± 0.1	0.7 ± 0.0	0.61
<i>Action Potential Rise Time [ms]</i>	0.5 ± 0.1	0.5 ± 0.1	0.95

The altered paired-pulse ratio of hippocampal field recordings and the presynaptic localization of Slc4a8 prompted us to examine synaptic transmission more closely. Presynaptic activity can be investigated by measuring evoked or spontaneous vesicle release, both of which originate from the same pool of vesicles (Hua et al., 2010). Spontaneous synaptic vesicle release was assessed by recording mEPSCs (Fig. 23A–F) and mIPSCs (Fig. 25A–D) in collaboration with Dr. L. Liebmann. While the amplitudes of the mEPSCs did not differ between genotypes (Fig. 23C; KO: 19.493±1.63 pA; WT: 20.49±1.61 pA; p=0.66; one-way ANOVA: F=1.51, p=0.21; n=38/32), the mean frequency was more than halved in pyramidal *CA1* neurons of *Slc4a8*^{-/-} mice (23D/inset Fig. 23F; KO: 0.31±0.03 Hz; WT: 1.11±0.25 Hz; one-way ANOVA: F=3.70, p=0.01 and Newman-Keuls test: p<0.01; p=0.002).

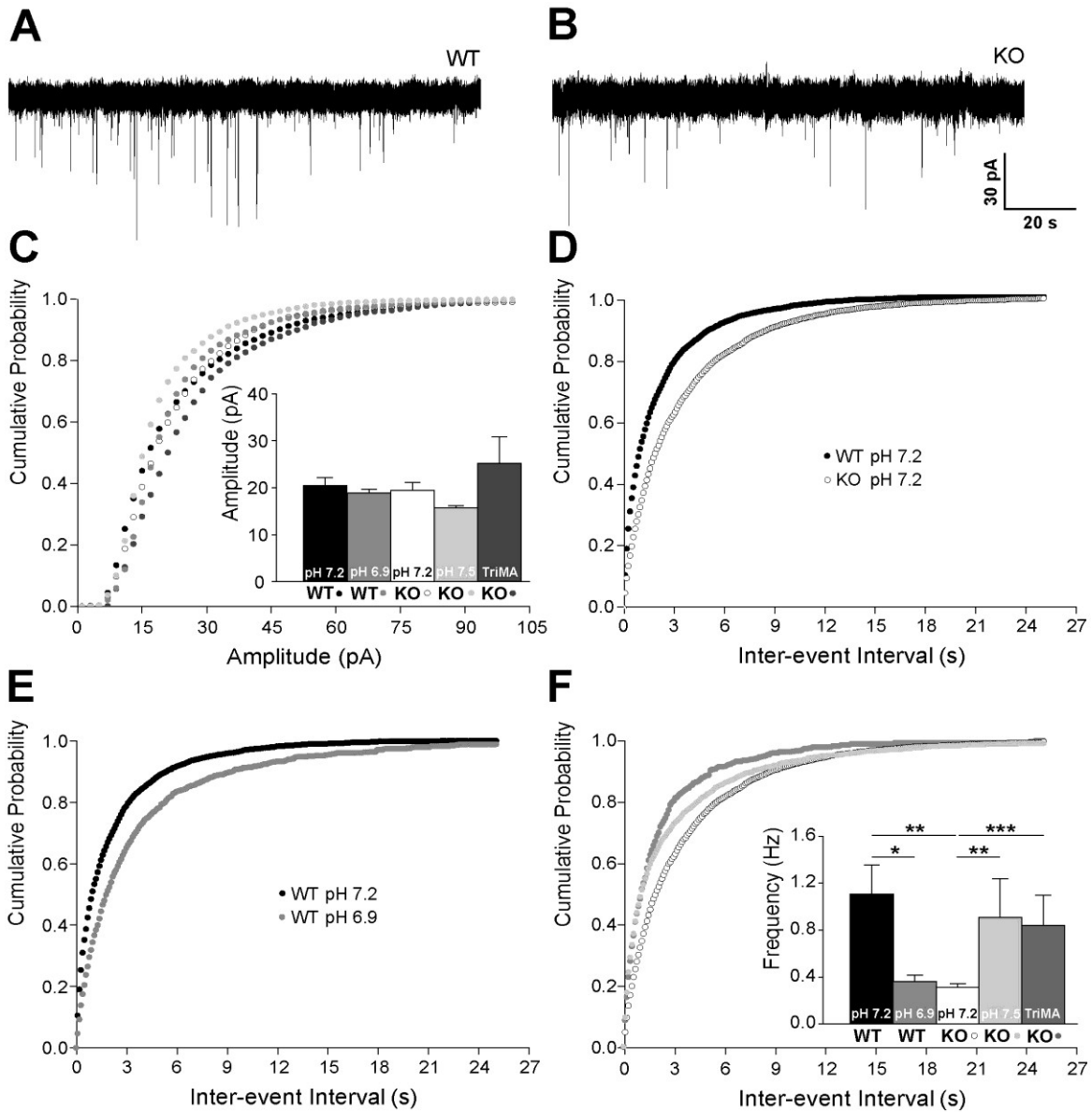


Figure 23. The frequency of mEPSCs is decreased in *Slc4a8*^{-/-} mice in a pH-dependent manner. **A, B**, Representative traces of mEPSC recordings of WT and *Slc4a8*^{-/-} *CA1* pyramidal cells at pH_o 7.2. **C**, Cumulative plots of mEPSC amplitudes at varying pH_i did not differ. Inset: means of mEPSC amplitudes (p=0.21; n=32/15/38/14/7). **D**, Cumulative plots of inter-event intervals revealed a shift to longer intervals in *Slc4a8*^{-/-} compared to WT (pH_o 7.2 p<0.001; n=38/32). **E**, Shifting the pH_o to 6.9 in WT diminished mEPSC frequencies (p<0.0001; n=32/15). **F**, Increasing pH_i by decreasing pCO₂ (pH_o 7.5) or by application of the weak base *TriMA* raised the mEPSC frequency of *Slc4a8*^{-/-} cells (pH_o 7.5 p=0.03; n=38/14; *TriMA* p=0.003; n=38/7) towards WT. Inset: means of mEPSC frequencies of WT and *Slc4a8*^{-/-} at different pH_i.

pH dependent modulation of mEPSC frequency in WT and *Slc4a8*^{-/-} neurons

To assess whether the electrophysiological changes could be explained by a compromised neuronal pH regulation, we manipulated the pH_i by varying pCO₂ at a constant extracellular bicarbonate concentration. Under these conditions, altering the pCO₂ changed extra- and intracellular pH in the same direction, with a decrease of pCO₂ resulting in an increase of pH_i and an increase of pCO₂ in a decrease of pH_i, as demonstrated by previous studies (Dulla et al., 2005; Lee et al., 1996) and confirmed by own pH recordings on cultured neurons (Fig. 24; ΔpH_i; 2.5 % CO₂: +0.26±0.04; 10 % CO₂: -0.19±0.06; one-way ANOVA: F=27.48 p<0.00001; Newman-Keuls test: p<0.01/p<0.001; n=22/39/17).

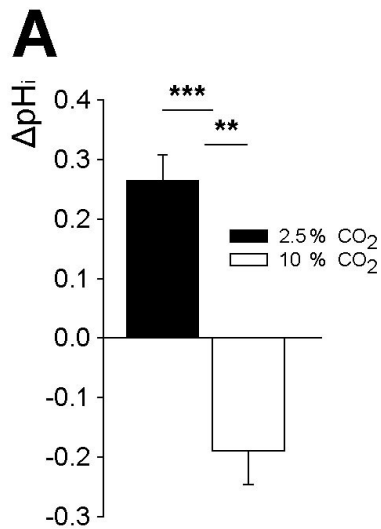


Figure 24. Alteration of pCO₂ results in changes in intracellular pH. A, Decreasing pCO₂ from 5 % to 2.5 % increased intracellular pH (n=39/22; p<0.001). In opposite, pH_i was decreased by raising CO₂ concentration to 10 % (n=39/17; p<0.01).

Lowering pH_o decreased the mean frequency of mEPSCs in WT to values obtained from *Slc4a8*^{-/-} slices (Fig. 23E; WT pH_o 7.2: 1.11±0.25 Hz; WT pH_o 6.9: 0.36±0.05 Hz; Newman-Keuls test: p>0.05 and Kolmogorov-Smirnov test: p=0.0001; n=32/15), whereas raising the pH increased the frequency distribution of mEPSCs in *Slc4a8*^{-/-} slices (Fig. 23F; KO pH_o 7.2: 0.31±0.03 Hz; KO pH_o 7.5: 0.91±0.33 Hz; Kolmogorov-Smirnov test: p=0.028; n=38/14). We additionally recorded mEPSCs in slices from *Slc4a8*^{-/-} mice upon substitution of 20mM NaCl by *TriMA*, a membrane-permeant weak base, which raises the pH_i without altering the extracellular pH_o (Eisner et al., 1989). Again, no significant differences in mEPSC amplitudes were observed (Fig.23C, KO: 19.49±1.63 pA; KO_{*TriMA*}: 25.23±5.61 pA; Kolmogorov-Smirnov test: p=0.20; n=38/7), but *TriMA* raised the mEPSC frequencies in *Slc4a8*^{-/-} slices (KO:

0.34±0.03 Hz; KO_{TriMA}: 0.84±0.25 Hz; Kolmogorov-Smirnov test: p=0.003; n=38/7) to mean values recorded from WT cells under control conditions (Fig.23F; KO_{TriMA}: 0.84±0.25 Hz; WT: 1.11±0.25 Hz; Newman-Keuls test: p>0.05 and Kolmogorov-Smirnov test: p=1.00; n=7/32).

In accordance with the immunofluorescence data that GAD and Slc4a8 only partially overlap, no differences were noted for mIPSC amplitudes (Fig. 25C; KO pH_o 7.2: 38.54±2.39 pA; WT pH_o 7.2: 39.43±2.10 pA; Students t-test: p=0.78; n=15/16) and frequencies (Fig. 25D; KO pH_o 7.2: 7.07±1.02 Hz; WT pH_o 7.2: 5.82±0.46 Hz; Students t-test: p=0.27).

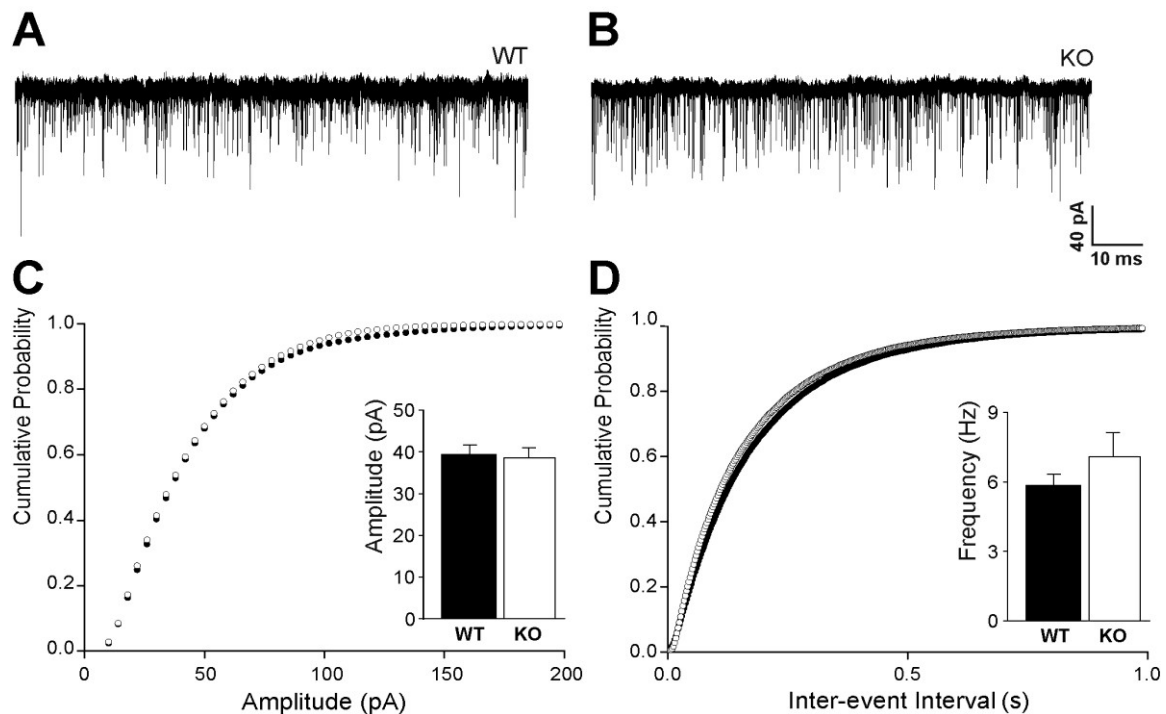


Figure 25. No change in frequency or amplitudes of mIPSC by deletion of Slc4a8. A, B, Representative traces of mIPSC recordings of WT and *Slc4a8*^{-/-} CA1 pyramidal neurons. C,D, Cumulative plots and means of mIPSC amplitude and frequencies did not differ between the genotypes (pH_o 7.2 p=0.78 and p=0.27; n=15/16).

Slc4a8 modulates presynaptic vesicle release

To finally pinpoint the defect of glutamatergic transmission in *Slc4a8*^{-/-} mice to the presynapse, vesicle release upon field stimulation was subsequently quantified by measuring

bouton destaining in FM1-43-labelled cultured hippocampal neurons (Fig. 26). No difference was observed in baseline punctual intensity (KO: 476.34 ± 18.02 a.u.; WT: 466.25 ± 18.09 a.u.; Students t-test: $p=0.69$; $n=116/134$). However, destaining and hence synaptic vesicle release upon repetitive stimulation was significantly diminished in *Slc4a8*^{-/-} cultures after approximately 900 action potentials ($(F_0 - F_{900})/F_0$; KO: 0.183 ± 0.007 ; WT: 0.206 ± 0.009 ; Students t-test: $p=0.035$; $n=116/134$). Following extensive stimulation with more than 1,500 action potentials, this difference disappeared ($(F_0 - F_{1500})/F_0$; KO: 0.307 ± 0.008 ; WT: 0.320 ± 0.010 ; Students t-test: $p=0.31$). Fitting single bouton destaining over time mono-exponentially, allowed the calculation of destaining τ . Analysis of the cumulative probability of τ (Fig. 26B) revealed a significantly different distribution between the two groups (Kolmogorov-Smirnov test: $p=0.002$), with an increase of mean τ in *Slc4a8*^{-/-} (144.59 ± 9.04 s; $n=54$) compared to WT neurons (112.43 ± 7.53 s; Students t-test: $p=0.0079$; $n=50$) (inset Fig. 26C).

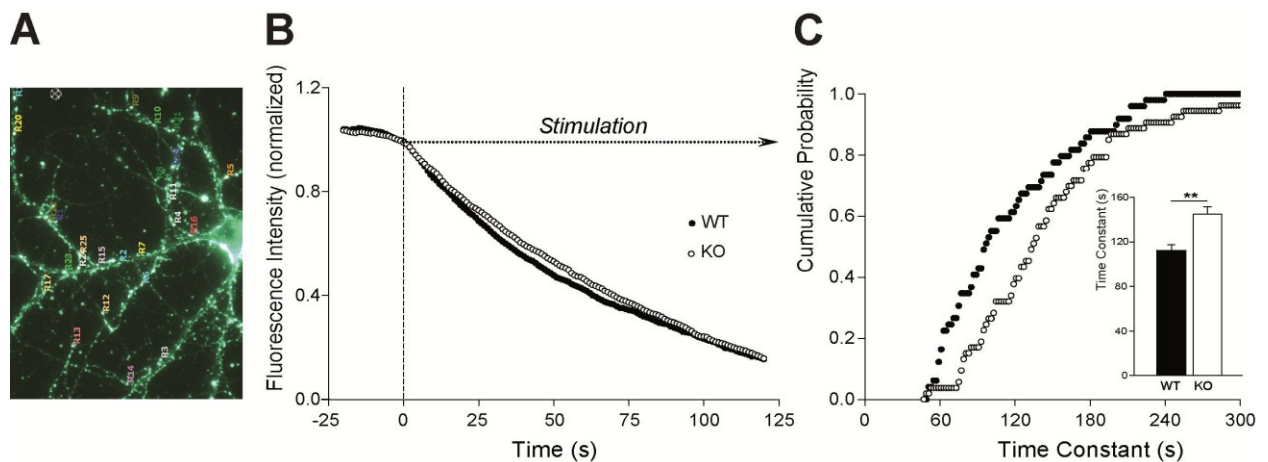


Figure 26. Impaired release of synaptic vesicles in *Slc4a8*^{-/-} hippocampal neurons. **A**, Synapses labeled with FM1-43 of a cultured hippocampal neuron. **B**, Time course of fluorescence destaining following field stimulation of cultured hippocampal WT and *Slc4a8*^{-/-} neurons upon vesicle labeling with FM1-43 ($n=54/50$). **C**, Cumulative plot of the time constants revealed a shift towards a higher τ in *Slc4a*^{-/-} neurons ($p=0.002$; $n=54/50$) equivalent with an increased mean τ . Inset: Mean τ also increased in *Slc4a8*^{-/-} synapses ($n=54/50$, $p<0.01$).

These findings could be corroborated electrophysiologically in collaboration with Dr. L. Liebmann: normalized eEPSC amplitudes decreased more rapidly per stimulus upon application of the open-channel NMDA receptor blocker MK-801 in WT compared to *Slc4a8*^{-/-} slices (Fig. 27A). The blocking rate of NMDA receptor eEPSCs was significantly delayed in *Slc4a8*^{-/-} slices (54.59±6.32 stimuli; n=8) compared to WT (27.56±3.64 stimuli; Students t-test: p=0.005; n=6) (Fig. 27B), whereas the input/output relationship of evoked NMDA current density did not differ between genotypes at all stimulus intensities tested (input/output relationship 0-60V: repeated measures ANOVA: F=1.01, p=0.32; n=16/11).

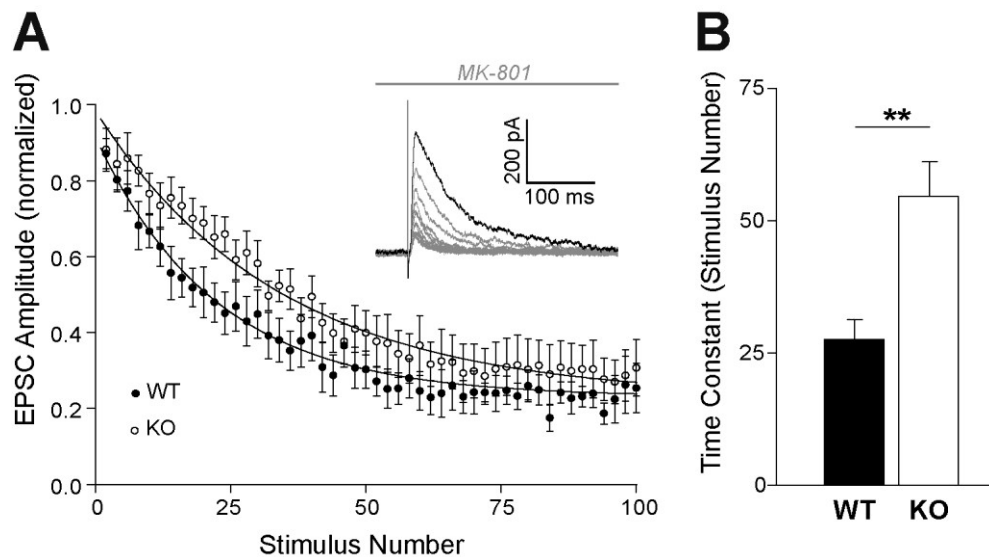


Figure 27. Electrophysiological analysis showed reduced released of glutamatergic vesicles in *Slc4a8*^{-/-} slices. **A**, Time course of the amplitude decrease of normalized NMDA currents in the presence of MK-801 (n=8/6). Inset: sample traces of NMDA receptor-mediated eEPSCs recorded from *CA1* pyramidal neurons in the presence of MK-801 upon repetitive stimulation of Schaffer collaterals. Mean τ was increased in *CA1* neurons of *Slc4a8*^{-/-} mice in the presence of MK-801 (**B**, n=8/6, p<0.01).

Taken together, these experiments show that deletion of *Slc4a8* results in a reduction of the number of released glutamatergic vesicles, although the pool of releasable vesicles appears to be unchanged.

Pyramidal cells and interneurons express Slc4a10

Besides strong expression of Slc4a10 protein in the choroid plexus, Slc4a10 was detected in cortical brain regions (olfactory bulb, cortex, and hippocampus) and the cerebellum (Jacobs et al., 2008). On the subcellular level, Slc4a10 mostly localized to dendrites and dendritic spines and was often found in juxtaposition of GAD positive presynapses. In contrast to Slc4a8, these data suggest a predominant postsynaptic expression of Slc4a10, mostly in neurons under GABAergic control. To further clarify the complementary expression patterns of Slc4a10 and Slc4a8, double immunofluorescent stainings for both transporters were performed as well as co-stainings of Slc4a10 protein with different synaptic markers.

Expression of Slc4a10 was confirmed in plasma-membranes of pyramidal cells in all hippocampal regions and, in contrast to the expression of Slc4a8, also in most parvalbumin-positive interneurons of the hippocampus (Fig. 28AB). GABAergic presynapses, labelled with VGAT (Fig. 28CD) or GAD (data not shown), were mostly found in juxtaposition to Slc4a10 positive dendrites (Fig. 28DE) as described previously (Jacobs et al., 2008). But in the pyramidal layer also some co-localization was observed (Fig. 28DF).

In addition, double immunostainings for Slc4a8 and Slc4a10 protein revealed that both transporters were expressed in the pyramidal cell layer but not all cells which expressed Slc4a10 were positive for Slc4a8 (Fig. 28G'-G''). Those cells most likely are the parvalbumin-positive interneurons, which only express Slc4a10. Expression patterns in other hippocampal cell layers differed. Dendrites in SRad stained positive for Slc4a10 protein but were not labelled by the Slc4a8 antibody. The Slc4a8 antibodies labelled the S-LM and the SOr more intensively, albeit some overlay in these layers (Fig. 28EF) was observed.

In conclusion, Slc4a10 and Slc4a8 were expressed in plasma-membranes of pyramidal cells of all hippocampal regions but only Slc4a10 was expressed in parvalbumin-positive interneurons. On the sub-cellular level, Slc4a8 protein was found predominantly in presynaptic, glutamatergic compartments, whereas Slc4a10 protein was mostly found in postsynaptic regions (dendrites, dendritic spines) of glutamatergic neurons but also in GABAergic neurons (e.g. in plasma-membrane and presynaptic terminals).

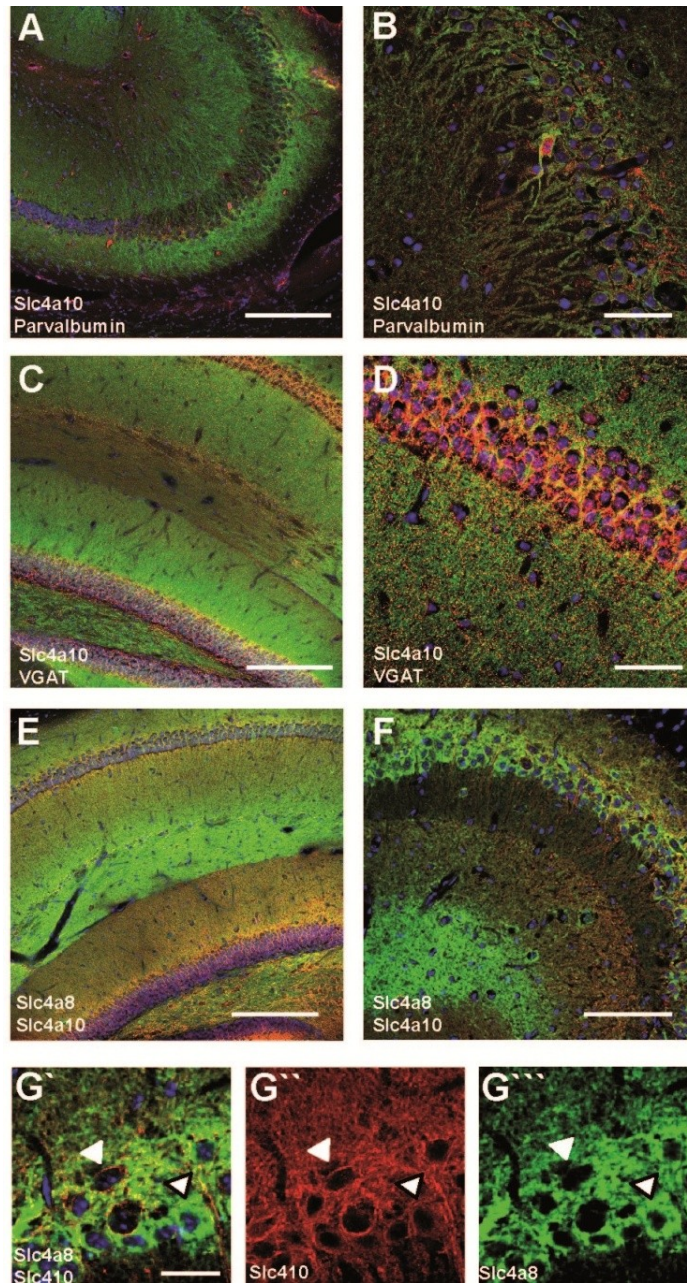


Figure 28. Interneurons and pyramidal cells express Slc4a10 A, B, Apart from expression in pyramidal cells, Slc4a10 (green) is expressed in parvalbumin-positive interneurons (red), shown in the CA3 region (scale bars 200 μm /50 μm). C, Double staining against Slc4a10 (green) and VGAT (red) as a marker for GABAergic presynapses, partially co-localize (scale bar 200 μm). Close up from SPyr of the CA1 region (D, scale bar 50 μm). Co-stainings of Slc4a8 (green) and Slc4a10 (red) protein revealed that both transporters partly co-localize (E, scale bar 200 μm) but differ in their expression pattern in some hippocampal regions e.g. in the SRad of the CA3 region (F, scale bar 100 μm). G'-G'''' Also in the pyramidal cell layers some neurons are Slc4a8 negative but Slc4a10 positive (white arrow), albeit most (pyramidal) neurons express both transporters (black framed white arrow; scale bar 25 μm).

Slc4a10 deletion alters field excitability and paired pulse depression

To examine the role of Slc4a10 in synaptic transmission, field potentials in acute WT and *Slc4a10*^{-/-} slices were recorded in the *CA1* region upon stimulation of Schaffer collaterals. In contrast to the decreased fEPSP amplitude in *Slc4a8*^{-/-} slices we found an increased fEPSP amplitude in Slc4a10 deficient mice with increasing stimulus intensities (Fig. 29A; repeated measures ANOVA: $F=5.38$, $p=0.03$; $n=23/18$) and also at half-maximal stimulus intensity (inset Fig. 29A; KO 5.86 ± 0.71 mV WT: 3.74 ± 0.42 mV; Students T-test: $p=0.013$; $n=16/18$). Paired pulse experiments revealed no change in short term plasticity (repeated measures ANOVA: $F=2.63$, $p=0.11$; $n=16/18$).

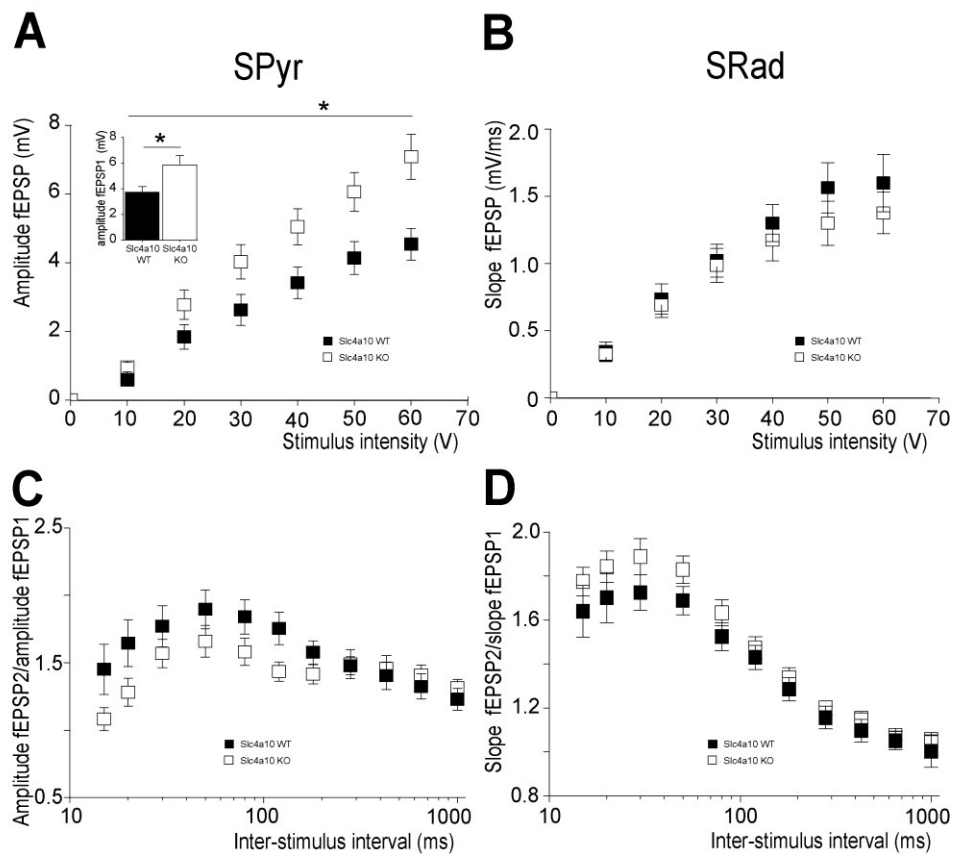


Figure 29. Increase in field excitability in *CA1* SPyr but not SRad of *Slc4a10*^{-/-} mice. **A**, Increased field-potential amplitude in SPyr upon stimulation with increasing stimulus intensities ($n=23/18$; $p=0.03$). Inset: At half maximal stimulus intensity fEPSP amplitude was larger in *Slc4a10*^{-/-} slices compared to WT ($n=20/20$; $p=0.01$). **B**, No differences in input/output relationship of fEPSP slope in the SRad ($n=18/21$; $p>0.05$). **C**, **D**, No differences in short term plasticity analysed by the paired pulse paradigm in the SPyr and SRad.

No significant differences were observed in recordings from the SRad (Fig. 29B; input/output relationship; repeated measures ANOVA: $F=0.47$, $p=0.50$; $n=20/20$; half-maximal stimulus intensity KO: 1.25 ± 0.14 mV/ms WT: 1.01 ± 0.12 mV/ms; Students t-test: $p=0.21$; $n=18/21$; paired pulse ratio: repeated measures ANOVA: $F=1.38$, $p=0.25$; $n=17/18$).

As *Slc4a10* is also broadly expressed in the cortex, we recorded field potentials from cortical layer 2/3 upon stimulation of layer 6 close to the corpus callosum in the occipital and the temporal lobe. No differences were observed in amplitudes of the field potentials, neither with increasing stimulus intensities (Fig. 30AB; position 1: repeated measures ANOVA: $F=0.70$, $p=0.41$; $n=23/24$; position 2: repeated measures ANOVA: $F=0.16$, $p=0.70$; $n=21/26$), nor in the response to half maximal stimulus response (position 1 KO: 3.58 ± 0.39 mV WT: 3.29 ± 0.38 ; Students t-test: $p=0.61$; $n=21/26$; position 2 KO: 2.78 ± 0.31 ; WT: 3.54 ± 0.39 ; Students t-test: $p=0.11$; $n=19/24$). But in the paired pulse paradigm an increase in the paired pulse depression with inter-stimulus intervals around 100 msec was found in the occipital lobe of *Slc4a10*^{-/-} slices (Fig. 30CD; position 1: repeated measures ANOVA: $F=4.30$, $p=0.04$; $n=21/26$; position 2: $F=2.05$, $p=0.16$; $n=19/24$).

Thus, contrary to the decreased excitatory synaptic transmission in *Slc4a8*^{-/-} mice our initial electrophysiological recordings revealed an increased excitability in the pyramidal cell layer of the hippocampus of *Slc4a10*^{-/-} mice and an increase in paired pulse depression with long inter-stimulus intervals in the cortex.

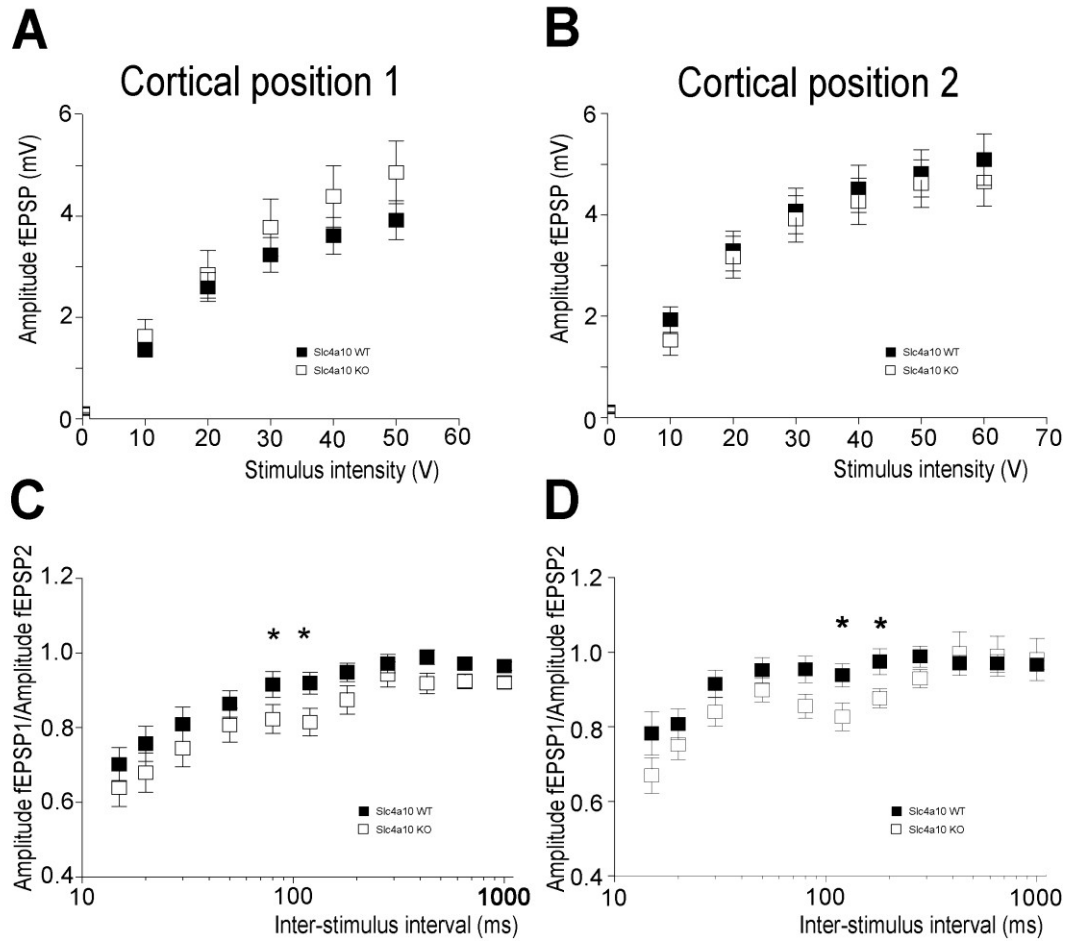


Figure 30. Altered paired-pulse depression at longer inter-stimulus intervals in the cortex of *Slc4a10*^{-/-} slices. **A, B,** No differences between genotypes could be detected in the input/output relationship at position 1 and 2 of the cortex. **C,** Paired pulse recordings from cortical position 1 revealed an increased paired pulse depression around 100 msec (n=21/26; p=0.04). **D,** A trend towards a strengthened paired pulse depression was also notable in recordings at position 2 of *Slc4a10*^{-/-} slices (n=19/24; p=0.16).

Discussion

Na⁺ dependent anion exchange has been described in nearly all mammalian cell types. With the help of a constitutive KO mouse model for Slc4a8, this thesis addressed the physiological function of Na⁺ dependent Cl⁻/HCO₃⁻ exchange in the mouse brain and kidney.

Physiological role of Slc4a8 in the mouse kidney

Earlier expression data for Slc4a8 from *in situ* hybridizations and a multiple tissue Northern blot suggested a relatively broad expression with the highest expression level in the adult and embryonic brain and a smaller splice variant in the testis (Kougioumtzes, 2006). *Slc4a8* mRNA was also detected in adult kidney, lung, intestines, oesophagus and in the thyroid gland. The expression in the kidney of adult mice was confirmed on mRNA and protein level. Within the mouse kidney Slc4a8 protein was detected in the renal cortex and more precisely in the cortical collecting duct.

Renal function of Slc4a8

Paracellular and transcellular transport mechanisms in the proximal nephron allow reabsorption of large parts of the salt and water reabsorption from the ultrafiltrate formed in the glomeruli. Transcellular transport of approximately 90 % of filtrated Na⁺ takes place in the proximal tubulus mediated by NHE3 and in the ascending loop of Henle mediated by NKCC2. However, the regulation of salt reabsorption almost exclusively takes place in the most distal part of the nephron, called the aldosterone sensitive distal nephron (for review, see Verrey, 2001 or Rozansky, 2006). The amiloride-sensitive, thiazide-insensitive ENaC in the principal cells of the connecting and collecting tubule and the thiazide-sensitive Na⁺/Cl⁻ co-transporter NCC, which is exclusively expressed in the distal convoluted tubules, are well known aldosterone targets in this segment. Early studies already showed that Na⁺-reabsorption in the cortical collecting duct is also thiazide sensitive (Tomita et al., 1985; Terada and Knepper,

1990). The results of this thesis and mainly those from the study performed in collaboration with Dr. D. Eladari (Leviel et al., 2010) suggest that the parallel action of Slc4a8 and the Cl⁻/HCO₃⁻ exchanger Pendrin account for this electroneutral thiazide-sensitive NaCl transport in the cortical collecting duct.

If Slc4a8 is important for salt reabsorption, one could expect a transcriptional up-regulation under conditions of increased Na⁺- reabsorption. Indeed, such an up-regulation of Slc4a8 protein was observed when WT mice were maintained under a Na⁺ restricted diet or when salt reabsorption was stimulated by application of the aldosterone analogue DOCP.

Similar to the situation in humans, where high daily salt intake rather provokes high blood pressure due to an increase in extracellular osmolarity (Meneton et al., 2005), Slc4a8 mediated Na⁺ reabsorption in mice seems to be of special physiological importance when increased salt retention is needed. This is further proven by the fact that no differences in baseline Na⁺-excretion between genotypes were detected under normal diet. Surprisingly, we observed a normal adaptation of constitutive *Slc4a8*^{-/-} mice to a Na⁺ depleted diet. The only notable difference was an increased urinary aldosterone concentration in Na⁺ depleted *Slc4a8*^{-/-} mice. Increased aldosterone concentrations could mediate an increased activation or expression of other aldosterone-sensitive pathways, especially of NCC or ENaC (Kim et al., 1998; Loffing et al., 2001).

The most plausible candidate for a compensatory up-regulation of another Na⁺ reabsorption mechanisms in *Slc4a8*^{-/-} is NCC. An up-regulation of the second major Na⁺-transporter in the distal nephron, ENaC, would be accompanied by an increase in electrical driving force for K⁺ secretion through stimulation of ROMK channels. This was not indicated by the normal urinary K⁺ excretion of *Slc4a8*^{-/-} in the metabolic experiments. Increased activity of NCC indeed could be confirmed in *Slc4a8*^{-/-} mice under Na⁺ restriction by monitoring the response to acute thiazide injection. In contrast to an indifferent response to the ENaC blocker amiloride, an exaggerated response to thiazides in *Slc4a8*^{-/-} mice by means of an increased amount of excreted Na⁺ was observed. These results suggest that the constitutive deletion of *Slc4a8* is compensated by an increased expression or activation of NCC, which in the meanwhile has been confirmed by Western blot analysis.

As described earlier from the classical point of view thiazides are believed to reduce vascular volume by blocking NCC in the distal convoluted tubulus (Ellison and Loffing, 2009). The

presented data suggest that the anti-hypertensive effect of thiazides may, at least partly, occur through inhibition of the newly identified Na⁺ reabsorption pathway involving Slc4a8 in the cortical collecting duct. Hence, a better understanding of Slc4a8 localization and activity in the kidney may pioneer a better treatment of potentially Slc4a8-mediated side effects of thiazides and the development of more specific treatment options in the future.

Physiological role of Slc4a8 in the mouse brain

Slc4a8 localizes to presynaptic nerve endings

Antibodies generated to detect Slc4a8 have been reported to label hippocampal pyramidal neurons (Damkier et al., 2007; Chen et al., 2008a) but not astrocytes (Chen et al., 2008a). With our new antibody (Leviel et al., 2010) various regions of the central nervous system including cerebellum, spinal cord, brainstem, hippocampus and cortex were stained. The broad neuronal expression of Slc4a8 appeared to be specific as the signals were absent in stainings of tissue from *Slc4a8*^{-/-} mice. Double stainings with GFAP, as well as immunoblot analysis from cell cultures, proved that neurons but not glial cells expressed detectable amounts of Slc4a8 protein. Co-stainings with pre- (vGLUT1, -2; synaptophysin; NF68) and postsynaptic markers (PSD-95; MAP2) were in accordance with a mainly presynaptic localization of the Slc4a8 protein. This was corroborated by immunoblot analysis of sub-cellular fractions of mouse brain lysates, Slc4a8 being enriched in synaptic junction membranes compared to synaptosomes and crude membrane preparations but absent from the postsynaptic density. Ultrastructural analysis of co-immuno labelled synaptosomes finally confirmed that Slc4a8 protein localizes to the same synaptic compartment as classical presynaptic markers (syntaxin, SNAP25).

Role of Slc4a8 in neuronal pH_i regulation

The transport direction of electroneutral transporters like Slc4a8 does not depend on the transmembrane potential. Because of the large Na⁺ gradient between the extracellular and

intracellular compartment, Slc4a8 mediates an inward transport of HCO_3^- , which is equivalent to acid extrusion from the cells and an increase of the intracellular buffering capacity. In accordance with a reduction of the buffering capacity, NH_4Cl -induced peak alkalosis and the concomitant rebound acidosis were increased in *Slc4a8*^{-/-} neurons. As the steady-state pH_i was decreased and the recovery from an acid load impaired in the somata of cultured hippocampal neurons of *Slc4a8*^{-/-} mice, Slc4a8 clearly plays an important role in pH_i regulation in these neurons. This confirms previous data from rat CA1 hippocampal neurons which displayed DIDS-sensitive HCO_3^- -dependent acid extrusion that required external Na^+ as well as internal Cl⁻ (Schwiening and Boron, 1994). Because of minor effects of amiloride on acid extrusion, it was further concluded that Na^+/H^+ exchange might be less relevant in rat CA1 hippocampal neurons. However, as acutely dissociated CA1 pyramidal neurons from *Nhe1* deficient mice displayed a more acidic steady-state pH_i and a lower rate of acid extrusion compared with cells from WT mice in HEPES-buffered media (Yao et al., 1999), further studies are required to resolve to what extent acid extrusion in the absence of Slc4a8 depends on Slc9a1, Slc4A10 or Slc4a7. In CA3 pyramidal neurons devoid of Slc4a10 in acute slice preparations the steady-state pH_i was unchanged but acid recovery was delayed (Jacobs et al., 2008).

The repeated association and dissociation of intracellular protons with intracellular macromolecules results in a surprisingly low diffusion rate in the cytosol (al-Baldawi and Abercrombie, 1992). Consequently, pH gradients have been described in cells with a polarized expression of pH-relevant transporters (Schwiening and Willoughby, 2002; Stewart et al., 1999). Because of the enrichment of Slc4a8 in presynaptic nerve endings, one may infer that the impact of the disruption of *Slc4a8* on pH_i regulation may be more pronounced in synaptic boutons compared to the soma. However, to our knowledge, a direct analysis of pH_i regulation in presynaptic boutons has not been possible to date. Quite recently, the pH-sensitive properties of the yellow fluorescent protein were successfully used to analyse the presynaptic pH in motor endplates (Zhang et al., 2010), but motor endplates are much larger in size (a few hundred μm^2 ; Albuquerque et al., 1974) compared to the small, central presynaptic terminals (a few tens of μm^2 , Rollenhagen and Lübke, 2010). Focal injections of BCECF-AM in combination with slice imaging as used for measuring calcium transients in small synaptic compartments with the calcium-sensitive dye Fura (Saggau et al., 1999) may help to establish adequate pH imaging in small compartments like central pre- and postsynaptic terminals.

The numerous studies dealing with pH regulation in synaptosomes are difficult to interpret, as these preparations include both pre- and postsynaptic compartments (Bai and Witzmann, 2007). Surprisingly, HCO₃⁻-dependent acid extrusion has so far not been described in synaptosome preparations, whereas there is wide consensus that synaptosomes display amiloride-sensitive Na⁺/H⁺ exchange (Chesler, 2003; Rocha et al., 2008).

Glutamatergic vesicle release is modulated by Slc4a8

Apart from subtle behavioural changes and the diminished seizure susceptibility (Kougioumtzes, 2006), field recordings in hippocampal slices provided the first indication that Slc4a8 may be relevant for neuronal excitability, as synchronous firing of *CA1* pyramidal neurons measured as the population spike amplitude was reduced in *Slc4a8*^{-/-} slices upon stimulation of Schaffer collaterals. The increased facilitation of a second pulse together with the localization of Slc4a8 protein pointed to a presynaptic defect of the projection of Schaffer collaterals onto pyramidal neurons. As glutamate uptake into synaptic vesicles is driven by the electrochemical proton gradient across the synaptic vesicle membrane (Maycox et al., 1988), we analysed the amplitudes of spontaneous mEPSCs as an indirect measure for the quantum of transmitter released per synaptic vesicle. Whereas the normal amplitude distribution indicated that the loading of glutamatergic synaptic vesicles in *Slc4a8*^{-/-} mice was not affected (Mathews and Diamond, 2003), the drastic decrease of mEPSC frequency revealed that synaptic vesicle release was impaired in the absence of Slc4a8. It has been shown that effects of varying pCO₂ on excitatory transmission are apparently caused by changes in pH_i (Lee et al., 1996). Lowering the pH_i by increasing pCO₂ in WT slices decreased mEPSC frequency to values as observed in *Slc4a8*^{-/-} mice. Whereas the frequency of spontaneous mEPSCs increased with increased pH in *Slc4a8*^{-/-} mice. Thus, these results support our hypothesis that the decrease of frequency could be attributed to a decrease of pH_i in presynaptic nerve endings.

Although the optical analysis of synaptic vesicle release could not distinguish between glutamatergic and GABAergic presynapses, which are thought to account for a minor fraction in cultured hippocampal neurons (Walker and Peacock, 1981; Feng et al., 2002), induced synaptic vesicle release upon repetitive field stimulation of cultured hippocampal neurons was significantly slowed. However, the overall synaptic vesicle pool appeared to be unaffected by disruption of Slc4a8, as the difference disappeared after more than 1,500 pulses. The

difference between genotypes was more pronounced in the electrophysiological analysis, which was specific for glutamatergic synaptic activity.

How can disruption of Slc4a8 affect neurotransmitter release?

The machinery for the release of synaptic vesicles is initiated by a rise in $[Ca^{2+}]_i$ (Schneggenburger and Neher, 2000). Nonetheless, other ions including Na^+ and H^+ have also been proposed to play a critical role. As Slc4a8 mediates Na^+ -coupled anion exchange, its activity increases the $[Na^+]_i$ concentration, which in turn may increase the $[Ca^{2+}]_i$ via the Na^+/Ca^{2+} exchanger (Mulkey and Zucker, 1992; Reuter and Porzig, 1995). Following this scenario, disruption of *Slc4a8* may result in a lower $[Ca^{2+}]_i$ and hence a reduction of spontaneous synaptic vesicle release. However, in view of the partial reversibility of the decreased synaptic vesicle release by increasing the pH, a direct pH-related effect may be more likely. As virtually all proteins depend on pH to maintain their structure and function, multiple effects may add up. For example, the opening and the conductivity of presynaptic voltage-gated calcium channels, which mediate the presynaptic Ca^{2+} influx, are strongly dependent on both extracellular and intracellular pH (Tombaugh and Somjen, 1997). Protons can directly bind to sensors within the pore of the channel and thereby reduce channel conductance (Prod'homme et al., 1987; Chen et al., 1996) and shield membrane-bound charges and thus shift the channel activation voltage to more positive values (Klöckner and Isenberg, 1994; Zhou and Jones, 1996). Neurotransmitter release, synaptic short-term plasticity as well as spontaneous vesicle release also depend on calcium release from intracellular stores (Emptage et al., 2001), which is mediated via inositol 1,4,5-trisphosphate and ryanodine receptors, both of which show strong pH dependence (Ma et al., 1988; Tsukioka et al., 1994). Ultimately, dysfunction of any of these presynaptic processes due to the decrease in pH_i at the presynaptic bouton could lead to a slowed release of glutamatergic vesicles in *Slc4a8*^{-/-} mice and thereby diminishes the postsynaptic response, i.e. less glutamate receptors are activated, and decrease the overall neuronal excitability (see also Fig. 31A).

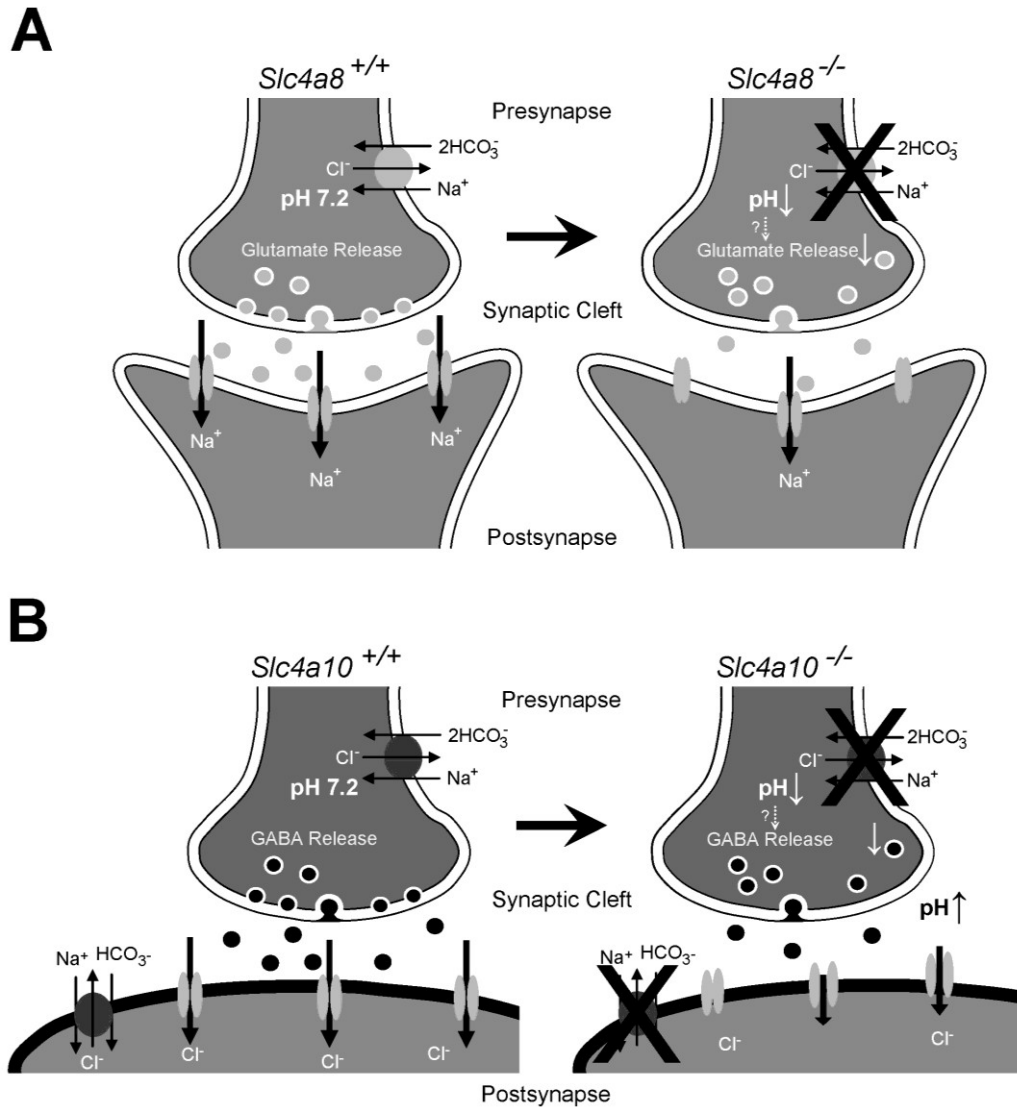


Figure 31. Possible roles of Slc4a8 and Slc4a10 for synapse physiology. **A**, Model illustrating the consequences of *Slc4a8* disruption on glutamate release. Slc4a8 is involved in presynaptic pH homeostasis. Upon disruption of *Slc4a8* the intracellular pH is diminished and glutamate release impaired. Accordingly, less postsynaptic glutamate receptors are activated but the pool of releasable vesicles appears to be unchanged. **B**, Pre- and postsynaptic expression of Slc4a10 on GABAergic synapses regulates vesicle release within the presynaptic terminal as well as the GABA_A receptor conductance on the postsynapse. The postsynaptic modulations may be caused by increasing the synaptic cleft pH and altering the Cl⁻ equilibrium potential. As a result, *Slc4a10* deletion would render GABAergic inhibition less effective.

Clinical relevance of these findings

As neuronal activity can result in sustained decreases of pH_i (Chesler and Kaila, 1992), the pH-dependent impairment of synaptic vesicle release may be even more relevant in situations with increased neuronal activity (Tong and Chesler, 1999; Zhan et al., 1998), including epileptic seizures (Xiong et al., 2000). Whereas a decrease of pH generally reduces neuronal excitability, it is increased by a rise of pH (Aram and Lodge, 1987). Hyperthermia-induced respiratory alkalosis is also considered as a key event in the pathogenesis of febrile seizures. In a rat pup model for febrile seizures, ictal activity was induced by respiratory alkalosis with a threshold of 0.2–0.3 pH units (Schuchmann et al., 2006) and could be stopped by suppressing alkalosis by increasing ambient pCO_2 . The impaired acid extrusion in *Slc4a8*^{-/-} neurons may thus explain why *Slc4a8*^{-/-} mice have reduced seizure susceptibilities in various paradigms, including the hyperthermia model (Kougioumtzes, 2006). Likewise, mice with a targeted disruption of *Slc4a10* were protected from seizure-related mortality (Jacobs et al., 2008), whereas the sensitivity to seizure-inducing agents was increased in mice with a disruption of the Na^+ -independent $\text{Cl}^-/\text{HCO}_3^-$ exchanger *Slc4a3*, which imposes an intracellular acid load (Hentschke et al., 2006). Some anticonvulsants, such as acetazolamide, reduce extracellular pH in the brain (Chen and Chesler, 1992), suggesting that acidosis may contribute to their anti-epileptic effects. As an exception to this rule, *Nhe1*-deficient mice develop slow-wave epilepsy (Cox et al., 1997), which may be explained by the secondary increase of the Na^+ current density in *CA1* pyramidal neurons of these mice (Gu et al., 2001; Xia et al., 2003) or selective neuronal death (Cox et al., 1997). Also, an important role of *Nhe1* for the regulation of synaptic cleft pH at GABAergic synapses has been proposed, where absence of *Nhe1*-induced acidosis could render GABAergic inhibition less effective (Dietrich and Morad, 2010). The reduced seizure threshold in *Slc4a8*^{-/-} mice (Kougioumtzes, 2006) suggests that inhibition of *Slc4a8* may be a target for anti-epileptic therapy. In this context, it is worth noting that GABAergic synaptic vesicle release was not affected by disruption of *Slc4a8* as judged from the amplitude and frequency distribution of mIPSCs in *CA1* pyramidal neurons, which corresponds with previous data showing that pH regulation in GABAergic presynaptic nerve endings was mainly mediated by *Nhe1* (Jang et al., 2006) and with our observation that co-localization of *Slc4a8* and GAD was only partial.

In conclusion, the results of this thesis show that the broadly expressed neuronal Na⁺-coupled anion exchanger Slc4a8 is enriched in presynaptic glutamatergic nerve terminals. As a key regulator of intracellular pH, Slc4a8 affects glutamatergic synaptic vesicle release in a pH-dependent way. Since consensus phosphorylation sites have been predicted for different members of the gene family (Boron et al., 2009), including *Slc4a8* (Grichtchenko et al., 2001), it is tempting to speculate that synaptic strength may be regulated via Slc4a8 in response to various signals. Interestingly, a splice variant of *Slc4a8* has been shown to include a consensus binding site for 14-3-3 proteins (Parker et al., 2008a), which are known to influence trafficking (Mrowiec and Schwappach, 2006) and activity (Allouis et al., 2006) of different ion transporters and channels. Thereby, Slc4a8 could have important consequences for synaptic transmission in both physiological and pathophysiological conditions.

Role of Slc4a10 in cortical brain regions

Comparison of hippocampal expression patterns of Slc4a10 and Slc4a8

Within the family of Slc4 HCO₃⁻ transporters *Slc4a8* shares the highest homology with the Na⁺-HCO₃⁻ co-transporter *Slc4a7/Nbcn1* (Pushkin et al., 1999a; Bok et al., 2003) and the Na⁺-coupled anion exchanger *Slc4a10/Ncbe* (Wang et al., 2000; Damkier et al., 2010) (see Fig. 2). Both transporters are shown to be expressed in the central nervous system (Jacobs et al., 2008; Park et al., 2010), where they mediate acid extrusion. Slc4a7 protein localizes to the postsynaptic side of neurons (Park et al., 2010). The closely related Na⁺-coupled anion exchanger Slc4a10 (Damkier et al., 2010; Wang et al., 2000) has mainly been detected in dendrites, dendritic spines and postsynaptic membranes (Jacobs et al., 2008), whereas Slc4a8 colocalized with presynaptic, mostly glutamatergic structures. In contrast to Slc4a10 and Slc4a7, it has been suggested that the Na⁺/H⁺ exchanger *Slc9a1/Nhe1* is present in GABAergic presynaptic nerve endings (Jang et al., 2006). Besides the different sub-cellular localization, Slc4a8 and Slc4a10 also differ in their cell-type specific expression. In the hippocampus, the major discrimination is between the GABAergic interneurons and the mostly glutamatergic pyramidal cells. Whereas Slc4a10 is expressed in both cell types, Slc4a8 is not expressed in most parvalbumin-positive interneurons. The expression data indicates that Slc4a10 activity

could influence both, postsynaptic responses to GABA in pyramidal cells as well as the presynaptic activity of GABAergic interneurons.

Deletion of Slc4a10 alters neuronal excitability antithetic to Slc4a8

Previous studies of our group revealed an increase in seizure threshold, comparable to the observations in the *Slc4a8*^{-/-} mice, and a diminished mortality upon seizure induction (Jacobs et al., 2008). Slc4a10 expressing cells (e.g. choroid plexus cells and CA3 pyramidal neurons) show an attenuated recovery to an induced acid load, which in turn can also influence neuronal excitability (Jacobs et al., 2008). The severe impairment of cerebrospinal fluid production and the resulting malformation of the *Slc4a10*^{-/-} brains complicate the interpretation of electrophysiological results, as morphological differences can always influence functional connectivity. Nonetheless neuronal excitability was analysed in the hippocampus and in the cortex in more detail.

In contrast to the results in the *Slc4a8*^{-/-} slices, increased population spike amplitudes were observed in the stratum pyramidale of *Slc4a10*^{-/-} compared to WT slice, whereas field responses in the SRad were unaltered. Considering that only ~6 % of synaptic inputs to pyramidal CA1 neurons are inhibitory and that the distal SRad has a very high (glutamatergic) spine density and the lowest ratio of inhibitory/excitatory inputs (Megías et al., 2001), the altered field response in the SPyr but not in the SRad indicates an altered inhibition in *Slc4a10*^{-/-} mice.

Interestingly, heterozygous deletions of large genomic regions spanning the human *SLC4A10* gene (2q24) have been associated to idiopathic epilepsies and mental retardation in humans (Gurnett et al., 2008; Krepischi et al., 2010). Albeit the causality between *SLC4A10* gene deletion and the phenotype needs to be proven, the present findings in homozygous *Slc4a10*^{-/-} mice might suggest that alteration in synaptic inhibition could be the functional correlate for these clinical observations. Analysis of heterozygous *Slc4a10*^{+/-} mice in *in vivo* epilepsy models as well as for the electrophysiological analysis might be helpful in the future.

The paired pulse paradigm for the analysis of changes in short term plasticity slices revealed no significant differences between homozygous *Slc4a10*^{-/-} and WT slices, neither in SRad nor in the pyramidal cell layer. However, paired stimuli with half-maximal intensity cannot reveal minor differences in synaptic inhibition, as it is overlaid by a strong paired pulse facilitation at

most inter-stimulus intervals (Madroñal et al., 2009). Future experiments (e.g. paired pulse experiments with low stimulus intensities (< 40 %) will investigate possible disturbances in paired pulse depression.

Field recordings in the occipital as well as the parietal cortex, revealed no differences in the amplitude of field responses to increasing stimulus intensities but the paired pulse paradigm revealed an increased paired pulse depression at longer inter-stimulus intervals (around 100 ms). Paired pulse depression in the range of around hundred milliseconds is mediated via GABA_B receptors (e.g. (Buonomano and Merzenich, 1998). Thus, these results suggest an increase in GABA_B-receptor mediated inhibition in *Slc4a10*^{-/-} mice which might be a compensatory change and could be related to the protection from fatal seizures *in vivo*.

Similar to Slc4a8, Slc4a10 apparently plays an important role in the regulation of neuronal activity. Its absence in the homozygous *Slc4a10*^{-/-} mouse results in an increased seizure threshold (Jacobs et al., 2008) whereas heterozygous human mutations have been associated with seizures (Gurnett et al., 2008; Krepischi et al., 2010). The predominant postsynaptic expression in pyramidal neurons in addition to the expression in GABAergic interneurons, complicate the interpretation of field potential results. For example the increased population spike amplitude could be due to a postsynaptic increase in excitability as well as a result of a decrease in inhibition. The transport capacity of Slc4a10 for HCO₃⁻ and Cl⁻ argues more in favour of an altered GABAergic inhibition, but this can only be revealed by single cell recordings, which allow the dissection of both systems. Interestingly, a relatively recent study by Dietrich and Morad (2010) showed that pharmacological inhibition of the Slc9a1/Nhe1, which localizes to the presynaptic site of GABAergic terminals (Jang et al., 2006), results in an altered postsynaptic response to GABA by modulation of the synaptic cleft pH. Deletion of Slc4a10 activity on either synapse site would result in an increased synaptic cleft pH, which than in turn would result in an inhibition of postsynaptic GABA_A receptors (Krishek et al., 1996). In contrast, an increase of cleft pH in glutamatergic synapses would accelerate the postsynaptic response to glutamate (Traynelis and Cull-Candy, 1990). Thus, besides the effect of a deregulation in intracellular pH, which could result in a diminished presynaptic vesicle release as described for *Slc4a8*^{-/-} mice, changes in extracellular pH could influence synaptic transmission and thereby the network excitability in toto (see Fig. 31B). To unravel the role of Slc4a10 our future plans include recordings of mIPSCs as well as mEPSCs and we are also

especially interested in measuring intracellular chloride concentrations, as those are of special importance for the GABAergic postsynaptic response.

Outlook

Although the relation between neuronal excitability and pH is known for a long time, a good understanding of active key players at the synaptic formations was missing. The results of this thesis along with results from other recent studies of our group (Hentschke et al., 2006; Jacobs et al., 2008) and other groups (Dietrich and Morad, 2010; Jang et al., 2006; Park et al., 2010) have advanced our understanding of the functional role of ion exchangers for synapse physiology and overall brain function considerably. It is very intriguing that all presynaptic ion exchangers identified so far increase pH_i . At the same time these ion transporters as well as the postsynaptic ones decrease extracellular pH, which seems to be of special importance at GABAergic synapses (see also Fig. 32). Yet, we are still lacking information on the exact (synaptic) localization and function of some ion exchangers, e.g. Slc4a3 or Slc4a7, and are still far from understanding the full machinery.

For a thorough understanding of the participant modulators, which is the basis of pharmacological targeting for clinical applications in the future, mouse models have been a valuable tool. Albeit good but mostly indirect evidence for Slc9a1 function in synaptic cleft acidification enabling efficient postsynaptic GABAergic inhibition has been described (Dietrich and Morad, 2010). The presented results suggest an additional contribution of Slc4a10 in this process. The severe epileptic phenotype in constitutive *Slc9a1* KO mice (Cox et al., 1997) and the lacking specificity of available inhibitors (e.g. lithium or amiloride) prompted us to generate a neuron-specific conditional mouse model for *Slc9a1*. The analysis will hopefully add or finally confirm the physiological role of Nhe1 for (GABAergic) synapse physiology.

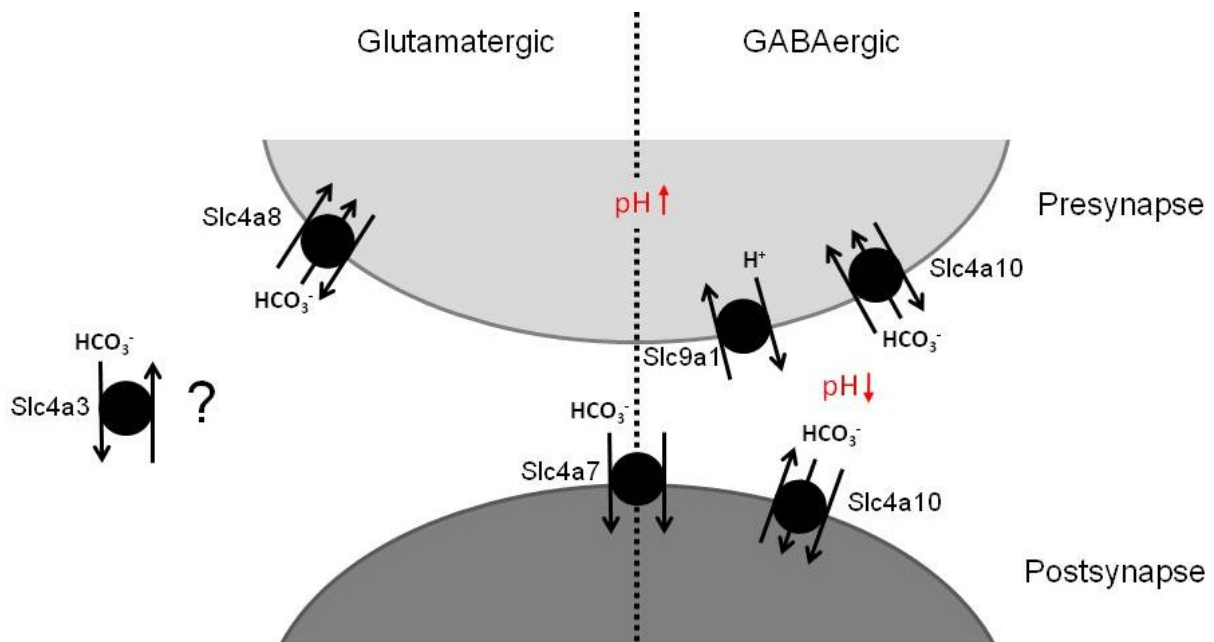


Figure 32. Model displaying ion exchangers possibly involved in synaptic pH regulation. The presynaptic localization of Slc4a8 at glutamatergic synapses and its importance for presynaptic pH and vesicle release was demonstrated by this thesis. Also, pre- and postsynaptic localization of Slc4a10 at mostly GABAergic synapses was shown. Indirect evidence suggests an important role of Slc9a1 at GABAergic presynapses, mostly for the synaptic cleft pH. The role of the postsynaptic Slc4a7 is not well understood. Whether or not Slc4a3 modulates synaptic activity remains unclear.

Both genes of interest investigated in this study, Slc4a8 and Slc4a10, transport Cl^- into the cell and consequently increase intracellular Cl^- . The present experiments mainly focussed on their pH regulatory capacity. However, alterations of the transmembrane Cl^- gradient can have major impact on neuronal excitability by determining the inhibitory GABA response at the postsynapse (Ben-Ari, 2002). Since the results of this study suggest that Slc4a10 deletion modulates synaptic inhibition it would be very interesting to analyze Cl^- concentration in *Slc4a10*^{-/-} neurons, e.g. by analysis of the GABA_A reversal potential (Kyrozi and Reichling, 1995).

It is well known that increased neuronal activity induces a sustained decrease in neuronal pH, which is probably due to activation of the $\text{Ca}^{2+}/\text{H}^+$ exchanger (Trapp et al., 1996), increased

production of metabolic acids (Chesler, 2003) and the short term incorporation of the vesicular H⁺-ATPase into the presynaptic membrane (Zhang et al., 2010). Therefore it would be interesting to analyse the role of Slc4a8 under conditions of increased neuronal activity in more detail. Electrophysiological experiments in which physiological and pathophysiological states of increased electrical activity are investigated, e.g. oscillations (Buzsáki, 2002; Colgin and Moser, 2010), different *in vitro* models of epilepsy (Jefferys, 2003; Kilb et al., 2007) or learning and memory (Neves et al., 2008) could both be of great interest. A better understanding of the role of Slc4a8 under these conditions is also essential for a better interpretation of the *in vivo* results, which showed a prolonged latency till seizure onset upon induction of epileptic seizures in the different models used (Kougioumtzes, 2006) and is a prerequisite for the potential use of specific Slc4a8 blockers as anticonvulsant treatment options in the future.

The strong expression of Slc4a8 protein in the S-LM, where the direct input from the perforant path terminates, suggests that *Slc4a8*^{-/-} slices show deficits in the mostly glutamatergic signal transduction within this region. The perforant path has been shown to modulate synaptic plasticity e.g. of the Schaffer collateral synapses and to be essential for the long-term memory consolidation (Remondes and Schuman, 2002, 2004). Although *Slc4a8*^{-/-} mice did not show deficits in spatial learning they showed some noticeable abnormalities when spatial memory was tested after 24 h (Kougioumtzes, 2006). Therefore, closer analysis of the perforant path and testing of long-term memory consolidation in the *Slc4a8*^{-/-} mice might elucidate the physiological role of Slc4a8 in more detail.

Conclusions

The Na⁺-dependent Cl⁻-HCO₃⁻ exchanger Slc4a8 is expressed in the renal cortex of mice and its expression is up-regulated under conditions of increased NaCl reabsorption. Mice devoid of Slc4a8 show no differences in urinary composition under standard feeding conditions and can adapt to Na⁺ restriction. Increased urinary aldosterone concentrations under Na⁺ restriction as well as an exaggerated response to acute thiazide treatment propose compensatory changes due to the absence of Slc4a8.

In the hippocampus, Slc4a8 is a key regulator for neuronal pH homeostasis. In the presence of extracellular bicarbonate steady state pH_i was decreased and acid recovery was impaired in Slc4a8 deficient neurons. Different approaches (immunohistochemistry, ultrastructural analysis and biochemical fractionation) showed that Slc4a8 protein localizes to excitatory presynaptic structures suggesting that Slc4a8 is essential to control presynaptic pH_i in principal neurons. Disruption of *Slc4a8* results in a pH dependent impairment of glutamatergic vesicle release *in vitro*, whereas GABA release is not affected. This finding and the decrease in hippocampal field excitability and altered synaptic plasticity *in vitro* are probably the functional correlate for the protection from seizures *in vivo*.

The closely related transporter Slc4a10 is expressed in pyramidal neurons, but also in interneurons. On the sub-cellular level, it localizes to the pre- and postsynaptic site of GABAergic synapses. First electrophysiological analysis showed a diminished field response in the pyramidal cell layer but not in the stratum radiatum of *Slc4a10*^{-/-} slices, suggesting alterations in the GABAergic inhibition.

Literature

- Aalkjaer, C., Frische, S., Leipziger, J., Nielsen, S., and Praetorius, J. (2004). Sodium coupled bicarbonate transporters in the kidney, an update. *Acta Physiol Scand* *181*, 505-512.
- Abuladze, N., Pushkin, A., Tatishchev, S., Newman, D., Sassani, P., and Kurtz, I. (2004). Expression and localization of rat NBC4c in liver and renal uroepithelium. *Am J Physiol Cell Physiol* *287*, C781-789.
- Agnati, L.F., Tinner, B., Staines, W.A., Väänänen, K., and Fuxe, K. (1995). On the cellular localization and distribution of carbonic anhydrase II immunoreactivity in the rat brain. *Brain Res* *676*, 10-24.
- al-Baldawi, N., and Abercrombie, R. (1992). Cytoplasmic hydrogen ion diffusion coefficient. *Biophys J* *61*, 1470-1479.
- Alberts, B., Johnson, A., Lewis, J., Raff, M., Roberts, K., and Walter, P. (2002). *Molecular Biology of the Cell*, 4 edn (New York: Garland Science).
- Albuquerque, E.X., Barnard, E.A., Porter, C.W., and Warnick, J.E. (1974). The density of acetylcholine receptors and their sensitivity in the postsynaptic membrane of muscle endplates. *Proc Natl Acad Sci U S A* *71*, 2818-2822.
- Allouis, M., Le Bouffant, F., Wilders, R., Pérez, D., Schott, J., Noireaud, J., Le Marec, H., Mérot, J., Escande, D., and Baró, I. (2006). 14-3-3 is a regulator of the cardiac voltage-gated sodium channel Nav1.5. *Circ Res* *98*, 1538-1546.
- Alper, S. (2009). Molecular physiology and genetics of Na⁺-independent SLC4 anion exchangers. *J Exp Biol* *212*, 1672-1683.
- Alper, S.L. (2006). Molecular physiology of SLC4 anion exchangers. *Exp Physiol* *91*, 153-161.
- Amaral, D.G., and Witter, M.P. (1989). The three-dimensional organization of the hippocampal formation: a review of anatomical data. *Neuroscience* *31*, 571-591.
- Aram, J., and Lodge, D. (1987). Epileptiform activity induced by alkalosis in rat neocortical slices: block by antagonists of N-methyl-D-aspartate. *Neurosci Lett* *83*, 345-350.
- Bai, F., and Witzmann, F. (2007). Synaptosome proteomics. *Subcell Biochem* *43*, 77-98.
- Baxter, K., and Church, J. (1996). Characterization of acid extrusion mechanisms in cultured fetal rat hippocampal neurones. *J Physiol* *493 (Pt 2)*, 457-470.
- Ben-Ari, Y. (2002). Excitatory actions of gaba during development: the nature of the nurture. *Nat Rev Neurosci* *3*, 728-739.
- Bennett, M.K., Calakos, N., and Scheller, R.H. (1992). Syntaxin: a synaptic protein implicated in docking of synaptic vesicles at presynaptic active zones. *Science* *257*, 255-259.
- Berg, J.M., Tymoczko, J.L., and Stryer, L. (2002). *Biochemistry*, 5 edn (W H Freeman).

- Bevensee, M., Cummins, T., Haddad, G., Boron, W., and Boyarsky, G. (1996). pH regulation in single CA1 neurons acutely isolated from the hippocampi of immature and mature rats. *J Physiol* 494 (Pt 2), 315-328.
- Blake-Palmer, K.G., and Karet, F.E. (2009). Cellular physiology of the renal H⁺ATPase. *Curr Opin Nephrol Hypertens* 18, 433-438.
- Bok, D., Galbraith, G., Lopez, I., Woodruff, M., Nusinowitz, S., BeltrandelRio, H., Huang, W., Zhao, S., Geske, R., Montgomery, C., *et al.* (2003). Blindness and auditory impairment caused by loss of the sodium bicarbonate cotransporter NBC3. *Nat Genet* 34, 313-319.
- Bonnet, U., Leniger, T., and Wiemann, M. (2000). Alteration of intracellular pH and activity of CA3-pyramidal cells in guinea pig hippocampal slices by inhibition of transmembrane acid extrusion. *Brain Res* 872, 116-124.
- Boron, W., Chen, L., and Parker, M. (2009). Modular structure of sodium-coupled bicarbonate transporters. *J Exp Biol* 212, 1697-1706.
- Boron, W., and De Weer, P. (1976). Intracellular pH transients in squid giant axons caused by CO₂, NH₃, and metabolic inhibitors. *J Gen Physiol* 67, 91-112.
- Boron, W.F., and Boulpaep, E.L. (1983). Intracellular pH regulation in the renal proximal tubule of the salamander. Basolateral HCO₃⁻ transport. *J Gen Physiol* 81, 53-94.
- Boron, W.F., and Boulpaep, E.L. (2003). *Medical Physiology, Vol 1* (Philadelphia: Elsevier Science).
- Boyarsky, G., Ganz, M., Sterzel, R., and Boron, W. (1988). pH regulation in single glomerular mesangial cells. I. Acid extrusion in absence and presence of HCO₃⁻. *Am J Physiol* 255, C844-856.
- Buch-Pedersen, M.J., Pedersen, B.P., Veierskov, B., Nissen, P., and Palmgren, M.G. (2009). Protons and how they are transported by proton pumps. *Pflugers Arch* 457, 573-579.
- Buonomano, D.V., and Merzenich, M.M. (1998). Net interaction between different forms of short-term synaptic plasticity and slow-IPSPs in the hippocampus and auditory cortex. *J Neurophysiol* 80, 1765-1774.
- Burwell, R.D. (2000). The parahippocampal region: corticocortical connectivity. *Ann N Y Acad Sci* 911, 25-42.
- Buzsáki, G. (2002). Theta oscillations in the hippocampus. *Neuron* 33, 325-340.
- Carlin, R., Grab, D., Cohen, R., and Siekevitz, P. (1980). Isolation and characterization of postsynaptic densities from various brain regions: enrichment of different types of postsynaptic densities. *J Cell Biol* 86, 831-845.
- Casey, J., Grinstein, S., and Orlowski, J. (2010). Sensors and regulators of intracellular pH. *Nat Rev Mol Cell Biol* 11, 50-61.
- Casey, J.R. (2006). Why bicarbonate? *Biochem Cell Biol* 84, 930-939.
- Chen, J., and Chesler, M. (1992). pH transients evoked by excitatory synaptic transmission are increased by inhibition of extracellular carbonic anhydrase. *Proc Natl Acad Sci U S A* 89, 7786-7790.

- Chen, L., Kelly, M., Parker, M., Bouyer, P., Gill, H., Felie, J., Davis, B., and Boron, W. (2008a). Expression and localization of Na-driven Cl-HCO₃⁻ exchanger (SLC4A8) in rodent CNS. *Neuroscience* *153*, 162-174.
- Chen, L.M., Kelly, M.L., Rojas, J.D., Parker, M.D., Gill, H.S., Davis, B.A., and Boron, W.F. (2008b). Use of a new polyclonal antibody to study the distribution and glycosylation of the sodium-coupled bicarbonate transporter NCBE in rodent brain. *Neuroscience* *151*, 374-385.
- Chen, X., Bezprozvanny, I., and Tsien, R. (1996). Molecular basis of proton block of L-type Ca²⁺ channels. *J Gen Physiol* *108*, 363-374.
- Chesler, M. (2003). Regulation and modulation of pH in the brain. *Physiol Rev* *83*, 1183-1221.
- Chesler, M., and Kaila, K. (1992). Modulation of pH by neuronal activity. *Trends Neurosci* *15*, 396-402.
- Chobanian, A.V., Bakris, G.L., Black, H.R., Cushman, W.C., Green, L.A., Izzo, J.L., Jones, D.W., Materson, B.J., Oparil, S., Wright, J.T., *et al.* (2003). Seventh report of the Joint National Committee on Prevention, Detection, Evaluation, and Treatment of High Blood Pressure. *Hypertension* *42*, 1206-1252.
- Codina, J., and DuBose, T.D. (2006). Molecular regulation and physiology of the H⁺,K⁺ -ATPases in kidney. *Semin Nephrol* *26*, 345-351.
- Colgin, L.L., and Moser, E.I. (2010). Gamma oscillations in the hippocampus. *Physiology (Bethesda)* *25*, 319-329.
- Cordat, E., and Casey, J. (2009). Bicarbonate transport in cell physiology and disease. *Biochem J* *417*, 423-439.
- Cox, G., Lutz, C., Yang, C., Biemesderfer, D., Bronson, R., Fu, A., Aronson, P., Noebels, J., and Frankel, W. (1997). Sodium/hydrogen exchanger gene defect in slow-wave epilepsy mutant mice. *Cell* *91*, 139-148.
- Dahl, L.K., and Love, R.A. (1954). Evidence for relationship between sodium (chloride) intake and human essential hypertension. *AMA Arch Intern Med* *94*, 525-531.
- Damkier, H., Aalkjaer, C., and Praetorius, J. (2010). Na⁺-dependent HCO₃⁻ import by the slc4a10 gene product involves Cl⁻ export. *J Biol Chem*.
- Damkier, H., Nielsen, S., and Praetorius, J. (2007). Molecular expression of SLC4-derived Na⁺-dependent anion transporters in selected human tissues. *Am J Physiol Regul Integr Comp Physiol* *293*, R2136-2146.
- Dietrich, C.J., and Morad, M. (2010). Synaptic Acidification Enhances GABA_A Signaling. *J Neurosci* *30*, 16044-16052.
- Dulla, C., Dobelis, P., Pearson, T., Frenguelli, B., Staley, K., and Masino, S. (2005). Adenosine and ATP link PCO₂ to cortical excitability via pH. *Neuron* *48*, 1011-1023.
- Dzhala, V.I., Talos, D.M., Sdrulla, D.A., Brumback, A.C., Mathews, G.C., Benke, T.A., Delpire, E., Jensen, F.E., and Staley, K.J. (2005). NKCC1 transporter facilitates seizures in the developing brain. *Nat Med* *11*, 1205-1213.

- Eisner, D.A., Kenning, N.A., O'Neill, S.C., Pocock, G., Richards, C.D., and Valdeolmillos, M. (1989). A novel method for absolute calibration of intracellular pH indicators. *Pflugers Arch* 413, 553-558.
- Eladari, D., and Hübner, C.A. (2011). Novel mechanisms for NaCl reabsorption in the collecting duct. *Curr Opin Nephrol Hypertens*.
- Ellison, D.H., and Loffing, J. (2009). Thiazide effects and adverse effects: insights from molecular genetics. *Hypertension* 54, 196-202.
- Emptage, N., Reid, C., and Fine, A. (2001). Calcium stores in hippocampal synaptic boutons mediate short-term plasticity, store-operated Ca²⁺ entry, and spontaneous transmitter release. *Neuron* 29, 197-208.
- Everett, L.A., Glaser, B., Beck, J.C., Idol, J.R., Buchs, A., Heyman, M., Adawi, F., Hazani, E., Nassir, E., Baxevanis, A.D., *et al.* (1997). Pendred syndrome is caused by mutations in a putative sulphate transporter gene (PDS). *Nat Genet* 17, 411-422.
- Feng, J., Chi, P., Blanpied, T., Xu, Y., Magarinos, A., Ferreira, A., Takahashi, R., Kao, H., McEwen, B., Ryan, T., *et al.* (2002). Regulation of neurotransmitter release by synapsin III. *J Neurosci* 22, 4372-4380.
- Franco, M., Sanchez-Lozada, L.G., Bautista, R., Johnson, R.J., and Rodriguez-Iturbe, B. (2008). Pathophysiology of salt-sensitive hypertension: a new scope of an old problem. *Blood Purif* 26, 45-48.
- Frömter, E. (1988). Mechanisms and regulation of ion transport in the renal collecting duct. *Comp Biochem Physiol A Comp Physiol* 90, 701-707.
- Gaffield, M.A., and Betz, W.J. (2006). Imaging synaptic vesicle exocytosis and endocytosis with FM dyes. *Nat Protoc* 1, 2916-2921.
- Gilmour, K.M. (2010). Perspectives on carbonic anhydrase. *Comp Biochem Physiol A Mol Integr Physiol* 157, 193-197.
- Glover, M., Zuber, A.M., and O'Shaughnessy, K.M. (2011). Hypertension, dietary salt intake, and the role of the thiazide-sensitive sodium chloride transporter NCCT. *Cardiovasc Ther* 29, 68-76.
- Gluck, S.L., Underhill, D.M., Iyori, M., Holliday, L.S., Kostrominova, T.Y., and Lee, B.S. (1996). Physiology and biochemistry of the kidney vacuolar H⁺-ATPase. *Annu Rev Physiol* 58, 427-445.
- Greger, R. (2000). Physiology of renal sodium transport. *Am J Med Sci* 319, 51-62.
- Grichtchenko, I., Choi, I., Zhong, X., Bray-Ward, P., Russell, J., and Boron, W. (2001). Cloning, characterization, and chromosomal mapping of a human electroneutral Na(+)-driven Cl-HCO₃ exchanger. *J Biol Chem* 276, 8358-8363.
- Grynkiewicz, G., Poenie, M., and Tsien, R.Y. (1985). A new generation of Ca²⁺ indicators with greatly improved fluorescence properties. *J Biol Chem* 260, 3440-3450.
- Gu, X., Yao, H., and Haddad, G. (2001). Increased neuronal excitability and seizures in the Na(+)/H(+) exchanger null mutant mouse. *Am J Physiol Cell Physiol* 281, C496-503.

- Gurnett, C.A., Veile, R., Zempel, J., Blackburn, L., Lovett, M., and Bowcock, A. (2008). Disruption of sodium bicarbonate transporter SLC4A10 in a patient with complex partial epilepsy and mental retardation. *Arch Neurol* 65, 550-553.
- Guyton, A.C., Coleman, T.G., Cowley, A.V., Scheel, K.W., Manning, R.D., and Norman, R.A. (1972). Arterial pressure regulation. Overriding dominance of the kidneys in long-term regulation and in hypertension. *Am J Med* 52, 584-594.
- Guyton, A.C., Manning, R.D., Hall, J.E., Norman, R.A., Young, D.B., and Pan, Y.J. (1984). The pathogenic role of the kidney. *J Cardiovasc Pharmacol* 6 *Suppl 1*, S151-161.
- Halestrap, A.P., and Meredith, D. (2004). The SLC16 gene family-from monocarboxylate transporters (MCTs) to aromatic amino acid transporters and beyond. *Pflugers Arch* 447, 619-628.
- Hentschke, M., Wiemann, M., Hentschke, S., Kurth, I., Hermans-Borgmeyer, I., Seidenbecher, T., Jentsch, T., Gal, A., and Hübner, C. (2006). Mice with a targeted disruption of the Cl⁻/HCO₃⁻ exchanger AE3 display a reduced seizure threshold. *Mol Cell Biol* 26, 182-191.
- Hertz, L., and Dienel, G. (2005). Lactate transport and transporters: general principles and functional roles in brain cells. *J Neurosci Res* 79, 11-18.
- Hirtz, D., Thurman, D.J., Gwinn-Hardy, K., Mohamed, M., Chaudhuri, A.R., and Zalutsky, R. (2007). How common are the "common" neurological disorders? *Neurology* 68, 326-337.
- Hua, Y., Sinha, R., Martineau, M., Kahms, M., and Klingauf, J. (2010). A common origin of synaptic vesicles undergoing evoked and spontaneous fusion. *Nat Neurosci* 13, 1451-1453.
- Hummler, E. (2003). Epithelial sodium channel, salt intake, and hypertension. *Curr Hypertens Rep* 5, 11-18.
- Höglund, P., Haila, S., Socha, J., Tomaszewski, L., Saarialho-Kere, U., Karjalainen-Lindsberg, M.L., Airola, K., Holmberg, C., de la Chapelle, A., and Kere, J. (1996). Mutations of the Down-regulated in adenoma (DRA) gene cause congenital chloride diarrhoea. *Nat Genet* 14, 316-319.
- Hübner, C., Stein, V., Hermans-Borgmeyer, I., Meyer, T., Ballanyi, K., and Jentsch, T. (2001). Disruption of KCC2 reveals an essential role of K-Cl cotransport already in early synaptic inhibition. *Neuron* 30, 515-524.
- Hübner, C.A., Hentschke, M., Jacobs, S., and Hermans-Borgmeyer, I. (2004). Expression of the sodium-driven chloride bicarbonate exchanger NCBE during prenatal mouse development. *Gene Expr Patterns* 5, 219-223.
- Jacobs, S., Ruusuvuori, E., Sipilä, S., Haapanen, A., Damkier, H., Kurth, I., Hentschke, M., Schweizer, M., Rudhard, Y., Laatikainen, L., *et al.* (2008). Mice with targeted Slc4a10 gene disruption have small brain ventricles and show reduced neuronal excitability. *Proc Natl Acad Sci U S A* 105, 311-316.
- Jang, I., Brodwick, M., Wang, Z., Jeong, H., Choi, B., and Akaike, N. (2006). The Na⁽⁺⁾/H⁽⁺⁾ exchanger is a major pH regulator in GABAergic presynaptic nerve terminals synapsing onto rat CA3 pyramidal neurons. *J Neurochem* 99, 1224-1236.
- Jefferys, J.G. (2003). Models and mechanisms of experimental epilepsies. *Epilepsia* 44 *Suppl 12*, 44-50.

- Kaech, S., and Banker, G. (2006). Culturing hippocampal neurons. *Nat Protoc* 1, 2406-2415.
- Kaila, K., and Voipio, J. (1987). Postsynaptic fall in intracellular pH induced by GABA-activated bicarbonate conductance. *Nature* 330, 163-165.
- Karmazyn, M., Gan, X.T., Humphreys, R.A., Yoshida, H., and Kusumoto, K. (1999). The myocardial Na(+)-H(+) exchange: structure, regulation, and its role in heart disease. *Circ Res* 85, 777-786.
- Katz, B., and Miledi, R. (1968). The role of calcium in neuromuscular facilitation. *J Physiol* 195, 481-492.
- Kearney, P.M., Whelton, M., Reynolds, K., Muntner, P., Whelton, P.K., and He, J. (2005). Global burden of hypertension: analysis of worldwide data. *Lancet* 365, 217-223.
- Kearney, P.M., Whelton, M., Reynolds, K., Whelton, P.K., and He, J. (2004). Worldwide prevalence of hypertension: a systematic review. *J Hypertens* 22, 11-19.
- Kilb, W., Sinning, A., and Luhmann, H.J. (2007). Model-specific effects of bumetanide on epileptiform activity in the in-vitro intact hippocampus of the newborn mouse. *Neuropharmacology* 53, 524-533.
- Kim, G.H., Masilamani, S., Turner, R., Mitchell, C., Wade, J.B., and Knepper, M.A. (1998). The thiazide-sensitive Na-Cl cotransporter is an aldosterone-induced protein. *Proc Natl Acad Sci U S A* 95, 14552-14557.
- Kiss, L., and Korn, S.J. (1999). Modulation of N-type Ca²⁺ channels by intracellular pH in chick sensory neurons. *J Neurophysiol* 81, 1839-1847.
- Klößner, U., and Isenberg, G. (1994). Calcium channel current of vascular smooth muscle cells: extracellular protons modulate gating and single channel conductance. *J Gen Physiol* 103, 665-678.
- Ko, S.B., Luo, X., Hager, H., Rojek, A., Choi, J.Y., Licht, C., Suzuki, M., Muallem, S., Nielsen, S., and Ishibashi, K. (2002). AE4 is a DIDS-sensitive Cl(-)/HCO(-)(3) exchanger in the basolateral membrane of the renal CCD and the SMG duct. *Am J Physiol Cell Physiol* 283, C1206-1218.
- Konstas, A.A., Koch, J.P., Tucker, S.J., and Korbmayer, C. (2002). Cystic fibrosis transmembrane conductance regulator-dependent up-regulation of Kir1.1 (ROMK) renal K⁺ channels by the epithelial sodium channel. *J Biol Chem* 277, 25377-25384.
- Kopito, R.R., Lee, B.S., Simmons, D.M., Lindsey, A.E., Morgans, C.W., and Schneider, K. (1989). Regulation of intracellular pH by a neuronal homolog of the erythrocyte anion exchanger. *Cell* 59, 927-937.
- Kougioumtzes, A. (2006). Herstellung und Charakterisierung einer KO-Maus für einen Natrium-abhängigen Anionenaustauscher. In Fakultät für Mathematik, Informatik und Naturwissenschaft (Hamburg, Universität Hamburg), p. 131.
- Krepischi, A.C., Knijnenburg, J., Bertola, D.R., Kim, C.A., Pearson, P.L., Bijlsma, E., Szuhai, K., Kok, F., Vianna-Morgante, A.M., and Rosenberg, C. (2010). Two distinct regions in 2q24.2-q24.3 associated with idiopathic epilepsy. *Epilepsia* 51, 2457-2460.

- Krishek, B.J., Amato, A., Connolly, C.N., Moss, S.J., and Smart, T.G. (1996). Proton sensitivity of the GABA(A) receptor is associated with the receptor subunit composition. *J Physiol* 492 (Pt 2), 431-443.
- Kyrozis, A., and Reichling, D.B. (1995). Perforated-patch recording with gramicidin avoids artifactual changes in intracellular chloride concentration. *J Neurosci Methods* 57, 27-35.
- Langley, O.K., Ghandour, M.S., Vincendon, G., and Gombos, G. (1980). Carbonic anhydrase: an ultrastructural study in rat cerebellum. *Histochem J* 12, 473-483.
- Lee, J., Taira, T., Pihlaja, P., Ransom, B., and Kaila, K. (1996). Effects of CO₂ on excitatory transmission apparently caused by changes in intracellular pH in the rat hippocampal slice. *Brain Res* 706, 210-216.
- Lennox, W. (1928). The effect on epileptic seizures of varying the composition of respired air. (*Journal of Clinical Investigations*), pp. 23-24.
- Leviel, F., Hübner, C., Houillier, P., Morla, L., El Moghrabi, S., Brideau, G., Hatim, H., Parker, M., Kurth, I., Kougioumtzes, A., *et al.* (2010). The Na⁺-dependent chloride-bicarbonate exchanger SLC4A8 mediates an electroneutral Na⁺ reabsorption process in the renal cortical collecting ducts of mice. *J Clin Invest* 120, 1627-1635.
- Liebmann, L., Karst, H., and Joëls, M. (2009). Effects of corticosterone and the beta-agonist isoproterenol on glutamate receptor-mediated synaptic currents in the rat basolateral amygdala. *Eur J Neurosci* 30, 800-807.
- Lingrel, J.B. (1992). Na,K-ATPase: isoform structure, function, and expression. *J Bioenerg Biomembr* 24, 263-270.
- Livak, K.J., and Schmittgen, T.D. (2001). Analysis of relative gene expression data using real-time quantitative PCR and the 2(-Delta Delta C(T)) Method. *Methods* 25, 402-408.
- Lodish, H., Berk, A., Zipursky, S.L., Matsudaira, P., Baltimore, D., and Darnell, J. (2000). *Molecular Cell Biology*, 4th edn (New York: W.H. Freeman and Company).
- Loffing, J., Zecevic, M., Féraillé, E., Kaissling, B., Asher, C., Rossier, B.C., Firestone, G.L., Pearce, D., and Verrey, F. (2001). Aldosterone induces rapid apical translocation of ENaC in early portion of renal collecting system: possible role of SGK. *Am J Physiol Renal Physiol* 280, F675-682.
- Loo, L.S., and McNamara, J.O. (2006). Impaired volume regulation is the mechanism of excitotoxic sensitization to complement. *J Neurosci* 26, 10177-10187.
- Luo, J., and Sun, D. (2007). Physiology and pathophysiology of Na(+)/H(+) exchange isoform 1 in the central nervous system. *Curr Neurovasc Res* 4, 205-215.
- Ma, J., Fill, M., Knudson, C., Campbell, K., and Coronado, R. (1988). Ryanodine receptor of skeletal muscle is a gap junction-type channel. *Science* 242, 99-102.
- Madroñal, N., Gruart, A., and Delgado-García, J.M. (2009). Differing presynaptic contributions to LTP and associative learning in behaving mice. *Front Behav Neurosci* 3, 7.
- Malo, M.E., and Fliegel, L. (2006). Physiological role and regulation of the Na⁺/H⁺ exchanger. *Can J Physiol Pharmacol* 84, 1081-1095.
- Mann, E.O., and Paulsen, O. (2007). Role of GABAergic inhibition in hippocampal network oscillations. *Trends Neurosci* 30, 343-349.

- Markovich, D. (2001). Physiological roles and regulation of mammalian sulfate transporters. *Physiol Rev* 81, 1499-1533.
- Mathews, G.C., and Diamond, J.S. (2003). Neuronal glutamate uptake Contributes to GABA synthesis and inhibitory synaptic strength. *J Neurosci* 23, 2040-2048.
- Maunsbach, A.B., Vorum, H., Kwon, T.H., Nielsen, S., Simonsen, B., Choi, I., Schmitt, B.M., Boron, W.F., and Aalkjaer, C. (2000). Immunoelectron microscopic localization of the electrogenic Na/HCO₃ cotransporter in rat and ambystoma kidney. *J Am Soc Nephrol* 11, 2179-2189.
- Maycox, P., Deckwerth, T., Hell, J., and Jahn, R. (1988). Glutamate uptake by brain synaptic vesicles. Energy dependence of transport and functional reconstitution in proteoliposomes. *J Biol Chem* 263, 15423-15428.
- Megías, M., Emri, Z., Freund, T.F., and Gulyás, A.I. (2001). Total number and distribution of inhibitory and excitatory synapses on hippocampal CA1 pyramidal cells. *Neuroscience* 102, 527-540.
- Meneton, P., Jeunemaitre, X., de Wardener, H.E., and MacGregor, G.A. (2005). Links between dietary salt intake, renal salt handling, blood pressure, and cardiovascular diseases. *Physiol Rev* 85, 679-715.
- Mitchell, W., and Grubbs, R. (1956). Inhibition of audiogenic seizures by carbon dioxide. *Science* 123, 223-224.
- Mrowiec, T., and Schwappach, B. (2006). 14-3-3 proteins in membrane protein transport. *Biol Chem* 387, 1227-1236.
- Mulkey, R., and Zucker, R. (1992). Posttetanic potentiation at the crayfish neuromuscular junction is dependent on both intracellular calcium and sodium ion accumulation. *J Neurosci* 12, 4327-4336.
- Müller, J. (1995). Aldosterone: the minority hormone of the adrenal cortex. *Steroids* 60, 2-9.
- Neves, G., Cooke, S.F., and Bliss, T.V. (2008). Synaptic plasticity, memory and the hippocampus: a neural network approach to causality. *Nat Rev Neurosci* 9, 65-75.
- Nyman, P.O. (1961). Purification and properties of carbonic anhydrase from human erythrocytes. *Biochim Biophys Acta* 52, 1-12.
- Oyler, G.A., Higgins, G.A., Hart, R.A., Battenberg, E., Billingsley, M., Bloom, F.E., and Wilson, M.C. (1989). The identification of a novel synaptosomal-associated protein, SNAP-25, differentially expressed by neuronal subpopulations. *J Cell Biol* 109, 3039-3052.
- Park, H., Rajbhandari, I., Yang, H., Lee, S., Cucoranu, D., Cooper, D., Klein, J., Sands, J., and Choi, I. (2010). Neuronal expression of sodium/bicarbonate cotransporter NBCn1 (SLC4A7) and its response to chronic metabolic acidosis. *Am J Physiol Cell Physiol* 298, C1018-1028.
- Park, M., Li, Q., Shcheynikov, N., Zeng, W., and Muallem, S. (2004). NaBC1 is a ubiquitous electrogenic Na⁺-coupled borate transporter essential for cellular boron homeostasis and cell growth and proliferation. *Mol Cell* 16, 331-341.
- Parker, M., Bouyer, P., Daly, C., and Boron, W. (2008a). Cloning and characterization of novel human SLC4A8 gene products encoding Na⁺-driven Cl⁻/HCO₃⁻ exchanger variants NDCBE-A, -C, and -D. *Physiol Genomics* 34, 265-276.

- Parker, M.D., Musa-Aziz, R., Rojas, J.D., Choi, I., Daly, C.M., and Boron, W.F. (2008b). Characterization of human SLC4A10 as an electroneutral Na/HCO₃ cotransporter (NBCn2) with Cl⁻ self-exchange activity. *J Biol Chem* 283, 12777-12788.
- Parkkila, S., Parkkila, A.K., Rajaniemi, H., Shah, G.N., Grubb, J.H., Waheed, A., and Sly, W.S. (2001). Expression of membrane-associated carbonic anhydrase XIV on neurons and axons in mouse and human brain. *Proc Natl Acad Sci U S A* 98, 1918-1923.
- Pierdomenico, S.D., Di Nicola, M., Esposito, A.L., Di Mascio, R., Ballone, E., Lapenna, D., and Cuccurullo, F. (2009). Prognostic value of different indices of blood pressure variability in hypertensive patients. *Am J Hypertens* 22, 842-847.
- Praetorius, J., Kim, Y.H., Bouzinova, E.V., Frische, S., Rojek, A., Aalkjaer, C., and Nielsen, S. (2004a). NBCn1 is a basolateral Na⁺-HCO₃⁻ cotransporter in rat kidney inner medullary collecting ducts. *Am J Physiol Renal Physiol* 286, F903-912.
- Praetorius, J., Nejsum, L.N., and Nielsen, S. (2004b). A SCL4A10 gene product maps selectively to the basolateral plasma membrane of choroid plexus epithelial cells. *Am J Physiol Cell Physiol* 286, C601-610.
- Prod'hom, B., Pietrobon, D., and Hess, P. (1987). Direct measurement of proton transfer rates to a group controlling the dihydropyridine-sensitive Ca²⁺ channel. *Nature* 329, 243-246.
- Purves, D., Augustine, G.J., Fitzpatrick, D., Katz, L.C., LaMantia, A.-S., McNamara, J.O., and Williams, S.M. (2001). *Neuroscience*, 2 edn (Sunderland: Sinauer Associates).
- Pushkin, A., Abuladze, N., Lee, I., Newman, D., Hwang, J., and Kurtz, I. (1999a). Cloning, tissue distribution, genomic organization, and functional characterization of NBC3, a new member of the sodium bicarbonate cotransporter family. *J Biol Chem* 274, 16569-16575.
- Pushkin, A., Yip, K.P., Clark, I., Abuladze, N., Kwon, T.H., Tsuruoka, S., Schwartz, G.J., Nielsen, S., and Kurtz, I. (1999b). NBC3 expression in rabbit collecting duct: colocalization with vacuolar H⁺-ATPase. *Am J Physiol* 277, F974-981.
- Quentin, F., Chambrey, R., Trinh-Trang-Tan, M.M., Fysekidis, M., Cambillau, M., Paillard, M., Aronson, P.S., and Eladari, D. (2004). The Cl⁻/HCO₃⁻ exchanger pendrin in the rat kidney is regulated in response to chronic alterations in chloride balance. *Am J Physiol Renal Physiol* 287, F1179-1188.
- Remondes, M., and Schuman, E. (2002). Direct cortical input modulates plasticity and spiking in CA1 pyramidal neurons. *Nature* 416, 736-740.
- Remondes, M., and Schuman, E. (2004). Role for a cortical input to hippocampal area CA1 in the consolidation of a long-term memory. *Nature* 431, 699-703.
- Reuter, H., and Porzig, H. (1995). Localization and functional significance of the Na⁺/Ca²⁺ exchanger in presynaptic boutons of hippocampal cells in culture. *Neuron* 15, 1077-1084.
- Rink, T.J., Tsien, R.Y., and Pozzan, T. (1982). Cytoplasmic pH and free Mg²⁺ in lymphocytes. *J Cell Biol* 95, 189-196.
- Rocha, M., Crockett, D., Wong, L., Richardson, J., and Sonsalla, P. (2008). Na(+)/H(+) exchanger inhibition modifies dopamine neurotransmission during normal and metabolic stress conditions. *J Neurochem* 106, 231-243.

- Rollenhagen, A., and Lübke, J.H. (2010). The mossy fiber bouton: the "common" or the "unique" synapse? *Front Synaptic Neurosci* 2, 2.
- Romero, M., Henry, D., Nelson, S., Harte, P., Dillon, A., and Sciortino, C. (2000). Cloning and characterization of a Na⁺-driven anion exchanger (NDAE1). A new bicarbonate transporter. *J Biol Chem* 275, 24552-24559.
- Romero, M.F., Fulton, C.M., and Boron, W.F. (2004). The SLC4 family of HCO₃⁻ transporters. *Pflugers Arch* 447, 495-509.
- Romero, M.F., Hediger, M.A., Boulpaep, E.L., and Boron, W.F. (1997). Expression cloning and characterization of a renal electrogenic Na⁺/HCO₃⁻ cotransporter. *Nature* 387, 409-413.
- Roos, A., and Boron, W.F. (1981). Intracellular pH. *Physiol Rev* 61, 296-434.
- Rozansky, D.J. (2006). The role of aldosterone in renal sodium transport. *Semin Nephrol* 26, 173-181.
- Russell, J., and Boron, W. (1976). Role of chloride transport in regulation of intracellular pH. *Nature* 264, 73-74.
- Ruusuvuori, E., Li, H., Huttu, K., Palva, J.M., Smirnov, S., Rivera, C., Kaila, K., and Voipio, J. (2004). Carbonic anhydrase isoform VII acts as a molecular switch in the development of synchronous gamma-frequency firing of hippocampal CA1 pyramidal cells. *J Neurosci* 24, 2699-2707.
- Saggau, P., Gray, R., and Dani, J.A. (1999). Optical measurements of calcium signals in mammalian presynaptic terminals. *Methods Enzymol* 294, 3-19.
- Schneggenburger, R., and Neher, E. (2000). Intracellular calcium dependence of transmitter release rates at a fast central synapse. *Nature* 406, 889-893.
- Schuchmann, S., Schmitz, D., Rivera, C., Vanhatalo, S., Salmen, B., Mackie, K., Sipilä, S., Voipio, J., and Kaila, K. (2006). Experimental febrile seizures are precipitated by a hyperthermia-induced respiratory alkalosis. *Nat Med* 12, 817-823.
- Schwiening, C., and Boron, W. (1994). Regulation of intracellular pH in pyramidal neurones from the rat hippocampus by Na(+)-dependent Cl(-)-HCO₃⁻ exchange. *J Physiol* 475, 59-67.
- Schwiening, C., and Willoughby, D. (2002). Depolarization-induced pH microdomains and their relationship to calcium transients in isolated snail neurones. *J Physiol* 538, 371-382.
- Schwiening, C.J., Kennedy, H.J., and Thomas, R.C. (1993). Calcium-hydrogen exchange by the plasma membrane Ca-ATPase of voltage-clamped snail neurons. *Proc Biol Sci* 253, 285-289.
- Shankar, S.S., and Brater, D.C. (2003). Loop diuretics: from the Na-K-2Cl transporter to clinical use. *Am J Physiol Renal Physiol* 284, F11-21.
- Shinnar, S., and Glauser, T.A. (2002). Febrile seizures. *J Child Neurol* 17 Suppl 1, S44-52.
- Somjen, G., and Tombaugh, G. (1998). pH modulation of neuronal excitability and central nervous system function. In *pH and brain function*, K. Kaila, and R. BR, eds. (New York: John Wiley), pp. 373-393.
- Sterling, D., and Casey, J.R. (2002). Bicarbonate transport proteins. *Biochem Cell Biol* 80, 483-497.

- Stewart, A., Boyd, C., and Vaughan-Jones, R. (1999). A novel role for carbonic anhydrase: cytoplasmic pH gradient dissipation in mouse small intestinal enterocytes. *J Physiol* 516 (Pt 1), 209-217.
- Supuran, C. (2008). Carbonic anhydrases--an overview. *Curr Pharm Des* 14, 603-614.
- Terada, Y., and Knepper, M.A. (1990). Thiazide-sensitive NaCl absorption in rat cortical collecting duct. *Am J Physiol* 259, F519-528.
- Thomas, J.A., Buchsbaum, R.N., Zimniak, A., and Racker, E. (1979). Intracellular pH measurements in Ehrlich ascites tumor cells utilizing spectroscopic probes generated in situ. *Biochemistry* 18, 2210-2218.
- Thomas, R. (1976). The effect of carbon dioxide on the intracellular pH and buffering power of snail neurones. *J Physiol* 255, 715-735.
- Tolner, E.A., Hochman, D.W., Hassinen, P., Otáhal, J., Gaily, E., Haglund, M.M., Kubová, H., Schuchmann, S., Vanhatalo, S., and Kaila, K. (2011). Five percent CO₂ is a potent, fast-acting inhalation anticonvulsant. *Epilepsia* 52, 104-114.
- Tombaugh, G., and Somjen, G. (1996). Effects of extracellular pH on voltage-gated Na⁺, K⁺ and Ca²⁺ currents in isolated rat CA1 neurons. *J Physiol* 493 (Pt 3), 719-732.
- Tombaugh, G., and Somjen, G. (1997). Differential sensitivity to intracellular pH among high- and low-threshold Ca²⁺ currents in isolated rat CA1 neurons. *J Neurophysiol* 77, 639-653.
- Tomita, K., Pisano, J.J., and Knepper, M.A. (1985). Control of sodium and potassium transport in the cortical collecting duct of the rat. Effects of bradykinin, vasopressin, and deoxycorticosterone. *J Clin Invest* 76, 132-136.
- Tong, C., and Chesler, M. (1999). Activity-evoked extracellular pH shifts in slices of rat dorsal lateral geniculate nucleus. *Brain Res* 815, 373-381.
- Tong, C.K., Brion, L.P., Suarez, C., and Chesler, M. (2000). Interstitial carbonic anhydrase (CA) activity in brain is attributable to membrane-bound CA type IV. *J Neurosci* 20, 8247-8253.
- Trapp, S., Lückermann, M., Kaila, K., and Ballanyi, K. (1996). Acidosis of hippocampal neurones mediated by a plasmalemmal Ca²⁺/H⁺ pump. *Neuroreport* 7, 2000-2004.
- Traynelis, S., and Cull-Candy, S. (1990). Proton inhibition of N-methyl-D-aspartate receptors in cerebellar neurons. *Nature* 345, 347-350.
- Tsukioka, M., Iino, M., and Endo, M. (1994). pH dependence of inositol 1,4,5-trisphosphate-induced Ca²⁺ release in permeabilized smooth muscle cells of the guinea-pig. *J Physiol* 475, 369-375.
- Tóth, Z.E., and Mezey, E. (2007). Simultaneous visualization of multiple antigens with tyramide signal amplification using antibodies from the same species. *J Histochem Cytochem* 55, 545-554.
- van Strien, N.M., Cappaert, N.L., and Witter, M.P. (2009). The anatomy of memory: an interactive overview of the parahippocampal-hippocampal network. *Nat Rev Neurosci* 10, 272-282.

- Verrey, F. (2001). Sodium reabsorption in aldosterone-sensitive distal nephron: news and contributions from genetically engineered animals. *Curr Opin Nephrol Hypertens* *10*, 39-47.
- Wagner, C.A., Devuyst, O., Bourgeois, S., and Mohebbi, N. (2009). Regulated acid-base transport in the collecting duct. *Pflugers Arch* *458*, 137-156.
- Wagner, C.A., and Geibel, J.P. (2002). Acid-base transport in the collecting duct. *J Nephrol* *15 Suppl 5*, S112-127.
- Walker, C., and Peacock, J. (1981). Development of GABAergic function of dissociated hippocampal cultures from fetal mice. *Brain Res* *254*, 541-555.
- Wang, C., Yano, H., Nagashima, K., and Seino, S. (2000). The Na⁺-driven Cl⁻/HCO₃⁻ exchanger. Cloning, tissue distribution, and functional characterization. *J Biol Chem* *275*, 35486-35490.
- Wang, Z., Conforti, L., Petrovic, S., Amlal, H., Burnham, C.E., and Soleimani, M. (2001). Mouse Na⁺: HCO₃⁻ cotransporter isoform NBC-3 (kNBC-3): cloning, expression, and renal distribution. *Kidney Int* *59*, 1405-1414.
- Westermann, M., Steiniger, F., and Richter, W. (2005). Belt-like localisation of caveolin in deep caveolae and its re-distribution after cholesterol depletion. *Histochem Cell Biol* *123*, 613-620.
- Wu, L.G., and Saggau, P. (1994). Presynaptic calcium is increased during normal synaptic transmission and paired-pulse facilitation, but not in long-term potentiation in area CA1 of hippocampus. *J Neurosci* *14*, 645-654.
- Xia, Y., Zhao, P., Xue, J., Gu, X., Sun, X., Yao, H., and Haddad, G. (2003). Na⁺ channel expression and neuronal function in the Na⁺/H⁺ exchanger 1 null mutant mouse. *J Neurophysiol* *89*, 229-236.
- Xiong, Z., Saggau, P., and Stringer, J. (2000). Activity-dependent intracellular acidification correlates with the duration of seizure activity. *J Neurosci* *20*, 1290-1296.
- Yao, H., Ma, E., Gu, X., and Haddad, G. (1999). Intracellular pH regulation of CA1 neurons in Na(+)/H(+) isoform 1 mutant mice. *J Clin Invest* *104*, 637-645.
- Zhan, R., Fujiwara, N., Tanaka, E., and Shimoji, K. (1998). Intracellular acidification induced by membrane depolarization in rat hippocampal slices: roles of intracellular Ca²⁺ and glycolysis. *Brain Res* *780*, 86-94.
- Zhang, Z., Nguyen, K.T., Barrett, E.F., and David, G. (2010). Vesicular ATPase inserted into the plasma membrane of motor terminals by exocytosis alkalinizes cytosolic pH and facilitates endocytosis. *Neuron* *68*, 1097-1108.
- Zhou, W., and Jones, S. (1996). The effects of external pH on calcium channel currents in bullfrog sympathetic neurons. *Biophys J* *70*, 1326-1334.
- Ziemann, A.E., Schnizler, M.K., Albert, G.W., Severson, M.A., Howard, M.A., Welsh, M.J., and Wemmie, J.A. (2008). Seizure termination by acidosis depends on ASIC1a. *Nat Neurosci* *11*, 816-822.

Appendix

Curriculum Vitae

Personal details:

Name: Anne Sinning **Adresse:** Kieserstr. 6
07749 Jena

Date of birth: 10.05.1983 **Telephone:** 0176 62075572

Place of birth: Kassel

Nationality: German **Email:** A.sinning@gmx.de

Education :

Academic studies

February 2008-August 2011

PhD thesis

Institute for Clinical Chemistry/ Human Genetics
University Hospital Jena

April 2006 – November 2007

Master of sciences in

Experimental and Clinical Neurosciences

University Regensburg / Elitenetwork Bavaria

Masterthesis:

*Calcium as a mediator between membrane and
genes plays a key role in circadian clock functions*

Department Neurophysiology

Leiden University Medical Center (Niederlande)

Final degree: Very good (1.2)

November 2005 – March 2006

Biomedicine

Gutenberg University Mainz

April 2003 – August 2005

Bachelor of sciences in *Molecular Biology*

Gutenberg University Mainz

Bachelor thesis:

Analysis of the expression and activation of protein kinases JNK and Akt after radiation of squamous head and neck cancer

University Hospital Mainz

Final degree: Very good (1.4)

Secondary education

1993-2002:

Abitur

Jacob-Grimm School Rotenburg/Fulda

Final degree: 1.9

Work experience abroad

Juli 2002- September 2002

Work as guest and children courier for Eurocamps (UK)
in La Mole (France)

October 2002- April 2003

Au-pair in Florida (USA)

Publications

Leviel F*, Hübner C*, Houillier P, Morla L, El Moghrabi S, Brideau G, Hatim H, Parker M, Kurth I, Kougioumtzes A, **Sinning A**, Pech V, Riemondy K, Miller R, Hummler E, Shull G, Aronson P, Doucet A, Wall S, Chambrey R, Eladari D (2010)

The Na⁺-dependent chloride-bicarbonate exchanger Slc4a8 mediates an electroneutral Na⁺ reabsorption process in the renal cortical collecting ducts of mice.

J Clin Invest **120**: 1627-1635

Sinning A*, Liebmann L*, Kougioumtzes A, Westermann M, Bruehl C, Hübner C (2011)

Synaptic glutamate release is modulated by the Na⁺-driven Cl⁻/HCO₃⁻ exchanger Slc4a8.

J Neurosci **31**: 7300-7311

Koch D, Spiwoks-Becker I*, Sabanov V*, **Sinning A**, Dugladze T, Stellmacher A, Ahuja R, Grimm J, Schuler S, Muller A, Angenstein F, Ahmed T, Diesler A, Moser M, tom Dieck S, Spessert R, Boeckers T, Fassler R, Hübner C, Balschun D, Gloveli T, Kessels M, Qualmann B (2011)

Proper synaptic vesicle formation and neuronal network activity critically rely on syndapin I

EMBO J **in press**

*authors contributed equally to this work

Acknowledgements

Welch ein Privileg Unbekanntes erforschen zu dürfen, mit etwas Glück neues Wissen zu schaffen und im besten Falle das Leben ein bisschen verständlicher oder gar besser zu machen. Allein dafür lohnt es sich.

Dass man diesen Weg mit anderen Wissenschaftlern teilt, sich gegenseitig ermutigt nicht aufzugeben und das große Ziel gemeinsam verfolgt, macht es einmalig.

Zuerst möchte ich mich bei Prof. Dr. Christian Hübner für das Thema, die andauernde Unterstützung meiner Projekte und vor allem für die Betreuung der Doktorarbeit bedanken. Ich habe immer die notwendige Anleitung und Unterstützung erhalten und zugleich auch den Freiraum bei der Entwicklung meiner eigenen Ideen geschätzt. Zunächst möchte ich mich auch bei Prof. Dr. Baniahmad, Prof. Dr. Valentin Stein, Prof. Dr. Witte und Dr. M. Rust für die mögliche Begutachtung dieser Arbeit bedanken.

Dass mein Spaß an der Wissenschaft gewachsen ist, die alltägliche Laborarbeit nicht langweilig wurde und ich die Frustrationen aber auch die Freuden der Forschung mit Euch teilen durfte, dafür ein ganz dickes Dankeschön an alle Mitglieder des "Hübner Labors".

Antje, danke, dass du immer Deine (Labor-) Erfahrung mit mir geteilt hast. Christopher, auch wenn mein Chaosprinzip und Deine Ordnungsliebe das ein oder andere Mal kollidiert sind, es war mir eine große Freude mit Dir zu arbeiten. Viel Erfolg weiterhin. Mukhran, Deine georgische Lebensfreude und Dein "gell" haben mir den ein oder anderen Tag geredet, Dir und Deiner Familie alles Gute. Katrin, Du Seele des Labors, danke ganz herzlich, dass Du uns immer so aufmerksam und mütterlich umsorgt hast. Alles Liebe! Lutz, dank je well, dafür dass unsere Zusammenarbeit so gut geklappt hat. Meera, vielen Dank für die Korrektur der Rechtschreibung. Christoph und Ralf, Danke für viel Eis, verlorene Wetten, Schokolade und "Mobbing", Ihr habt mir großen Spaß in den Alltag gebracht.

Ingo und seinem Team, den Mitarbeiter der klinischen Chemie, des humangenetischen Institutes und des Tierstalles sowie allen, die ich zu erwähnen vergessen habe: vielen lieben Dank.

Für eine tolle Zeit in Paris möchte ich auch Prof. Dr. Dominique Eladari, Dr. Regine Chambrey und Dr. Fabien Sohet danken. Merci. In diesem Zusammenhang bedanke ich mich auch recht herzlich bei allen weiteren Kollaborationspartnern für die nette Zusammenarbeit und vor allem für das großzügige Teilen von Erfahrungen und so manchem Labortrick.

Am Ende möchte ich mich noch bei meinen Freunden und vor allem bei meiner Familie bedanken, die mich wirklich immer unterstützen, an mich glauben und mir vertrauen. Euch verdanke ich so viel.

Zuletzt und doch am tiefsten danke ich Dir, Olli. Du bist mein liebster Weggefährte, mein treuester Unterstützer und Beschützer und nun auch meine Familie. Danke für alles.

Ehrenwörtliche Erklärung

Hiermit erkläre ich, dass mir die Promotionsordnung der Medizinischen Fakultät der Friedrich-Schiller-Universität bekannt ist, ich die Dissertation selbst angefertigt habe und alle von mir benutzten Hilfsmittel, persönlichen Mitteilungen und Quellen in meiner Arbeit angegeben sind, mich folgende Personen bei der Auswahl und Auswertung des Materials sowie bei der Herstellung des Manuskripts unterstützt haben: Prof. Dr. C.A. Hübner, Dr. L. Liebmann, M. Malik und Dr. A. Hübner, die Hilfe eines Promotionsberaters nicht in Anspruch genommen wurde und dass Dritte weder unmittelbar noch mittelbar geldwerte Leistungen von mir für Arbeiten erhalten haben, die im Zusammenhang mit dem Inhalt der vorgelegten Dissertation stehen, dass ich die Dissertation noch nicht als Prüfungsarbeit für eine staatliche oder andere wissenschaftliche Prüfung eingereicht habe und dass ich die gleiche, eine in wesentlichen Teilen ähnliche oder eine andere Abhandlung nicht bei einer anderen Hochschule als Dissertation eingereicht habe.

Jena, 23.08.2011